DEVELOPING A HIGH THERMAL CONDUCTIVITY NUCLEAR FUEL WITH SILICON CARBIDE ADDITIVES

By

JIWEI WANG

A DISSERTATION PRESENTED TO THE GRADUATE SCHOOL
OF THE UNIVERSITY OF FLORIDA IN PARTIAL FULFILLMENT
OF THE REQUIREMENTS FOR THE DEGREE OF
DOCTOR OF PHILOSOPHY

UNIVERSITY OF FLORIDA

2008

To my parents, Li Wang and Shaofen Liu, for their love and support.

ACKNOWLEDGMENTS

I would like to thank Professor James Tulenko, my advisor and the supervisory committee chair, for his guidance and support. I would also like to thank Dr. Ronald Baney, my supervisory committee co-chair, for his patience and instruction. Without their help, this work would not have been possible.

I would like to thank Dr. Samim Anghaie for being on my supervisory committee and his kindness for providing the equipments at the Innovative Nuclear Space Powder and Propulsion Institute. I would also like to thank my supervisory committee member Dr. Edward Dugan for his help on the computer codes.

I would like to thank Shirvan Daryoosh at Innovative Nuclear Space Powder and Propulsion Institute for his help on the experiment equipments. I would also like to thank Department of energy for the funding of this study. Finally, I would like to thank my family for their consistent support through the many years of my education.

TABLE OF CONTENTS

page

LIST OF TABLES

LIST OF FIGURES

LIST OF ABBREVIATIONS

AC	Alternating current
AHPCS	Allylhydridopolycarbosilane
BOL	Beginning of life
CVD	Chemical vapor deposition
DSC	Differential scanning calorimetry
EOC	End of cycle
EOL	End of life
FTIR	Fourier transform infrared spectroscopy
LOCA	Lost of coolant accident
MTC	Moderator temperature Coefficient
MTS	Methyltrichlorosilane
PACVD	Photo assisted chemical vapor deposition
PECVD	Plasma enhanced chemical vapor deposition
SCB	Silacyclobutane
SEM	Scanning electron microscopy
SiC	Silicon carbide
TD	Theoretical Density
TMS	Trimethylsilane
XRD	X-ray diffraction
UO_2	Uranium dioxide

Abstract of Dissertation Presented to the Graduate School
of the University of Florida in Partial Fulfillment of the
Requirements for the Degree of Doctor of Philosophy

DEVELOPING A HIGH THERMAL CONDUCTIVITY NUCLEAR FUEL WITH SILICON CARBIDE ADDITIVES

By

Jiwei Wang

August 2008

Chair: James Tulenko
Major: Nuclear Engineering Sciences

Uranium dioxide (UO_2) is the most common fuel material utilized in commercial nuclear power reactors. The main disadvantage of UO_2 is its low thermal conductivity. During a reactor's operation, there is a large temperature gradient in the UO_2 fuel pellet, causing a very high centerline temperature, and introducing thermal stresses, which lead to extensive fuel pellet cracking. These cracks will add to the release of fission product gases after high burnup. The high fuel operating temperature also increases the rate of fission gas release and the fuel pellet swelling caused by both fission gases bubbles and thermal expansion. The amount of fission gas release and fuel swelling limits the life time of UO_2 fuel in reactor.

The objective of this research is to increase the thermal conductivity of UO_2 while not significantly affecting the neutronic property of UO_2. The concept is to incorporate another high thermal conductivity material, silicon carbide (SiC), into the UO_2 pellet. Silicon carbide is expected to form a conductive percolation pathway in the UO_2 for heat to flow out of the fuel pellet, thus increasing the UO_2 thermal conductivity.

Three methods were studied to incorporate SiC into UO_2. Firstly, chemical vapor deposition (CVD) process was used to coat UO_2 particles with a SiC layer prior to the low temperature sintering process of UO_2. Secondly, allylhydridopolycarbosilane (AHPCS), a pre-

ceramic polymer, was used to generate a SiC coating on UO_2 particles prior to the low temperature sintering process of UO_2. Thirdly, silicon carbide whiskers were mixed with UO_2 particles prior to the low temperature sintering method of UO_2.

Though pellets with high density were not achieved by the first and second methods, pellets of 95% TD were achieved by pressureless sintering of UO_2 with 5 vol% SiC whiskers and hot press sintering of UO_2 with 5 vol%, 10 vol% and 15 vol% SiC whiskers. The thermal conductivity of the pellets will be measured at Idaho National Laboratory. The thermal conductivity data will not be discussed in this dissertation.

CHAPTER 1
INTRODUCTION

Uranium dioxide (UO_2) is the most common fuel material in commercial nuclear power reactors. UO_2 has the advantages of a high melting point, good high-temperature stability, good chemical compatibility with cladding and coolant and resistance to radiation. The main disadvantage of UO_2 is its low thermal conductivity. During a reactor's operation, because the thermal conductivity of UO_2 is very low, for example, about 2.8 W/m-K at 1000 ^oC [1], there is a large temperature gradient in the UO_2 fuel pellet, causing a very high centerline temperature and introducing thermal stresses, which lead to extensive fuel pellet cracking. These cracks will add to the release of fission product gases after high burnup. The high fuel operating temperature also increases the rate of fission gas release and the fuel pellet swelling caused by fission gases bubbles. The amount of fission gas release and fuel swelling limits the life time of UO_2 fuel in a reactor.

The objective of this research is to increase the thermal conductivity of UO_2 while not significantly affecting the neutronic property of UO_2. The concept is to incorporate another material with high thermal conductivity into UO_2. It has been reported that a 50% increase in the thermal conductivity of UO_2 has been achieved by adding 5 w% molybdenum (Mo) at 1000 ^oC [2], however, Mo has a large thermal neutron absorption cross section, which negates its use in thermal reactors. It has also been reported that a 25% increase in the thermal conductivity of UO_2 has been achieved by adding 1.2 w% BeO [3], however, BeO is a very toxic material for handling.

Silicon carbide (SiC) is chosen in this research because the thermal conductivity of single crystal SiC is sixty times higher than that of UO_2 at room temperature and thirty times higher at

800 ^{o}C [4]. Silicon carbide also has the advantage of a low thermal neutron absorption cross section, high melting point, good chemical stability and good irradiation stability [5].

The neutronic properties of UO_2 will be affected by the addition of the SiC whiskers. The effect of SiC whiskers on the neutronic property of a UO_2 pellet was simulated by CASMO-3 [6], a multi-group two-dimensional transport theory code. The CASMO-3 result set the limit of the amount of SiC additives that could be added to UO_2 without significantly affecting the neutronic property of UO_2.

Several studies have shown that SiC whiskers can increase the thermal conductivity of matrix materials. Russell et al. [7] reported the thermal conductivity of 30 vol% VLS SiC whisker-mullite composite was three times higher at room temperature than that of single phase mullite in the perpendicular direction to the hot pressing direction, and two times higher in the parallel direction to the hot pressing direction. Johnson et al. [8] reported that the thermal conductivity of 30 vol% SiC whisker-osumilite glass composite was four times higher at room temperature than that of single phase mullite in the perpendicular direction to the hot pressing direction, and two times higher in the parallel direction to the hot pressing direction. Hesselman et al. [9] showed the thermal conductivity of 30 vol% VLS SiC whisker-lithium aluminosilicate glass composite was five times higher at room temperature than that of lithium aluminosilicate glass in the perpendicular direction to the hot pressing direction, and three times higher in the parallel direction to the hot pressing direction. Hesselman et al. [9] suggested that a SiC whisker "percolation" pathway was formed, and heat was conducted through SiC whiskers, bypassing the matrix.

Solomon et al [10, 11] have tried to increase the thermal conductivity of UO_2 by impregnating a SiC pre-ceramic polymer into a high dense UO_2 pellet with 10 to 12 vol% open

porosity and transferring the SiC pre-ceramic polymer to a crystalline form at 1300 ^{o}C. There was no improvement in the thermal conductivity of UO_2 because the maximum density of SiC was 75% TD even after several impregnation, which due to the blockage of the open porosity by the SiC during the impregnation and the low crystallization temperature.

Uranium dioxide pellets are usually produced by sintering the green pellets at about 1700 ^{o}C in hydrogen atmosphere. The high sintering temperature around 1700 ^{o}C is necessary to achieve the required high density of 95% TD. However, based on the study by Allen et al. [12], UO_2 reacts with SiC at the temperature above 1377 ^{o}C, evolving CO and SiO, forming uranium carbide, uranium silicide and $U_3C_3Si_2$. A two-stage low temperature sintering method of UO_2 was studied to avoid the reaction between UO_2 and SiC. Fuhrman et al. [13] have reported that UO_2 pellets of 95% to 97% theoretical density (TD) were achieved by sintering at 1200 ^{o}C in nitrogen for one hour followed by one hour reduction in hydrogen, using a uranium oxide powder with extra oxygen (O/U ~ 2.37). Langrod [14] has also achieved UO_2 pellets of above 95% TD using mixture of UO_2 and U_3O_8 (O/U ~ 2.30) by sintering at 1300 ^{o}C in argon or nitrogen atmosphere for two hours followed by reduction in hydrogen.

Three methods were studied to incorporate SiC into UO_2. Firstly, a chemical vapor deposition (CVD) process was used to coat UO_2 particles with a SiC layer prior to the low temperature sintering process. Secondly, a SiC pre-ceramic polymer, allylhydridopolycarbosilane (AHPCS), was used to coat UO_2 particles prior to the low temperature sintering process. Thirdly, SiC whiskers were mixed with UO_2 particles prior to the low temperature sintering process.

Though pellets with high density were not achieved by the first and second methods, pellets of 95% TD were achieved by pressureless sintering of UO_2 with 5 vol% SiC whiskers and

hot press sintering of UO_2 with 5 vol%, 10 vol% and 15 vol% SiC whiskers. The thermal conductivity of the pellets will be measured at Idaho National Laboratory. The thermal conductivity data will not be discussed in this dissertation.

CHAPTER 2
LITERATURE REVIEW

Properties of Uranium Dioxide

The properties of uranium dioxide (UO_2) have been investigated for decades. UO_2 has a cubic fluorite (CaF_2) type crystal structure with a lattice parameter of 0.5468nm [15]. The theoretical density of UO_2 is 10.96 g/cm^3 [16]. The melting point of UO_2 is about 2850 ^oC [17]. UO_2 also has the advantages of good high temperature stability, good chemical compatibility with cladding and coolant and resistance to radiation [18].

The thermal conductivity is one of the most important properties of UO_2, because it determines the fuel temperature, thus directly affect the behavior and performance of fuel pellet in a reactor. Based on the experiment data, Fink [1] pointed out that the thermal conductive of 95% dense UO_2 can be calculated by Equation 2-1, which is plotted in Figure 2-1.

$$k = \frac{100}{7.5408 + 17.692t + 3.6142t^2} + \frac{6400}{t^{5/2}} \exp\left(\frac{-16.35}{t}\right) \qquad (2\text{-}1)$$

Where t = T (K)/1000 and k is the thermal conductivity of 95% dense UO_2 in W/m-K.

Uranium dioxide is easily oxidized in air. The uranium oxide with O/U ratio greater than 2.0 is called hyperstoichiometric UO_2; the uranium oxide with O/U ratio less than 2.0 is called hypostoichiometric UO_2. The oxidation of UO_2 in air is a two-step reaction: $UO_2 \rightarrow U_3O_7/U_4O_9 \rightarrow U_3O_8$. The intermediate oxidation products, U_4O_9 and U_3O_7, are derivatives of the fluorite structure in which clusters of interstitial oxygen atoms are centered on unoccupied cubic sites in the lattice, with accompanying displacement of neighboring U atoms [19]. U_3O_8 has an orthorhombic lattice structure [20]. The density of U_3O_8 is 8.38 g/cm3, which is 24% less than UO_2. The density decrease results in an undesirable volume increase in the fuel.

The thermal conductivity of hyperstoichiometric UO_2 [21]is shown in Figure 2-2. The excess oxygen atoms act as phonon scattering centers, thus reduce the thermal conductivity of UO_2. The thermal conductivity of $(U_{0.8}Pu_{0.2})O_x$ ($x < 2.0$) [22] is shown in Figure 2-3. The defects in the UO_2 crystal lattice also act as phonon scattering centers, thus reduce the thermal conductivity of UO_2. In addition, hypostoichiometric UO_2 could contain uranium metal which could be highly reactive with other materials; hyperstoichiometric UO_2 may have an oxygen partial pressure sufficient to cause interaction with other materials [23]. The O/U ratio of an unknown $UO_{2.x}$ powder can be determined by measuring the weight difference of $UO_{2.x}$ and U_3O_8 oxidized by $UO_{2.x}$, or $UO_{2.x}$ and UO_2 reduced by $UO_{2.x}$ (for hyperstoichiometric UO_2).

The thermal conductivity of irradiated UO_2 is affected by the changes that take place in the fuel during irradiation. During irradiation, fission products accumulate in the UO_2 matrix and cause the fuel swelling. The fission products dissolved in the UO_2 lattice serve as phonon scattering centers, thus reduce the thermal conductivity of UO_2 fuel; the precipitated fission products have a much higher thermal conductivity than UO_2 and have a positive contribution to the thermal conductivity of UO_2 fuel. The fission product gases initially form in irradiated fuel as dispersed atoms within the UO_2 lattice, then form small bubbles. The small bubbles within the UO_2 lattice also serve as phonon scattering centers, thus reduce the thermal conductivity [24]. At temperature below 1000 ^oC, uranium dioxide retains essentially all the fission gases, but above this temperature the gases are released, little remains in those region of the fuel where the temperature exceeds 1800 ^oC [18]. Radiation damage from neutrons, α-decay and fission products increase the number of lattice defects and consequently reduces the thermal conductivity of UO_2 fuel. The thermal conductivities of UO_2 before and after irradiation are shown in Figure 2-4 [24]. The radiation-induced decrease in the thermal conductivity of UO_2 is

large at low temperature. Oxygen and uranium defects are known to anneal at around 500 K and 1000 K, respectively. This explains why most changes in the thermal conductivity of UO_2 are seen below 1000 K [24].

Properties of Silicon Carbide

Silicon carbide (SiC) is a ceramic compound of silicon and carbon, which was discovered by Edward Goodrich Acheson around 1893. Several polytypes of SiC exist, the most common polytype is α-SiC (6H-SiC) and the cubic form is β-SiC (3C-SiC). Only β-SiC is considered in this research because of its property of isotropic expansion when heated. The density of β-SiC is 3.21 g/cm^3 [25]. The melting temperature of β-SiC is about 2700 ^{o}C [5]. Silicon carbide has low thermal neutron absorption cross section. The neutron cross-section for silicon, carbon and other relative nuclides are shown in Table 2-1 [26].

One of the most attractive properties of SiC is its high thermal conductivity. The thermal conductivity of single crystal SiC measured by Slack at room temperature is 490 W/m-K [4], which is higher than copper, 398 W/m-K. The thermal conductivity of polycrystalline β-SiC by CVD process is lower, about 70 W/m-K at room temperature [27]. Figure 2-5 shows the thermal conductivities of single crystal SiC and polycrystalline β-SiC versus temperature. The single crystal SiC has higher purity and less defects than the polycrystalline β-SiC. The boundaries in the polycrystalline β-SiC can also serve as phonon scattering centers. Figure 2-6 shows the thermal conductivity of polycrystalline β-SiC before and after irradiation [28]. The thermal conductivity of unirradiated SiC decreases with increasing temperature. The thermal conductivity of SiC is mainly controlled by the lattice vibration waves (Phonons). The phonon-phonon scatterings increase with increasing temperature, which decrease the phonon mean free path and consequently decrease the thermal conductivity.

The thermal conductivity of SiC decreases by a factor between 3 and 9 at room temperature when SiC was irradiated with fast neutrons fluence of 2.7-7.7×10^{21} n/cm^2 (E>0.18 MeV) at 550 ^{o}C-1100 ^{o}C [28]. During fast neutron irradiation, point defects are introduced in the SiC lattice structure. These defects act as the scattering centers for phonons, so the thermal conductivity is sharply reduced as a consequence. The phonon mean free path is determined by the mean free path of defects, so the thermal conductivity is almost independent of temperature after irradiation.

Amorphous SiC was studied by Snead [29] using transmission electron microscopy (TEM) after irradiation of β-SiC with fast neutron of 2.6 ×10^{25} n/m^2 (E>0.1 MeV) at 53 ^{o}C. The thermal conductivity of amorphous SiC is only 5.4 W/m-K at 800 ^{o}C, only slightly higher than UO_2. The annealing effect was also observed by Snead. The SiC crystallites grow slowly in the ~800-1100 ^{o}C temperature range and that the crystallite growth rate was approximately linear with annealing temperature; the SiC crystallites grow rapidly in the temperature range of 1100-1150 ^{o}C, with both faster growth of the existing crystallites and rapid nucleation of new crystallites throughout the amorphous material. No amorphous SiC is found after annealing at 1150 ^{o}C for 30 min [29].

Silicon carbide has good chemical stability because of the protective silicon oxide (SiO_2) layer formed on it. Silicon carbide is not attacked by any acids or alkalis or molten salts at room temperature. Verral reported that the SiC lost 2% at 573 K in deoxygenated water of pH 10.3 after 90 days and less than 2% at 573K in deoxygenated water of pH 3 after 32 days [5]. Hirayama also reported the weight loss increased with increasing pH value. The weight loss in the oxygenated solution was more than that in the deoxygenated solution [30]. Verral reported that there was no significant interaction between SiC and Zircaloy-4 at 1273 K. At 1773 K there

was a diffusion-based reaction to form ZrC and free SiC, but the SiC Zircaloy cladding interaction was no worse than the UO_2-Zircaloy cladding interaction [5].

Silicon carbide has been used as a layer in tristructral isotropic (TRISO) fuel particles for gas cooled nuclear reactors. There are four layers on the spherical UO_2 particle of TRISO fuel: a porous pyrolytic carbon buffer layer, a dense pyrolytic carbon layer, a SiC layer and another pyrolytic carbon layer. The SiC layer acts as a diffusion barrier to fission products and a pressure vessel of the particle [31]. Silicon carbide has shown the capability to maintain its properties under high irradiation and temperature conditions. There is a slightly expansion at the fluences up to 5×10^{26}n/m2 and irradiation temperature below 1000 ^{o}C; at higher temperature, irradiation creates voids that cause continuing expansion, but the structural integrity is not affected. The irradiation has a negligible effect on the strength of SiC [27].

Silicon carbide has also been used as electronic devices operating under extreme conductions of power and temperature because of its wide band gap, high breakdown electric field strength, high saturated electron drift velocity and high thermal conductivity. Because of high purity requirement of the semiconductor device, the SiC is usually produced by a chemical vapor deposition process.

Silicon carbide is commonly manufactured by combining silica sand (SiO_2) and carbon at high temperature, between 1600 ^{o}C to 2500 ^{o}C. The purity of the SiC crystals produced is relatively low compared to the more expensive chemical vapor deposition (CVD) process.

Pre-ceramic polymers can also used to produce crystalline silicon carbide. Allylhydridopolycarbosilane (AHPCS) was successfully converted to crystalline β-SiC at 1600 ^{o}C by Zheng et al. [32]. Silicon carbide fibers were also produced from the pre-ceramic polymer [33]. The fibers were used to improve the mechanical properties of the matrix materials.

Besides SiC fibers, SiC whiskers were also produced to improve the mechanical properties of the matrix material. The two main methods to produce SiC whiskers are Rice Hull method and vapor-liquid-solid (VLS) method. The SiC whiskers are single crystal. The strengths, Young's module and thermal conductivity can be extremely high. The SiC whiskers were not only used to increase the mechanical properties [34, 35], but also the thermal conductivity of the matrix materials [7-9].

Table 2-1. Neutronic cross sections (barns) [26].

	σ_{abs}(th)	σ_s(th)	σ_s(epi)
C	0.0032	4.8	4.66
Si	0.00019	4.2	3.7
O	0.13	5	3.4
Zr	0.18	8	6.2
Be	0.01	7	6.11
Mo	2.5	7	6.0

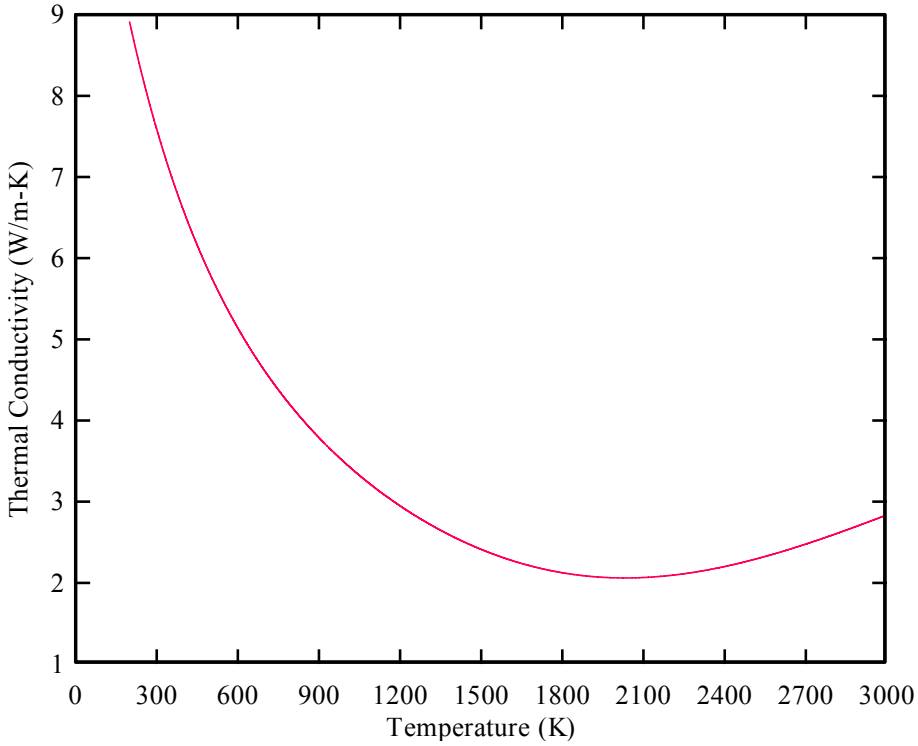

Figure 2-1. Thermal conductivity of UO_2 [1].

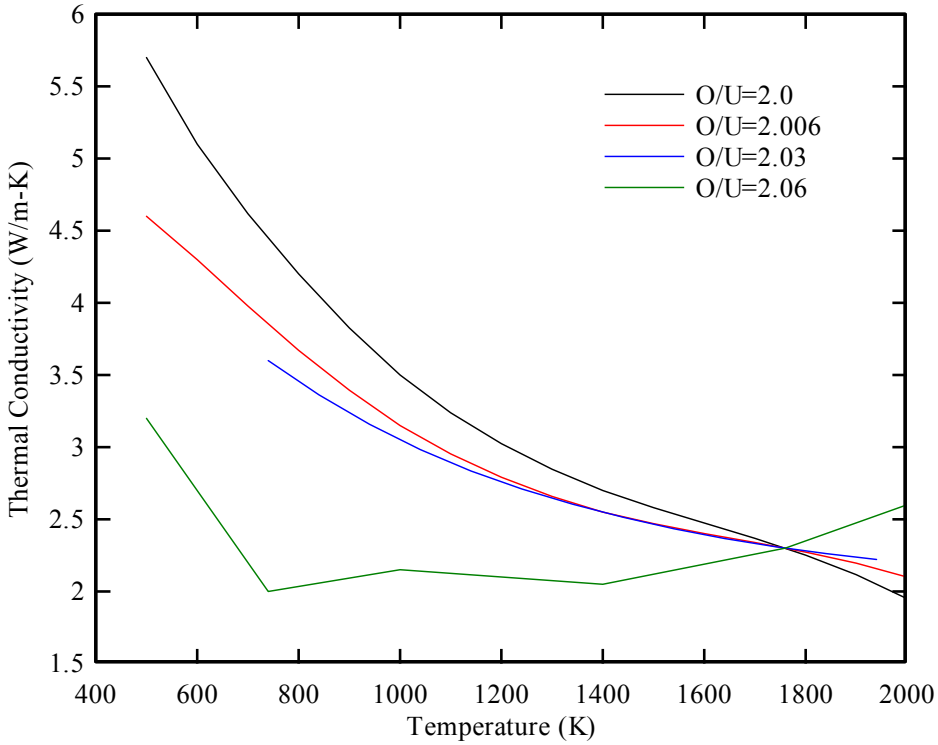

Figure 2-2. Thermal conductivity of hyperstoichiometric UO_2 [21].

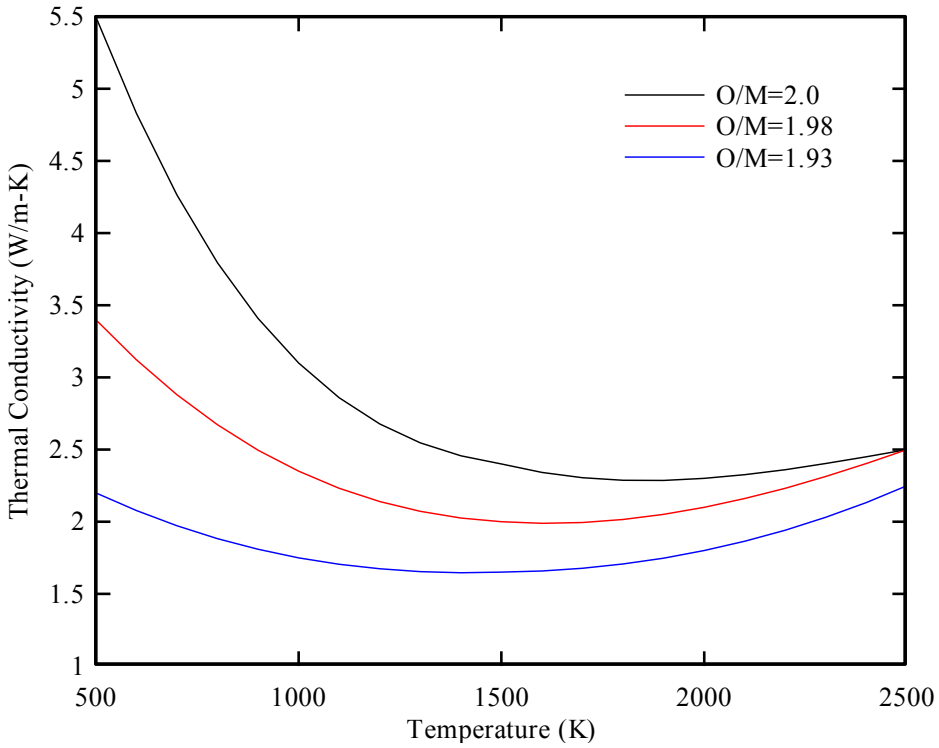

Figure 2-3. Thermal conductivity of $(U_{0.8}Pu_{0.2})O_x$ [22].

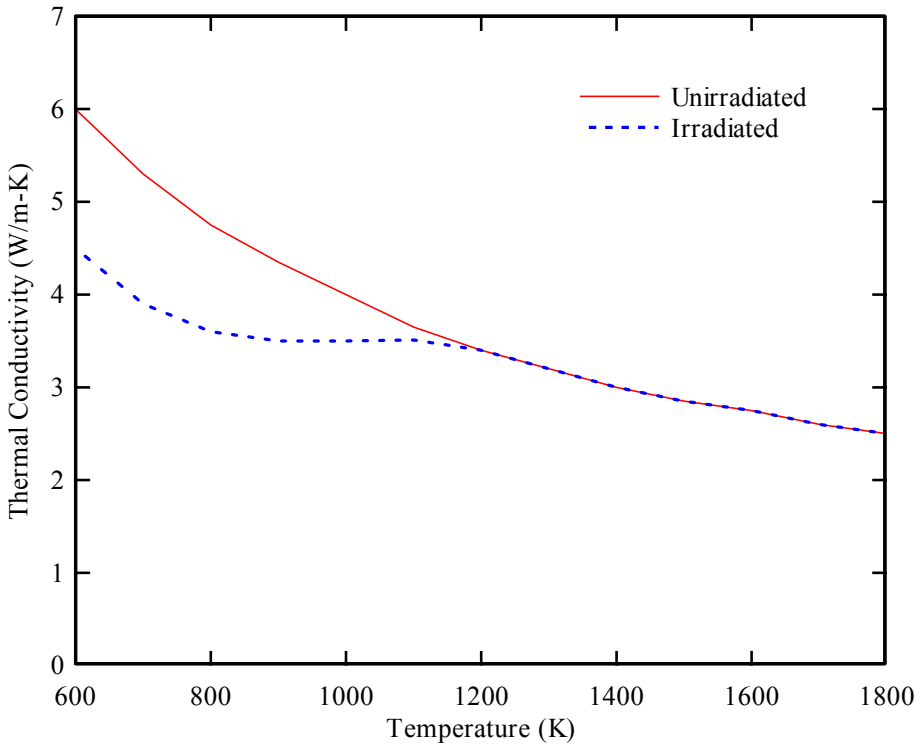

Figure 2-4. Thermal conductivity of UO_2 before and after irradiation [24].

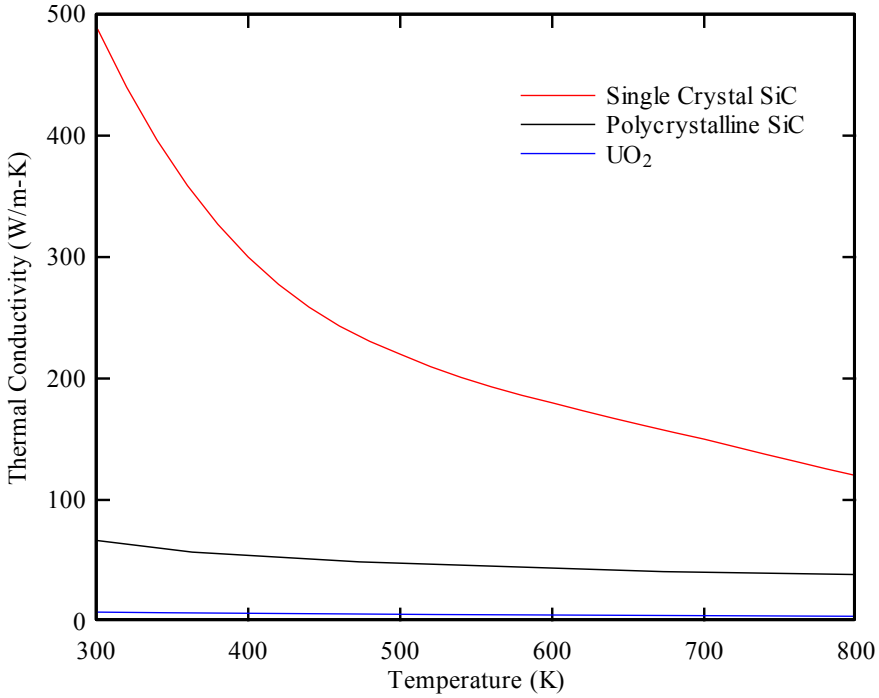

Figure 2-5. Thermal conductivity of single crystal SiC and polycrystalline SiC compared to UO_2 [1], [4], [27].

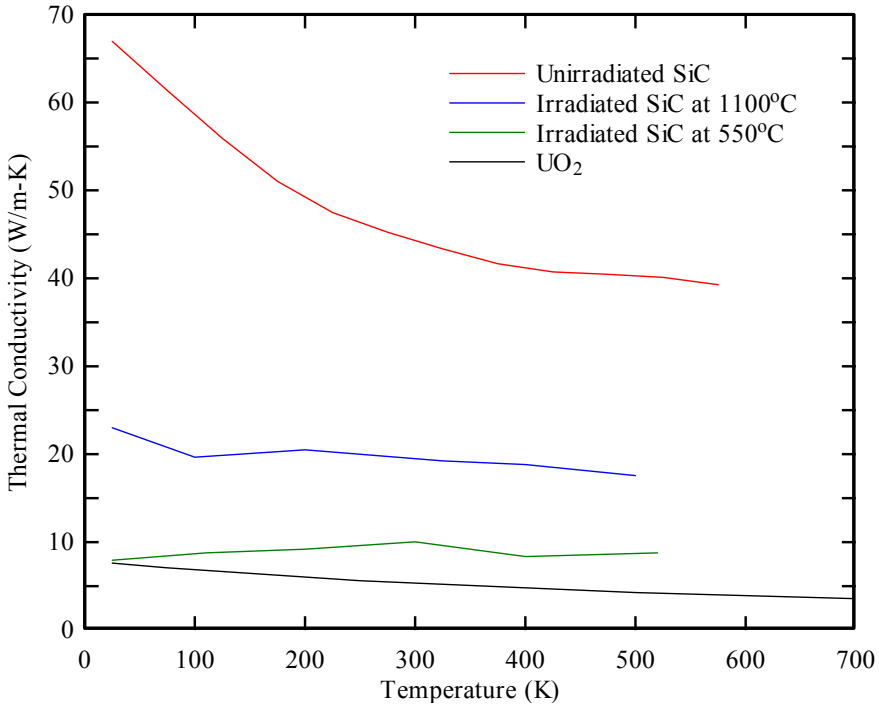

Figure 2-6. Thermal conductivity of SiC before and after irradiation compared to UO_2 [1], [27], [28].

CHAPTER 3
NEUTRONIC CALCULATION

Introduction

The effect of silicon carbide (SiC) additives on the neutronic properties of uranium dioxide (UO_2) should be studied before the experiments. CASMO-3 [6], a multi-group two-dimensional transport theory code, was used to simulate the burnup of UO_2 fuel and UO_2 fuel with SiC additives. The simulation utilized a Framatome Mark-B 15X15 assembly design. The power of the assembly is 14.37 MW. There are 208 fuel rods, 16 guide tubes and 1 instrument tube per assembly. The cross section view of Mark-B assembly is shown in Figure 3-1. The enrichment of the fuel is 4.66%.

Methods and Results

The K-infinity versus burnup of UO_2 fuel compared to UO_2 with 5 w% and 10 w% SiC is shown in Table 3-1 and Figure 3-2. The K-infinity of UO_2 fuel is less than that of UO_2 with 5 w% and 10 w% SiC at the beginning of life (BOL) because SiC replaces uranium-238, which has a large resonance absorption cross section. As the fuel burns up, the K-infinity of UO_2 fuel decreases slower than that of UO_2 with 5 w% and 10 w% SiC because the thermal utilization factor in UO_2 decreases slower than in UO_2 with SiC. At the end of life (EOL), 60 GWD/MTU, the K-infinity of UO_2 with 5 w% SiC and 10 w% SiC are about 7% and 14% less than the K-infinity of UO_2 fuel, respectively. The Doppler coefficient and moderator temperature coefficient (MTC) versus burnup of UO_2 fuel compared to UO_2 with 5 w% and 10 w% SiC are shown in Table 3-2, Table 3-3, Figure 3-3 and Figure 3-4. The Doppler coefficient of UO_2 fuel is less than that of UO_2 with 5 w% and 10 w% SiC at BOC, but larger than that of UO_2 with SiC at the end of cycle (EOC). The MTC of UO_2 fuel is less than UO_2 with SiC throughout the burnup. All the Doppler coefficients and MTCs of UO_2 fuel and UO_2 with SiC fuel are negative.

Because volume percentage is always used when considering SiC whiskers-matrix composite, the K-infinity versus burnup of UO_2 fuel compared to UO_2 with 5 vol%, 10 vol% and 15 vol% SiC is shown in Table 3-1 and Figure 3-5. The 5 vol% SiC is equal to 1.5 w% SiC, the 10 vol% SiC is equal to 3.2% SiC and 15 vol% SiC is equal to 4.9% SiC. At 60 GWD/MTU, the K-infinity of UO_2 with 5 vol%, 10 vol% and 15 vol% SiC are about 2.1%, 4.5% and 7.2% less than the K-infinity of UO_2 fuel. The Doppler coefficient and moderator temperature coefficient (MTC) versus burnup of UO_2 fuel compared to UO_2 with 5 vol%, 10 vol% and 15 vol% SiC are shown in Table 3-2, Table 3-3, Figure 3-6 and Figure 3-7.

Discussion

In this research, the limit of the amount of SiC additives was set to 5 w% to limit the change of K-infinity at EOL to 7 %. Because the SiC additives will affect the thermal conductivity of the fuel, thus affecting the fuel temperature, the effect of fuel temperature change on the neutronic properties of the fuel has to be considered.

Assuming there was 50% increase in thermal conductivity of UO_2 with SiC additives compared to UO_2 fuel, the centerline temperature of the fuel rod was calculated according to Equation 3-1. The results are shown in Table 3-13. The centerline temperature of UO_2 with SiC was 275 ^{o}C lower than the centerline temperature of UO_2 fuel.

$$T_{cl} - T_m = \frac{q'}{2\pi r_f}\left[\frac{r_f}{2k_f} + \frac{1}{h_g} + \frac{t_c}{k_c} + \frac{r_f}{h_s(r_f + t_c)}\right] \quad (3\text{-}1)$$

Where T_{cl} is the fuel centerline temperature (K)

T_m is the moderator temperature (K)

q' is the linear power density (W/cm)

r_f is the radius of fuel pellet (cm)

k_f is the average thermal conductivity of fuel (W/(cm*K))

h_g is the gap heat transfer coefficient (0.5---1.1) (W/(cm^2*K))

k_c is the thermal conductivity of cladding (W/(cm*K)

h_s is the coefficient of convective heat transfer (2.8---4.5) (W/(cm^2*K)

t_c is the clad thickness (cm)

Based on the centerline temperature calculation, a 200 ^oC decrease in fuel temperature of UO_2 with SiC was assumed in the CASMO-3 calculation. (Different amount of SiC will change the fuel temperature differently. In this research, the changes of fuel temperatures of UO_2 with different amount of SiC were assumed to be the same, 200 ^oC, for simplicity) The K-infinity versus burnup of UO_2 fuel compared to UO_2 with 5 vol%, 10 vol% and 15 vol% SiC, which are 200 ^oC lower in fuel temperature, is shown in Table 3-4 and Figure 3-8. At 60 GWD/MTU, the K-infinity of UO_2 with 5 vol%, 10 vol% and 15 vol% SiC are about 2.4%, 4.9% and 7.6% less than the K-infinity of UO_2 fuel. The differences in K-infinity are larger than that of UO_2 with SiC without considering the temperature change. The Doppler coefficient of UO_2 with SiC is less than UO_2, as shown in Table 3-5 and Figure 3-9. The MTC of UO_2 with SiC is still larger than UO_2, as shown in Table 3-6 and Figure 3-10. All the Doppler coefficients and MTC of UO_2 fuel and UO_2 with SiC fuel are negative.

The effect of SiC additives on the neutronic properties of UO_2 fuel at boron let down situation was also studied. Considering a core with three batches (equal amount of fuel), a batch of fresh fuel, a batch of fuel burned once and a batch of fuel burned twice. The power distribution of the three batches was 1.25:1:0.75. In steady state, the cycle burnup of batch one was 25 GWD/MTU; the cycle burnup of batch two was 20 GWD/MTU; and the cycle burnup of batch three was 15 GWD/MTU. The boron concentration is shown in Figure 3-11. During boron let down, the boron concentration changed from 1400 ppm at 0 GWD/MTU of fuel assembly to

10 ppm at 25 GWD/MTU of fuel assembly, from 1400 ppm at 25.01 GWD/MTU of fuel assembly to 10 ppm at 45 GWD/MTU of fuel assembly and from 1400 ppm at 45.01 GWD/MTU of fuel assembly to 10 ppm at 60 GWD/MTU of fuel assembly. The K-infinity versus burnup of UO_2 fuel compared to UO_2 with SiC fuel is shown in Table 3-7 and Figure 3-12. The K-infinity versus burnup of UO_2 core compared with UO_2 with SiC core is shown in Table 3-8 and Figure 3-13. At EOC, which is 25 GWD/MTU of the fresh fuel assembly, the K-infinity of the core of UO_2 with 5 vol%, 10 vol% and 15 vol% SiC are about 2.1%, 4.5% and 7.2% less than the K-infinity of the core of UO_2 fuel. The Doppler coefficient of UO_2 with SiC is less than UO_2, as shown in Table 3-9 and Figure 3-14. The Doppler coefficient of the core of UO_2 with SiC is less than the core of UO_2, as shown in Table 3-10 and Figure 3-15. All the Doppler coefficients are negative. The MTC of UO_2 with SiC is still larger than UO_2, as shown in Table 3-11 and Figure 3-16. The MTC of UO_2 with 10 vol% and 15 vol% SiC are positive at the 0.5 GWD/MTU of the fuel assembly. However, all the MTCs of the core are negative, as shown in Table 3-12 and Figure 3-17.

Table 3-1. K-infinity versus burnup of UO_2 fuel compared to UO_2 with SiC fuel.

Equivalent burnup (GWD/MTU)	UO_2	UO_2 + 5 w% SiC	UO_2 + 10 w% SiC	UO_2 + 5 vol% SiC	UO_2 + 10 vol% SiC	UO_2 + 15 vol% SiC
0	1.41154	1.42005	1.42592	1.41447	1.41739	1.4202
0.5	1.35996	1.36314	1.36451	1.3611	1.36221	1.36321
5	1.30833	1.30575	1.30048	1.30778	1.30685	1.30565
10	1.2556	1.24631	1.23368	1.25296	1.2499	1.24615
15	1.20872	1.19317	1.17308	1.20426	1.19899	1.19276
20	1.16617	1.14419	1.11601	1.15981	1.15238	1.14363
25	1.12643	1.0977	1.06056	1.11807	1.10839	1.09698
30	1.08863	1.05264	1.00586	1.07824	1.06614	1.05181
35	1.05234	1.00885	0.95243	1.03983	1.02516	1.00776
40	1.01733	0.96639	0.90124	1.00261	0.98546	0.96512
45	0.98355	0.92576	0.85395	0.96676	0.94723	0.92432
50	0.95128	0.88752	0.8124	0.93259	0.91097	0.88604
55	0.9207	0.85269	0.7779	0.90049	0.87735	0.85108
60	0.89211	0.82183	0.75079	0.87075	0.84677	0.82025

Table 3-2. Doppler coefficient (pcm/K) versus burnup of UO_2 fuel compared to UO_2 with SiC fuel.

Equivalent burnup (GWD/MTU)	UO_2	UO_2 + 5 w% SiC	UO_2 + 10 w% SiC	UO_2 + 5 vol% SiC	UO_2 + 10 vol% SiC	UO_2 + 15 vol% SiC
0	-1.56	-1.50	-1.47	-1.53	-1.52	-1.50
0.5	-1.58	-1.54	-1.51	-1.56	-1.55	-1.53
5	-1.65	-1.61	-1.59	-1.62	-1.62	-1.60
10	-1.79	-1.76	-1.76	-1.76	-1.76	-1.76
15	-1.94	-1.93	-1.95	-1.93	-1.92	-1.93
20	-2.09	-2.09	-2.13	-2.08	-2.08	-2.09
25	-2.23	-2.24	-2.28	-2.22	-2.22	-2.24
30	-2.35	-2.37	-2.44	-2.34	-2.35	-2.37
35	-2.46	-2.49	-2.56	-2.45	-2.45	-2.49
40	-2.54	-2.59	-2.67	-2.54	-2.56	-2.59
45	-2.62	-2.67	-2.75	-2.62	-2.64	-2.67
50	-2.69	-2.74	-2.82	-2.70	-2.71	-2.74
55	-2.74	-2.79	-2.86	-2.75	-2.77	-2.79
60	-2.79	-2.84	-2.87	-2.80	-2.81	-2.82

Table 3-3. MTC (pcm/K) versus burnup of UO_2 fuel compared to UO_2 with SiC fuel.

Equivalent burnup (GWD/MTU)	UO_2	UO_2 + 5 w% SiC	UO_2 + 10 w% SiC	UO_2 + 5 vol% SiC	UO_2 + 10 vol% SiC	UO_2 + 15 vol% SiC
0	-34.40	-31.02	-27.20	-33.63	-32.49	-30.93
0.5	-32.32	-29.18	-25.58	-31.63	-30.48	-29.10
5	-36.84	-34.10	-30.75	-36.31	-35.14	-34.01
10	-42.27	-39.80	-36.48	-41.84	-40.61	-39.71
15	-47.05	-44.66	-41.20	-46.69	-45.41	-44.57
20	-51.29	-48.91	-45.00	-50.98	-49.71	-48.86
25	-55.32	-52.68	-47.97	-54.98	-53.66	-52.60
30	-58.90	-55.94	-50.20	-58.53	-57.14	-55.83
35	-62.25	-58.66	-51.33	-61.76	-60.29	-58.55
40	-65.37	-60.96	-51.43	-64.67	-63.04	-60.76
45	-67.92	-62.66	-50.51	-67.15	-65.44	-62.47
50	-70.38	-63.67	-48.75	-69.20	-67.28	-63.50
55	-72.58	-64.21	-46.67	-70.87	-68.66	-63.92
60	-74.45	-64.29	-44.81	-72.24	-69.71	-64.02

Table 3-4. K-infinity versus burnup of UO_2 fuel compared to UO_2 with SiC fuel (200 ^oC less in fuel temperature).

Equivalent burnup (GWD/MTU)	UO_2	UO_2 + 5 vol% SiC	UO_2 + 10 vol% SiC	UO_2 + 15 vol% SiC
0	1.41154	1.42088	1.42376	1.42653
0.5	1.35996	1.36718	1.36825	1.36921
5	1.30833	1.31363	1.31263	1.31139
10	1.2556	1.25868	1.25552	1.2517
15	1.20872	1.20967	1.20427	1.1979
20	1.16617	1.16473	1.15711	1.14813
25	1.12643	1.12235	1.11237	1.10064
30	1.08863	1.08171	1.06922	1.05442
35	1.05234	1.0424	1.02721	1.00921
40	1.01733	1.00417	0.98639	0.96531
45	0.98355	0.96728	0.947	0.92324
50	0.95128	0.93209	0.90964	0.88379
55	0.9207	0.899	0.87501	0.84784
60	0.89211	0.8684	0.84362	0.8163

Table 3-5. Doppler coefficient (pcm/K) versus burnup of UO_2 fuel compared to UO_2 with SiC fuel (200 ^oC less in fuel temperature).

Equivalent burnup (GWD/MTU)	UO_2	UO_2 + 5 vol% SiC	UO_2 + 10 vol% SiC	UO_2 + 15 vol% SiC
0	-1.56	-1.67	-1.65	-1.64
0.5	-1.58	-1.71	-1.69	-1.68
5	-1.65	-1.78	-1.76	-1.75
10	-1.79	-1.92	-1.92	-1.91
15	-1.94	-2.10	-2.10	-2.11
20	-2.09	-2.27	-2.27	-2.28
25	-2.23	-2.42	-2.42	-2.44
30	-2.35	-2.55	-2.56	-2.59
35	-2.46	-2.67	-2.68	-2.71
40	-2.54	-2.78	-2.79	-2.82
45	-2.62	-2.86	-2.89	-2.92
50	-2.69	-2.95	-2.97	-3.00
55	-2.74	-3.02	-3.04	-3.07
60	-2.79	-3.07	-3.09	-3.12

Table 3-6. MTC (pcm/K) versus burnup of UO_2 fuel compared to UO_2 with SiC fuel (200 ^oC less in fuel temperature).

Equivalent burnup (GWD/MTU)	UO_2	UO_2 + 5 vol% SiC	UO_2 + 10 vol% SiC	UO_2 + 15 vol% SiC
0	-34.40	-32.74	-31.54	-30.15
0.5	-32.32	-30.75	-29.62	-28.32
5	-36.84	-35.33	-34.34	-33.15
10	-42.27	-40.74	-39.81	-38.71
15	-47.05	-45.46	-44.54	-43.44
20	-51.29	-49.63	-48.77	-47.59
25	-55.32	-53.59	-52.58	-51.26
30	-58.90	-57.06	-55.93	-54.40
35	-62.25	-60.22	-58.85	-56.98
40	-65.37	-62.99	-61.33	-59.05
45	-67.92	-65.33	-63.39	-60.52
50	-70.38	-67.29	-64.76	-61.28
55	-72.58	-68.77	-65.67	-61.42
60	-74.45	-69.97	-66.18	-61.18

Table 3-7. K-infinity versus burnup of UO_2 fuel compared to UO_2 with SiC fuel (200 ^oC less in fuel temperature) at boron let-down.

Equivalent burnup (GWD/MTU)	UO_2	UO_2 + 5 vol% SiC	UO_2 + 10 vol% SiC	UO_2 + 15 vol% SiC
0	1.27265	1.27525	1.27131	1.26663
0.5	1.23342	1.23469	1.22975	1.22414
5	1.2104	1.21074	1.20511	1.1987
10	1.18497	1.18436	1.17774	1.17014
15	1.16305	1.16153	1.15393	1.14514
20	1.1442	1.14159	1.13303	1.12307
25	1.12757	1.12383	1.11428	1.1031
25.01	1.02681	1.01685	1.00175	0.98436
25.4	1.02499	1.01488	0.99968	0.98215
29	1.01752	1.00657	0.99079	0.97252
33	1.00981	0.99784	0.98129	0.96208
37	1.00246	0.98941	0.97203	0.95173
41	0.9957	0.98157	0.96336	0.94212
45	0.98974	0.97463	0.95579	0.93381
45.01	0.89612	0.87443	0.84991	0.82166
45.3	0.8952	0.87343	0.84887	0.82061
48	0.89583	0.87401	0.84983	0.82219
51	0.89699	0.87504	0.85112	0.82397
54	0.89835	0.87629	0.85257	0.82588
57	0.90022	0.87812	0.85472	0.82861
60	0.90282	0.88088	0.858	0.83272

Table 3-8. K-infinity versus burnup of UO_2 core compared to UO_2 with SiC core (200 ^oC less in fuel temperature) at boron let-down.

Equivalent burnup of fresh fuel assembly (GWD/MTU)	UO_2	UO_2 + 5 vol% SiC	UO_2 + 10 vol% SiC	UO_2 + 15 vol% SiC
0	1.0966	1.0889	1.0761	1.0613
0.5	1.0794	1.0711	1.0578	1.0426
5	1.0675	1.0585	1.0449	1.0292
10	1.0546	1.0449	1.0306	1.0142
15	1.0433	1.0328	1.0180	1.0009
20	1.0337	1.0224	1.0069	0.9891
25	1.0254	1.0134	0.9974	0.9791

Table 3-9. Doppler coefficient (pcm/K) versus burnup of UO_2 fuel compared to UO_2 with SiC fuel (200 ^oC less in fuel temperature) at boron let-down.

Equivalent burnup (GWD/MTU)	UO_2	UO_2 + 5 vol% SiC	UO_2 + 10 vol% SiC	UO_2 + 15 vol% SiC
0	-1.75	-1.88	-1.88	-1.88
0.5	-1.77	-1.91	-1.91	-1.90
5	-1.79	-1.94	-1.93	-1.94
10	-1.90	-2.05	-2.05	-2.06
15	-2.03	-2.19	-2.19	-2.21
20	-2.14	-2.32	-2.32	-2.34
25	-2.23	-2.42	-2.42	-2.44
25.01	-2.46	-2.67	-2.70	-2.74
25.4	-2.46	-2.67	-2.71	-2.75
29	-2.50	-2.73	-2.76	-2.80
33	-2.54	-2.77	-2.80	-2.85
37	-2.58	-2.81	-2.84	-2.88
41	-2.60	-2.84	-2.86	-2.90
45	-2.60	-2.85	-2.86	-2.91
45.01	-2.87	-3.17	-3.23	-3.30
45.3	-2.87	-3.17	-3.22	-3.30
48	-2.86	-3.15	-3.19	-3.26
51	-2.84	-3.13	-3.17	-3.23
54	-2.82	-3.11	-3.14	-3.20
57	-2.80	-3.08	-3.11	-3.14
60	-2.77	-3.04	-3.07	-3.09

Table 3-10. Doppler coefficient (pcm/K) versus burnup of UO_2 core compared to UO_2 with SiC core (200 ^oC less in fuel temperature) at boron let-down.

Equivalent burnup of fresh fuel assembly (GWD/MTU)	UO_2	UO_2 + 5 vol% SiC	UO_2 + 10 vol% SiC	UO_2 + 15 vol% SiC
0	-2.27	-2.47	-2.49	-2.52
0.5	-2.27	-2.48	-2.50	-2.54
5	-2.30	-2.51	-2.52	-2.56
10	-2.35	-2.56	-2.58	-2.62
15	-2.41	-2.63	-2.65	-2.68
20	-2.46	-2.68	-2.69	-2.73
25	-2.49	-2.72	-2.73	-2.76

Table 3-11. MTC (pcm/K) versus burnup of UO_2 fuel compared to UO_2 with SiC fuel (200 ^oC less in fuel temperature) at boron let-down.

Equivalent burnup (GWD/MTU)	UO_2	UO_2 + 5 vol% SiC	UO_2 + 10 vol% SiC	UO_2 + 15 vol% SiC
0	-5.21	-2.63	-0.21	2.48
0.5	-3.48	-0.97	1.38	4.00
5	-12.86	-10.44	-8.36	-5.90
10	-23.56	-21.19	-19.29	-17.11
15	-33.90	-31.66	-29.99	-28.04
20	-44.25	-42.20	-40.89	-39.25
25	-55.11	-53.38	-52.40	-51.09
25.01	-20.51	-16.52	-13.03	-8.73
25.4	-21.27	-17.31	-13.79	-9.50
29	-28.91	-25.03	-21.67	-17.54
33	-37.87	-34.15	-31.04	-27.00
37	-47.29	-43.83	-40.93	-37.23
41	-57.26	-54.15	-51.71	-48.49
45	-67.81	-65.27	-63.46	-60.92
45.01	-25.70	-18.81	-12.33	-3.93
45.3	-26.41	-19.54	-13.12	-4.72
48	-34.17	-27.70	-21.65	-13.84
51	-43.33	-37.24	-31.73	-24.59
54	-53.09	-47.49	-42.58	-36.20
57	-63.45	-58.49	-54.32	-48.84
60	-74.53	-70.45	-67.16	-62.87

Table 3-12. MTC (pcm/K) versus burnup of UO_2 core compared to UO_2 with SiC core (200 ^oC less in fuel temperature) at boron let-down.

Equivalent burnup of fresh fuel assembly (GWD/MTU)	UO_2	UO_2 + 5 vol% SiC	UO_2 + 10 vol% SiC	UO_2 + 15 vol% SiC
0	-15.43	-11.30	-7.52	-2.86
0.5	-15.14	-11.06	-7.30	-2.68
5	-23.54	-19.62	-16.12	-11.77
10	-33.27	-29.52	-26.32	-22.28
15	-43.16	-39.67	-36.78	-33.14
20	-53.39	-50.25	-47.85	-44.73
25	-64.20	-61.61	-59.78	-57.31

Table 3-13. Centerline temperature of UO_2 fuel compared to UO_2 with SiC.

	T_m	q'	r_f	k_f	h_g	k_c	h_s	t_c	Tcl (K)	Tcl (^oC)
UO_2 with SiC	600	270	0.47	0.041	0.5	0.15	2.8	0.06731	1383	1110
					1.1		4.5		1272	999
UO_2	600	270	0.47	0.027	0.5	0.15	2.8	0.06731	1648	1375
					1.1		4.5		1538	1265

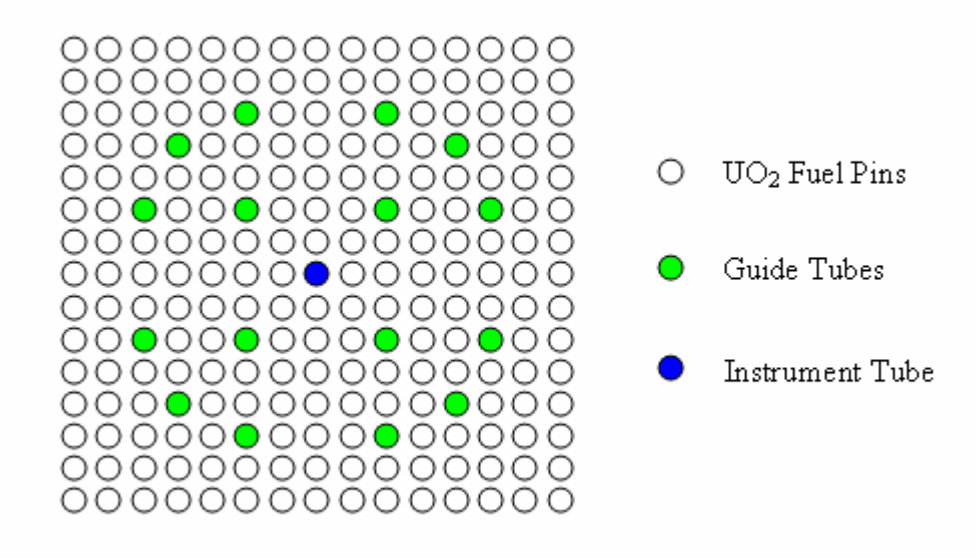

Figure 3-1. Crystal River 15X15 assembly design.

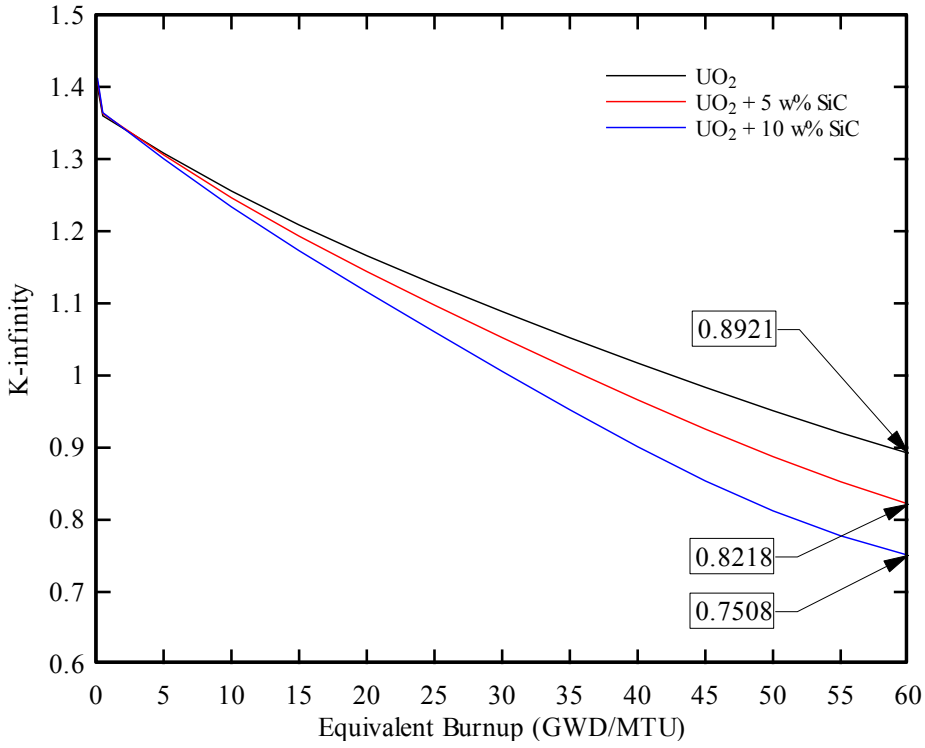

Figure 3-2. K-infinity versus burnup of UO_2 fuel compared to UO_2 with SiC fuel.

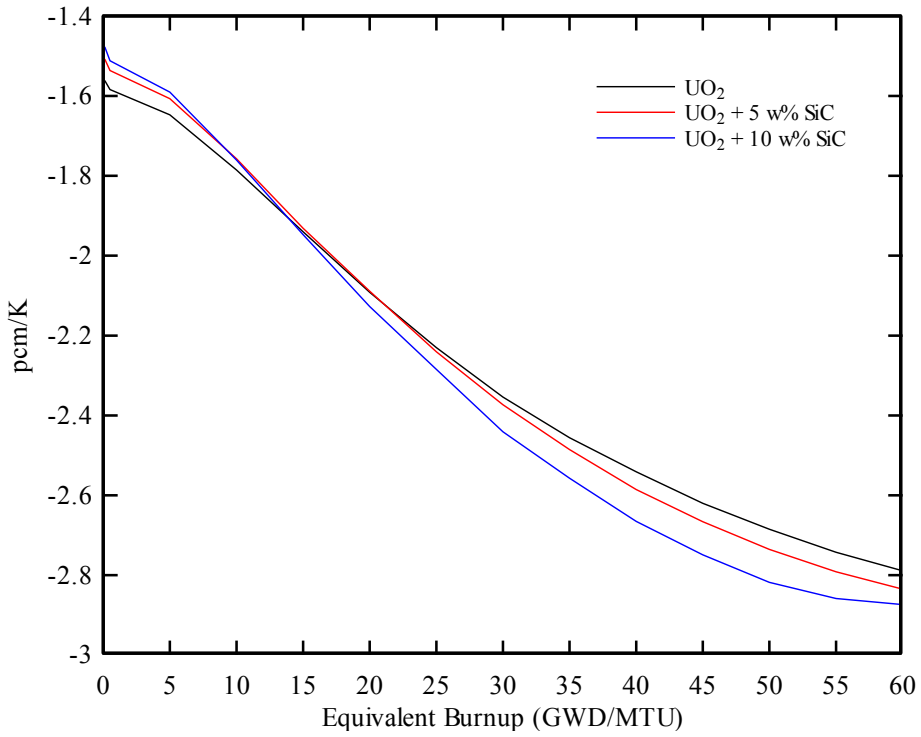

Figure 3-3. Doppler coefficient versus burnup of UO_2 fuel compared to UO_2 with SiC fuel.

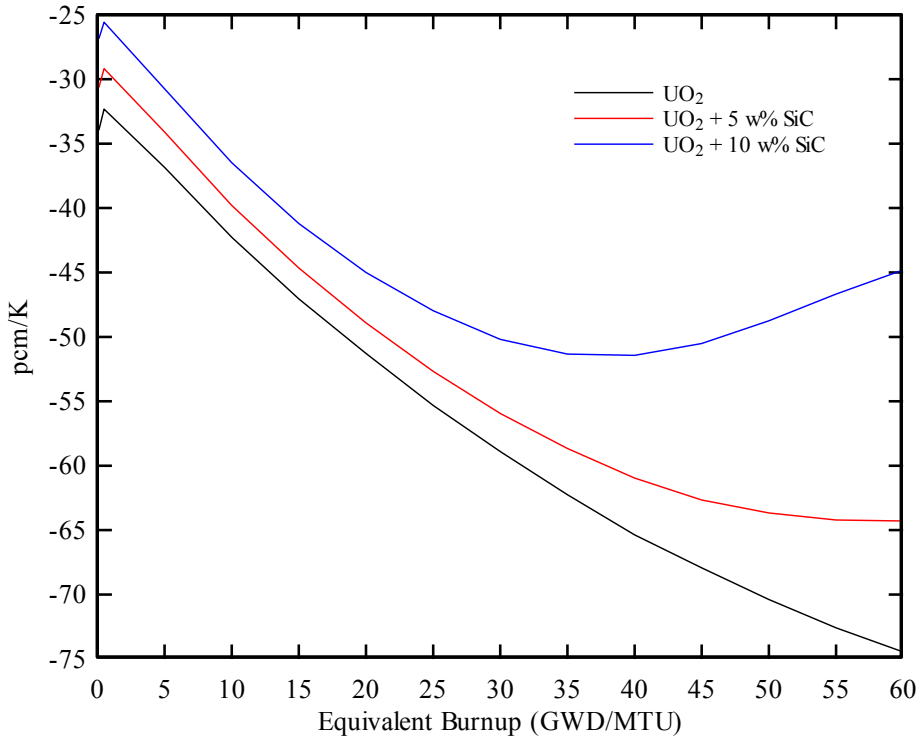

Figure 3-4. Moderator temperature coefficient versus burnup of UO_2 fuel compared to UO_2 with SiC fuel.

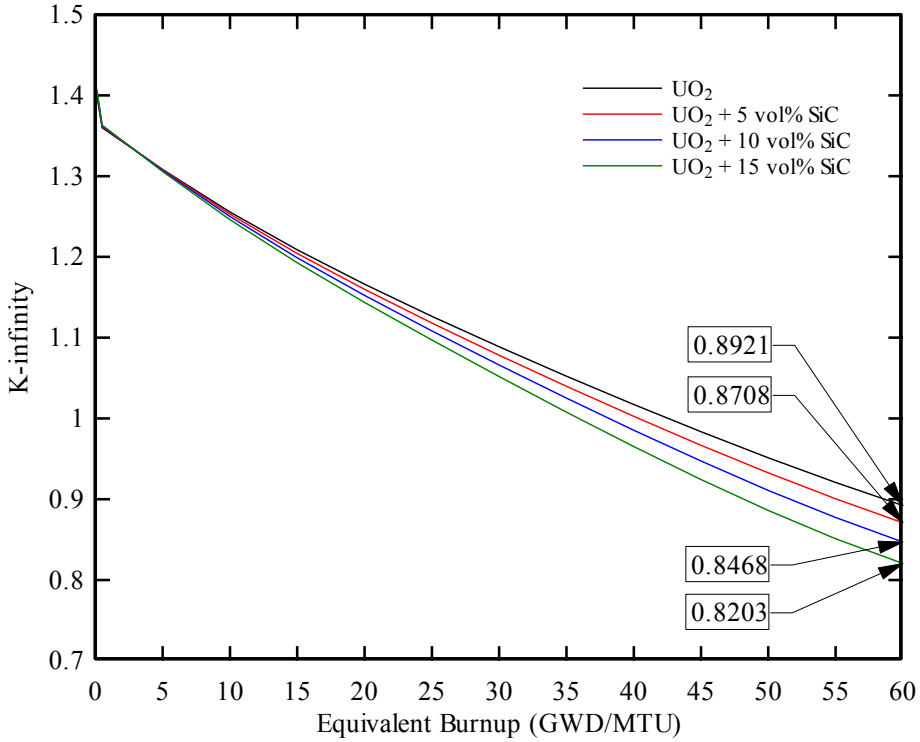

Figure 3-5. K-infinity versus burnup of UO_2 fuel compared to UO_2 with SiC fuel.

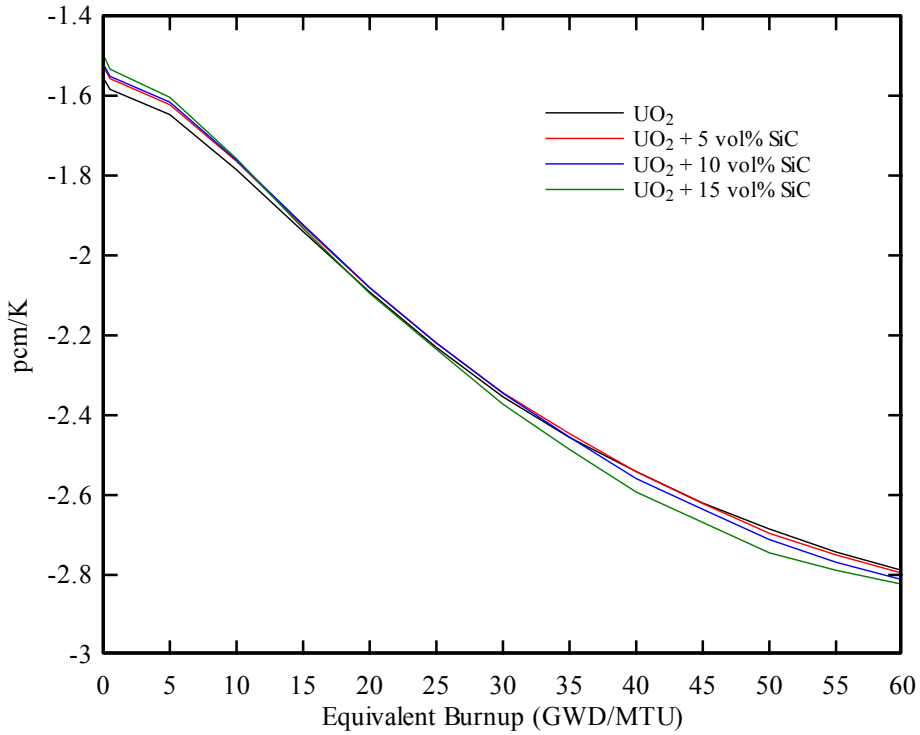

Figure 3-6. Doppler coefficient versus burnup of UO_2 fuel compared to UO_2 with SiC fuel.

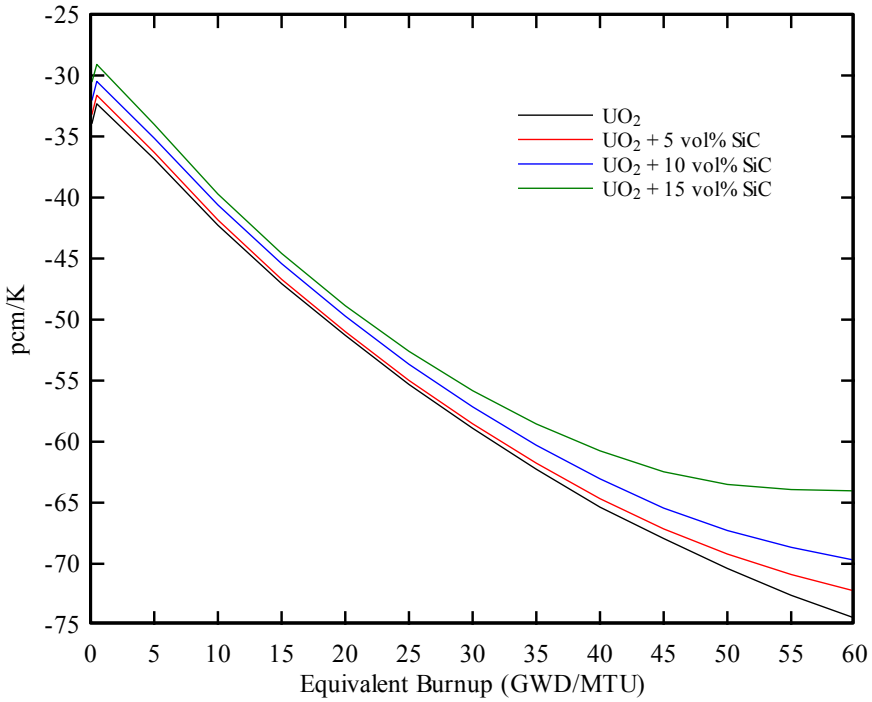

Figure 3-7. Moderator temperature coefficient versus burnup of UO_2 fuel compared to UO_2 with SiC fuel.

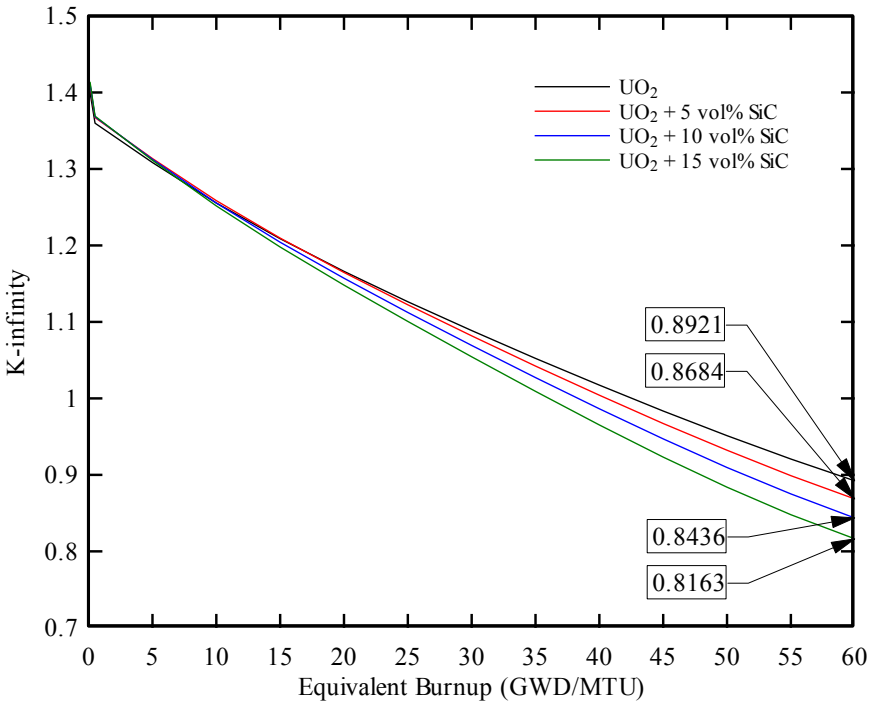

Figure 3-8. K-infinity versus burnup of UO_2 fuel compared to UO_2 with SiC fuel (200 ^{o}C less in fuel temperature).

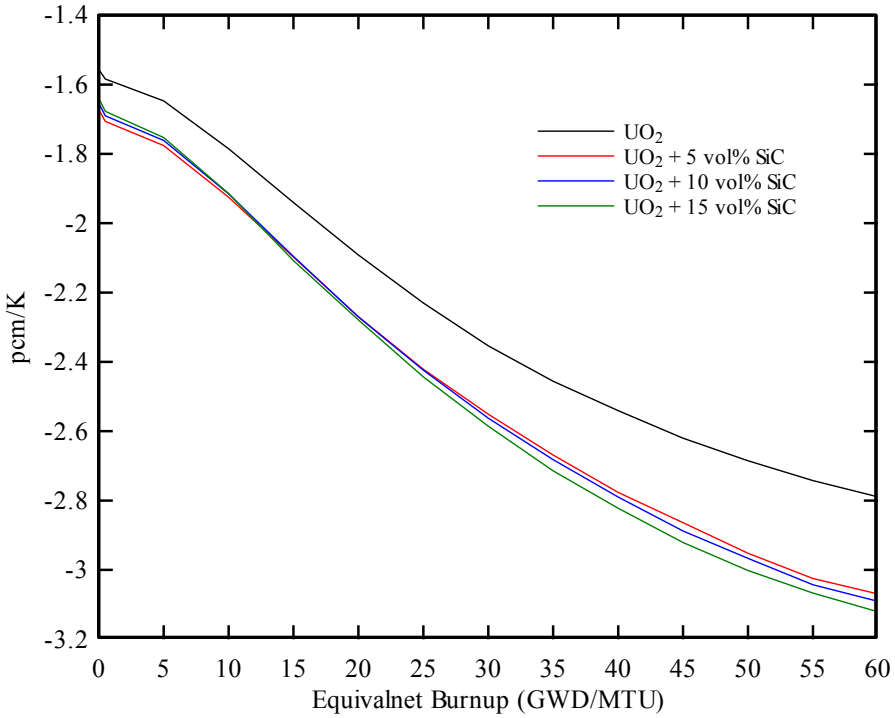

Figure 3-9. Doppler coefficient versus burnup of UO_2 fuel compared to UO_2 with SiC fuel (200 ^{o}C less in fuel temperature).

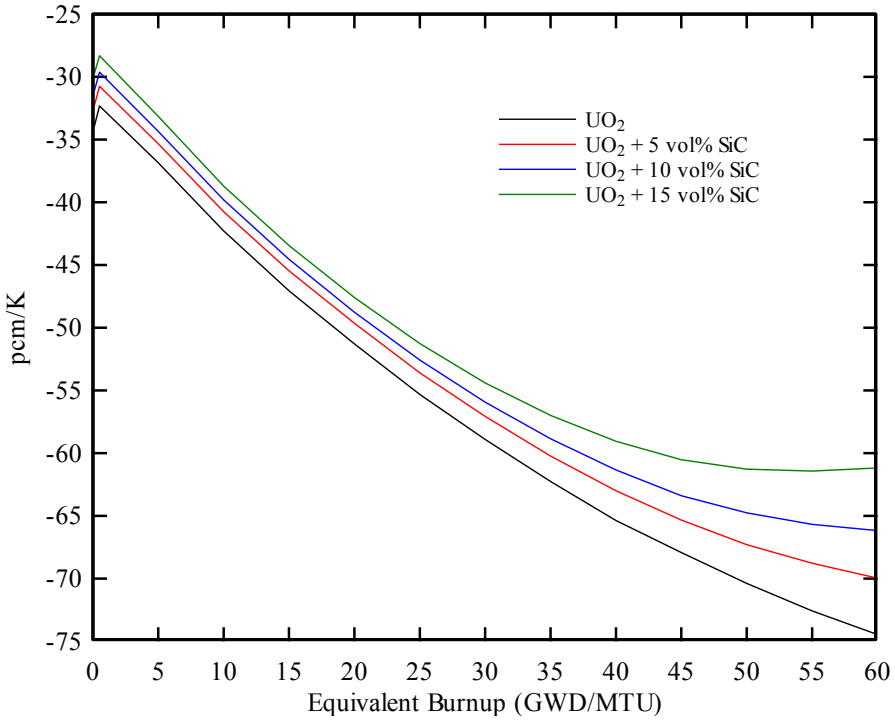

Figure 3-10. Moderator temperature coefficient versus burnup of UO_2 fuel compared to UO_2 with SiC fuel (200 ^{o}C less in fuel temperature).

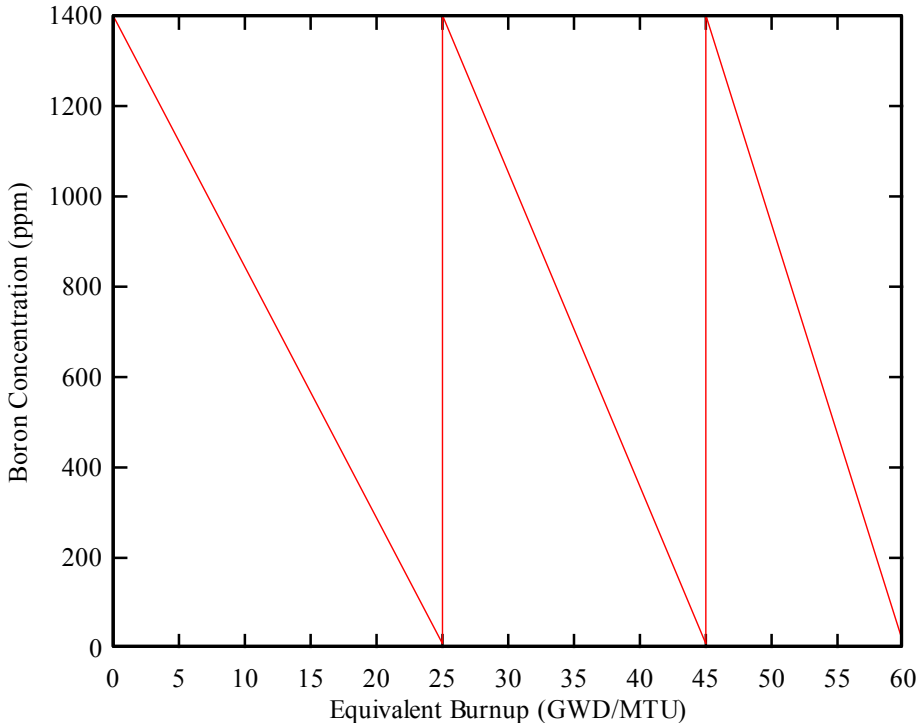

Figure 3-11. Boron concentration versus burnup at boron let-down.

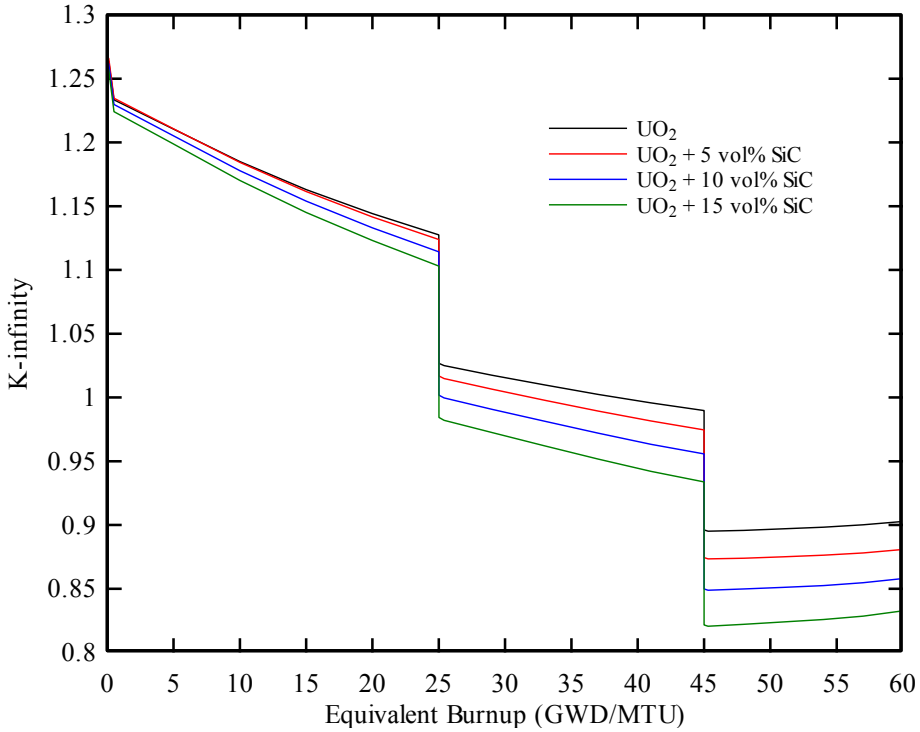

Figure 3-12. K-infinity versus burnup of UO_2 fuel compared to UO_2 with SiC fuel (200 ^oC less in fuel temperature) at boron let-down.

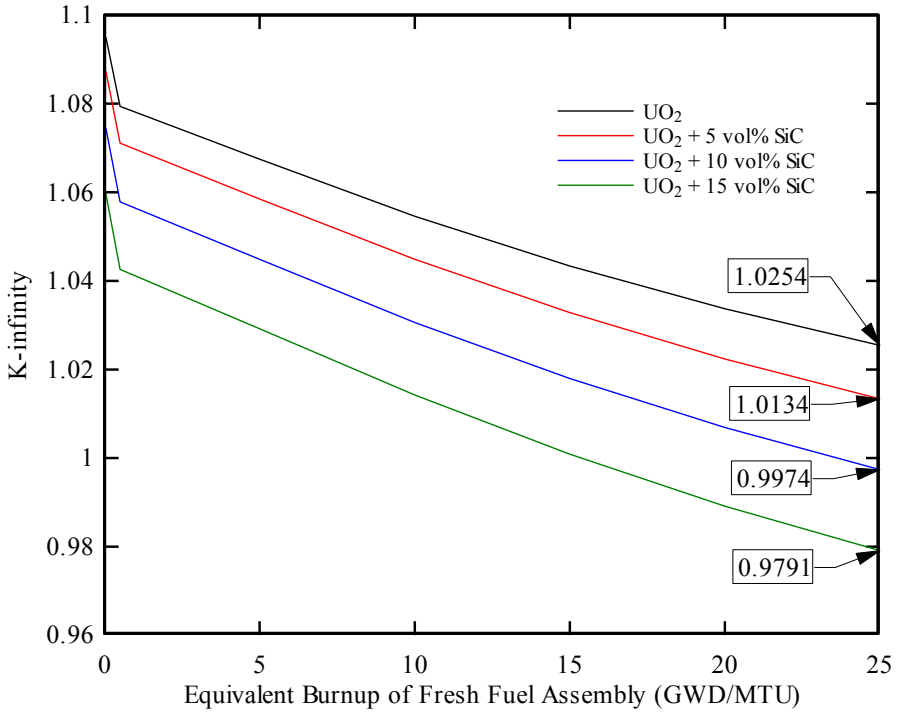

Figure 3-13. K-infinity versus burnup of UO_2 core compared to UO_2 with SiC core (200 ^oC less in fuel temperature) at boron let-down.

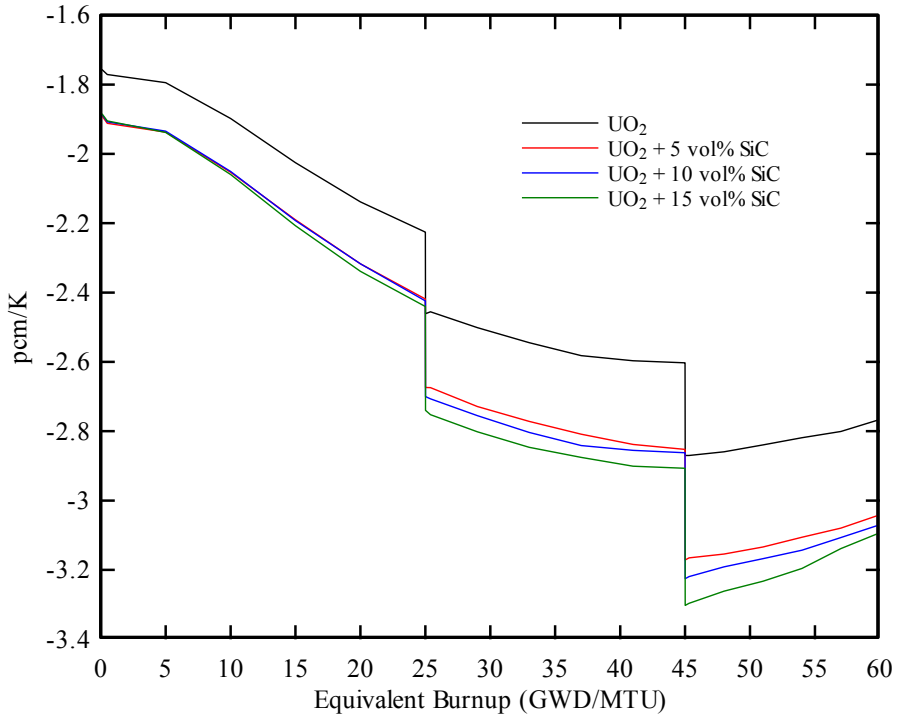

Figure 3-14. Doppler coefficient (pcm/K) versus burnup of UO_2 fuel compared to UO_2 with SiC fuel (200 ^oC less in fuel temperature) at boron let-down.

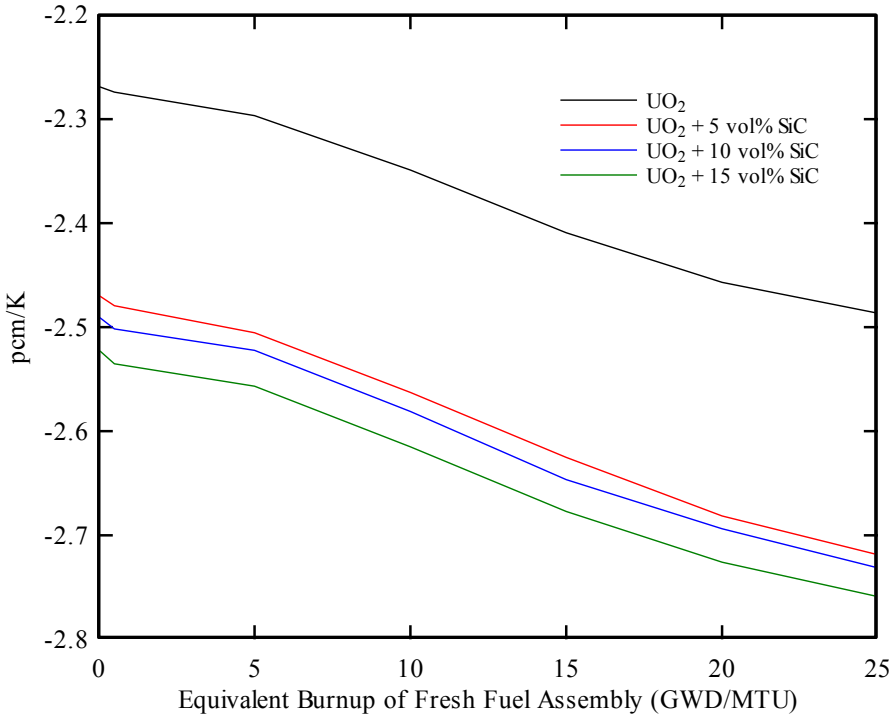

Figure 3-15. Doppler coefficient (pcm/K) versus burnup of UO_2 core compared to UO_2 with SiC core (200 ^oC less in fuel temperature) at boron let-down.

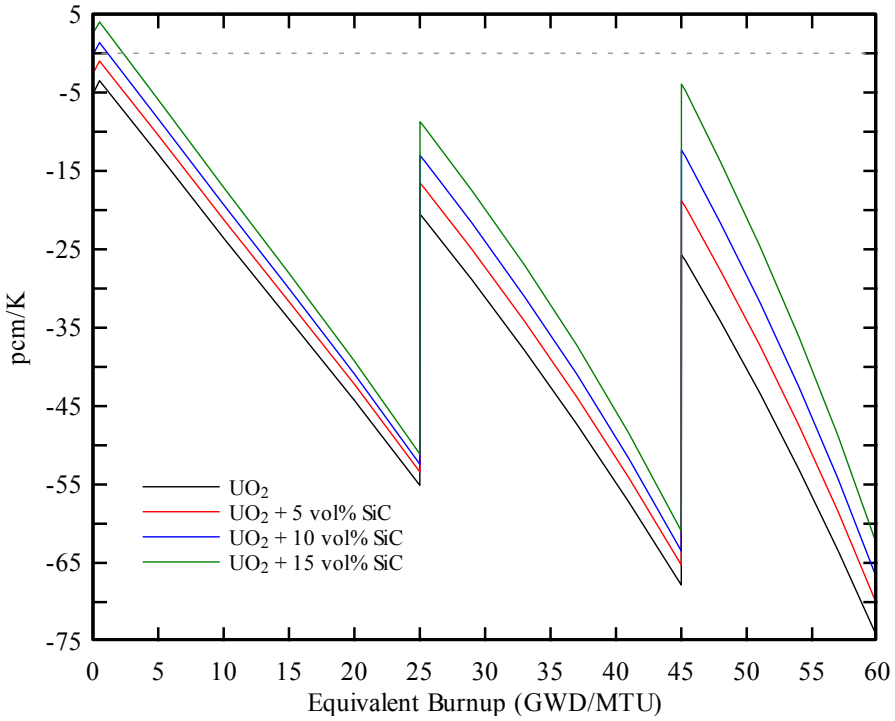

Figure 3-16. Moderator temperature coefficient (pcm/K) versus burnup of UO_2 fuel compared to UO_2 with SiC fuel (200 ^oC less in fuel temperature) at boron let-down.

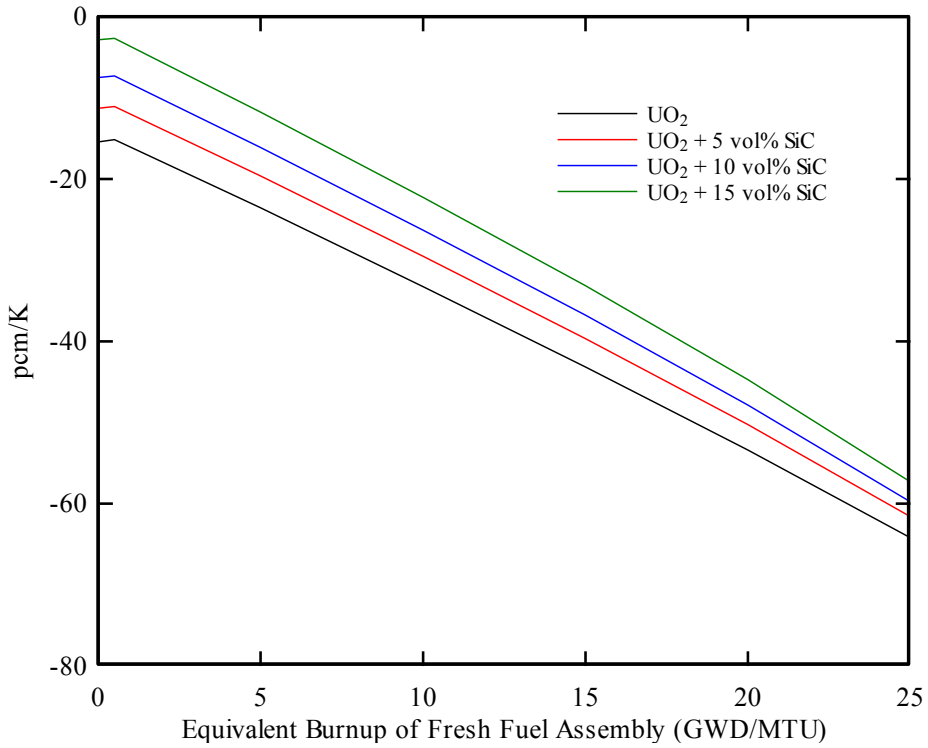

Figure 3-17. Moderator temperature coefficient (pcm/K) versus burnup of UO_2 core compared to UO_2 with SiC core (200 ^{o}C less in fuel temperature) at boron let-down.

CHAPTER 4
REACTION BETWEEN URAINIUM OXIDE AND SILICON CARBIDE

Background

There are very few papers about the reaction between uranium dioxide (UO_2) and silicon carbide (SiC). G. C Allen et al. [12] have reported that UO_2 reacts with SiC at a measurable rate above 1377 ^oC. The reactions were described as Equation 4-1 to Equation 4-5.

$$UO_2 + 2SiC \leftrightarrow USi_2 + 2CO \quad (4\text{-}1)$$

$$UO_2 + 2SiC \leftrightarrow UC_2 + 2SiO \quad (4\text{-}2)$$

$$USi_2 \leftrightarrow USi_{1.67} + 0.33Si \quad (4\text{-}3)$$

$$5Si + 3UC_2 \leftrightarrow U_3C_3Si_2 + 3SiC \quad (4\text{-}4)$$

$$UO_2 + 3UC_2 \leftrightarrow 4UC + 2CO \quad (4\text{-}5)$$

W. Lippmann et al. [36] have confirmed the reaction between UO_2 and SiC at the temperature above 1700 ^oC in a system where gaseous products were free to escape. However, they also found that there was no reaction up to 1800 ^oC in a system where gaseous products were sealed. Solomon et al. [10] also observed reactions between UO_2 and SiC at 1400 ^oC after fifteen hours.

Experiments and Results

UO_2 and SiC powder were sintered together at 1300 ^oC and 1650 ^oC to verify the literature result. Before the sintering process, the uranium oxide powder from Framatome/Areva was characterized for its oxygen to uranium ratio and particle size distribution.

Oxygen to Uranium Ratio of Uranium Oxide Powder

The powder was oxidized to U_3O_8 and the weight difference was measured to determine the O/U ratio of the uranium oxide powder from Framatome/Areva. The powder was oxidized in air at 350 ^oC for 24 hours. The weight change indicated the O/U ratio of received uranium oxide

powder was 2.10. The generated U_3O_8 was reduced to $UO_{2.0}$ in argon and 5% hydrogen environment at 900 ^oC for 4 hours. The received uranium oxide powder was oxidized in air at 140 ^oC for 24 hours. The O/U ratio calculated by weight difference was 2.27.

Figure 4-1 shows the uranium oxide powder with different O/U ratio. The received $UO_{2.10}$ powder was dark brown; the $UO_{2.27}$ was black; the U_3O_8 powder was dark green; and the $UO_{2.0}$ powder was orange. The X-ray diffraction (XRD) results of the four uranium oxide powders are shown in Figure 4-2 to Figure 4-5. The XRD peaks of $UO_{2.10}$ and $UO_{2.27}$ were close to the peaks of $UO_{2.0}$, the extra oxygen in $UO_{2.10}$ and $UO_{2.27}$ slightly broadens and offsets the peaks of $UO_{2.0}$. The XRD peaks of U_3O_8 were totally different from the peaks of $UO_{2.0}$ because the crystal structures were different.

Particle Size Distribution of Uranium Oxide Powder

The particle size of received $UO_{2.10}$ powder was characterized by sieve analysis. Ten gram $UO_{2.10}$ powder was sieved through a series of screens with standardized mesh size. The sieve was shaken for half an hour on an Octagon digital sieve shaker. The sieve and shaker are shown in Figure 4-6. The powder between two screens was weighed and recorded in Table 4-1. The experiments were repeated for three times. The average value was plotted in Figure 4-7. There was about a 4% powder loss in the sieving process.

Sintering UO_2 and SiC at 1300 ^oC and 1650 ^oC

The received uranium oxide powder was ball milled with the β-SiC powders (30 nm in particle size, from Alfa Aesar) for half an hour. The weight ratio of SiC to UO_2 is one. Figure 4-8 shows the X-ray diffraction (XRD) pattern of the 30 nm β-SiC. The mixture powders were cold pressed at 200MPa, then sintered at 1300 ^oC in argon atmosphere. The pellet after sintering is shown in Figure 4-9. The X-ray diffraction result (Figure 4-10) showed no new peaks at 1300 ^oC.

When the sintering temperature was increased to 1650 ^{o}C, the X-ray diffraction result (Figure 4-12) showed that $USi_{1.88}$ was formed. The pellet after sintering is shown in Figure 4-11.

Discussion

The experiment result was different from Allen's result [12] because the ratio of SiC to UO_2 used by Allen et al. was 2.5. Uranium dioxide pellets are usually produced by sintering the green pellets at about 1700 ^{o}C in hydrogen atmosphere. High temperature around 1700 ^{o}C is necessary to achieve the required high density of over 95% of theoretical. The reaction between UO_2 and SiC at 1377 ^{o}C has to be avoided to successfully incorporate SiC into UO_2.

Table 4-1. Particle size distribution of received uranium oxide powder.

Particle Size (μm)	Weight (g)	Weight (g)	Weight (g)	Average (g)
<25	0.6767	0.5633	0.6769	0.6390
>25 and < 45	1.9094	1.9317	1.9308	1.9240
>45 and <53	1.0295	1.1097	1.0454	1.0615
>53 and <63	0.8636	0.8886	0.9009	0.8844
>63 and <90	2.4028	2.4171	2.3799	2.3999
>90 and <150	1.4126	1.4529	1.4846	1.4500
>150 and <250	0.4147	0.4447	0.4161	0.4252
>250	0.8482	0.8681	0.8153	0.8439

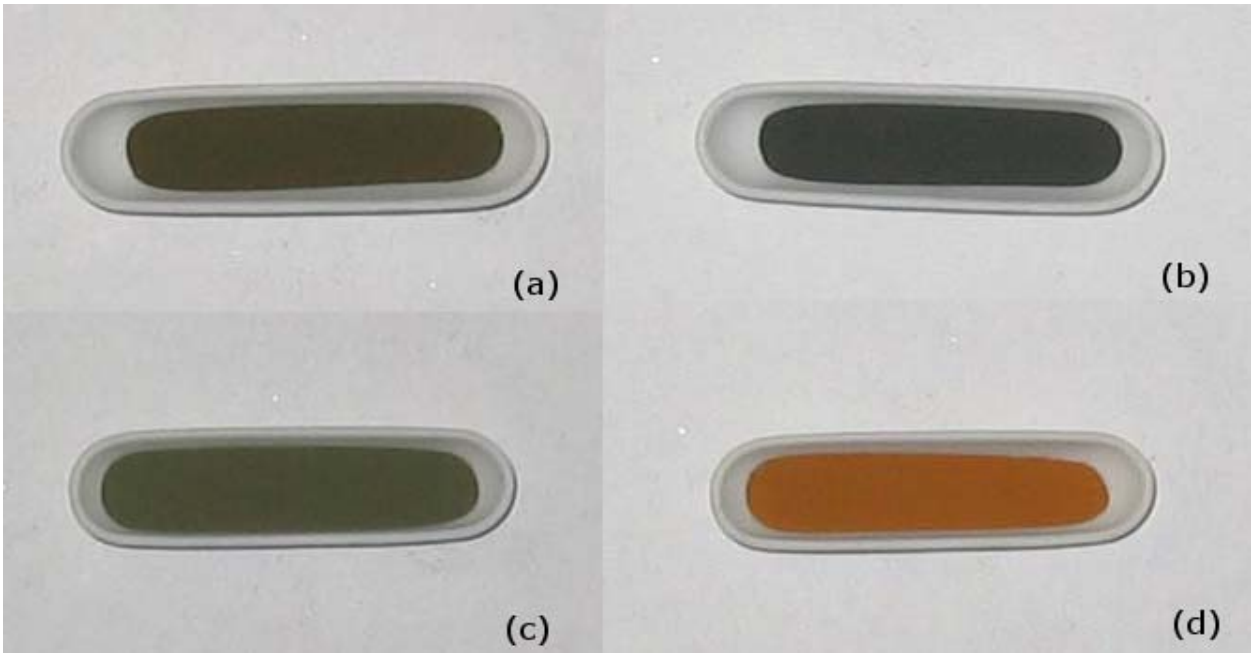

Figure 4-1. Uranium oxide powders with different O/U ratio. A) $UO_2.10$. B) $UO_{2.27}$. C) U_3O_8. D) UO_2.

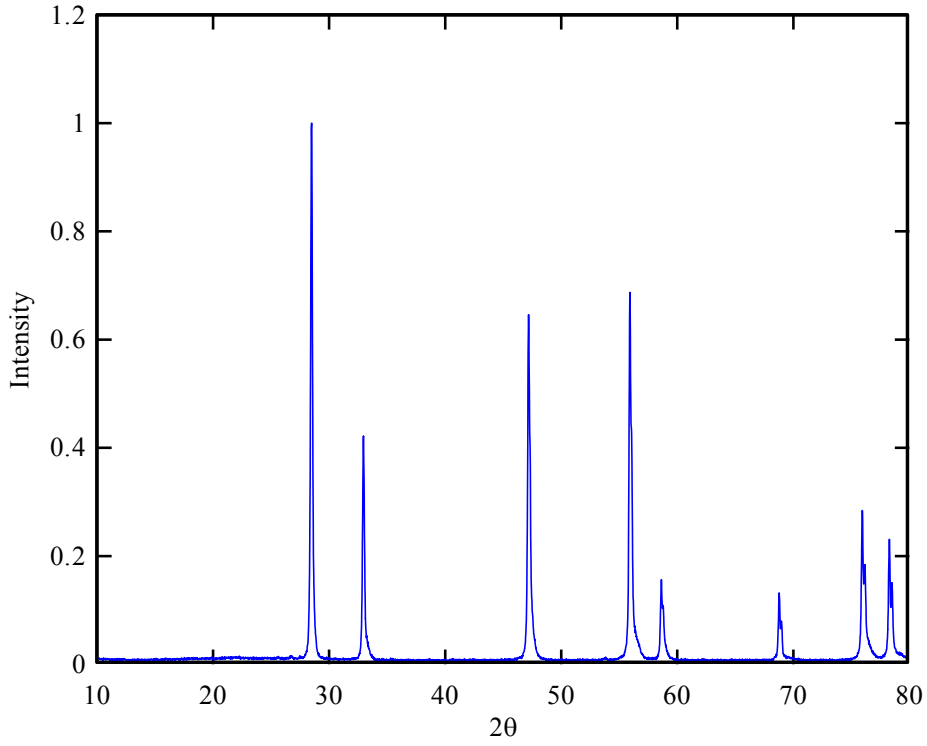

Figure 4-2. X-ray diffraction pattern of $UO_{2.10}$ powder.

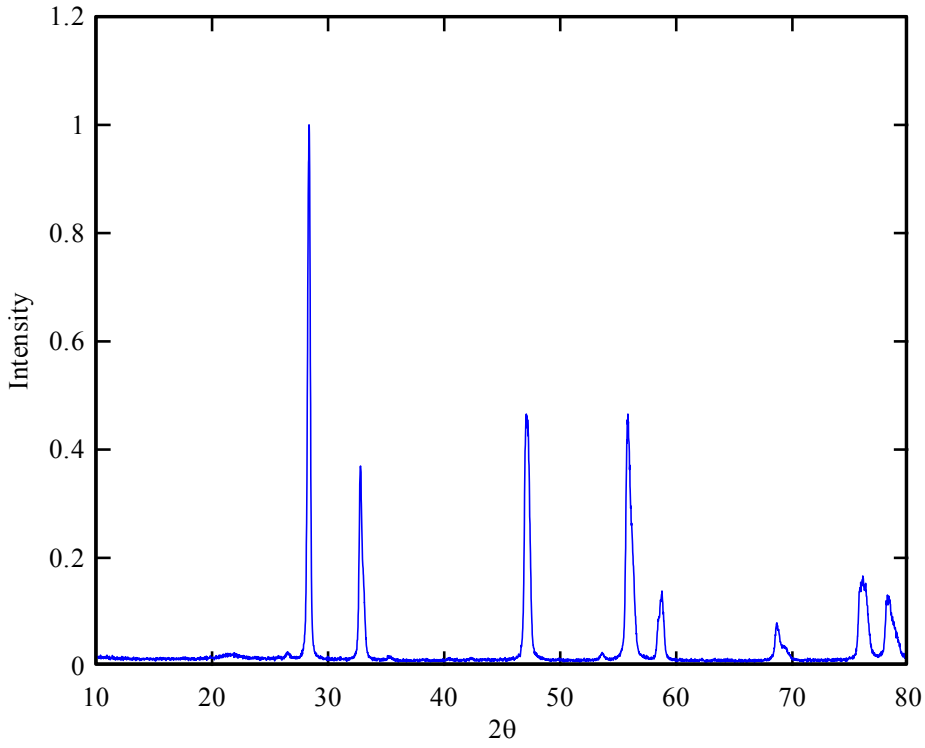

Figure 4-3. X-ray diffraction pattern of $UO_{2.27}$ powder.

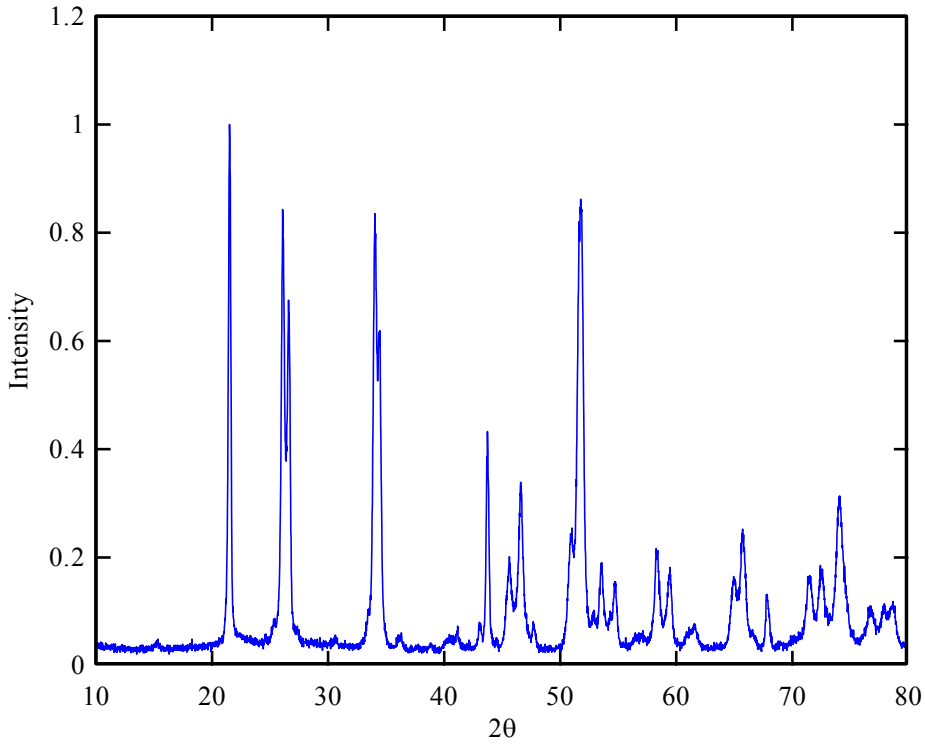

Figure 4-4. X-ray diffraction pattern of U_3O_8 powder.

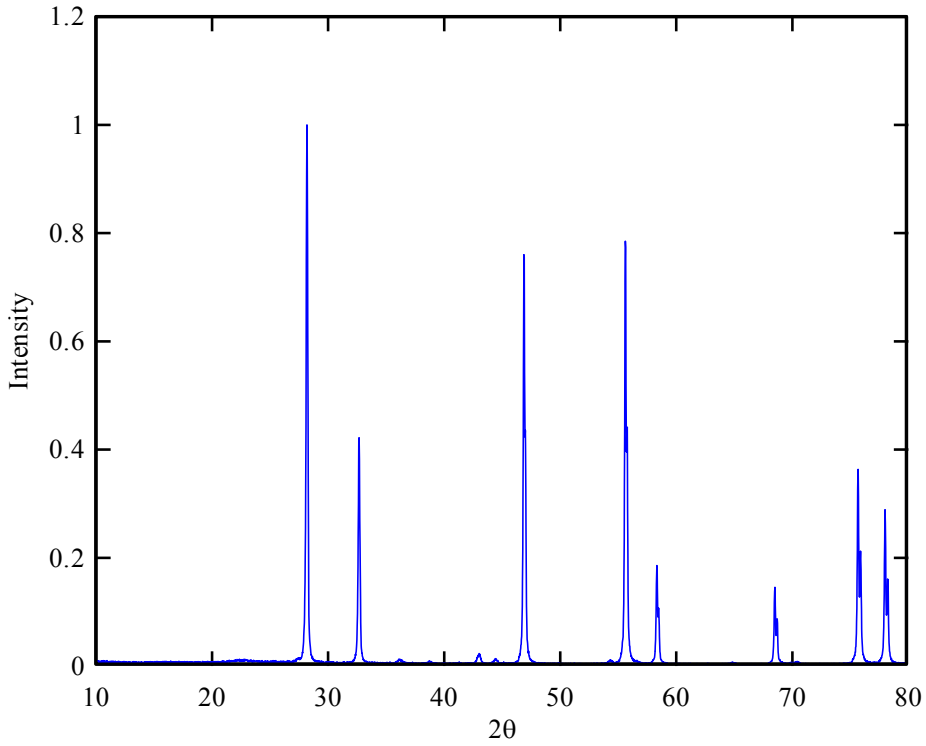

Figure 4-5. X-ray diffraction pattern of $UO_{2.0}$ powder.

Figure 4-6. Sieve and shaker for analyzing particle size distribution.

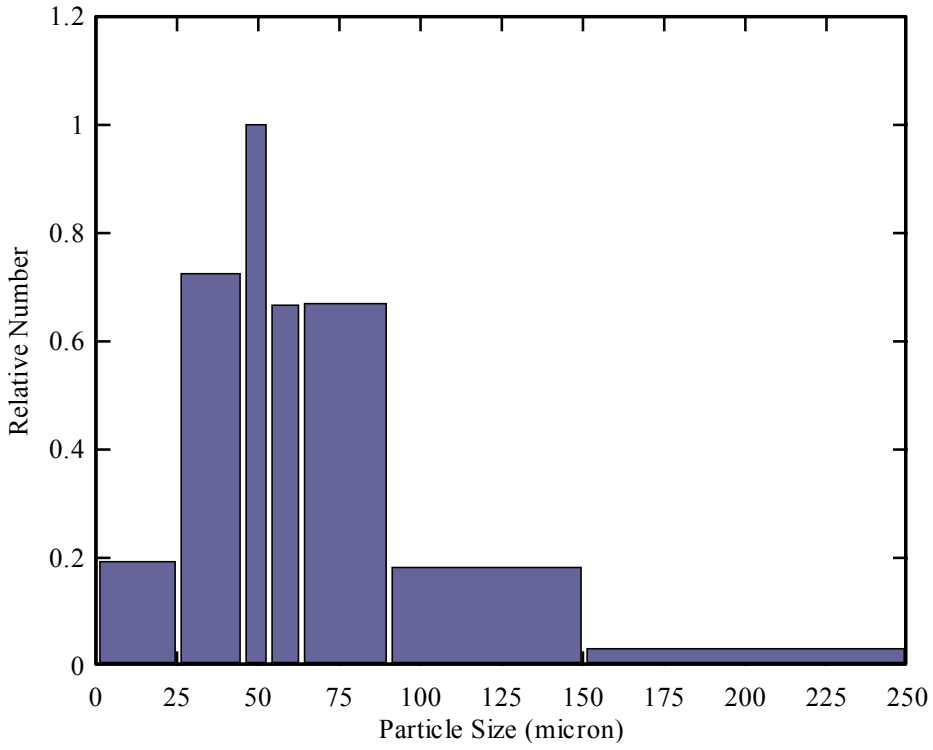

Figure 4-7. Particle size distribution of received uranium oxide powder.

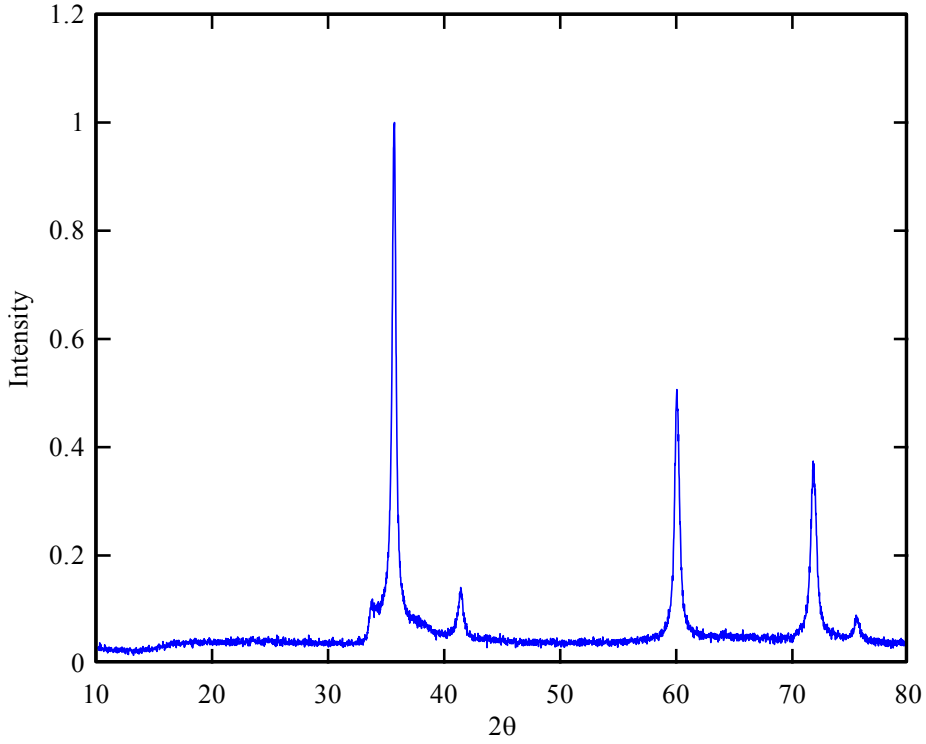

Figure 4-8. X-ray diffraction pattern of 30nm β-SiC from Alfa Aesar.

Figure 4-9. Uranium dioxide-silicon carbide pellet after sintering at 1300 °C.

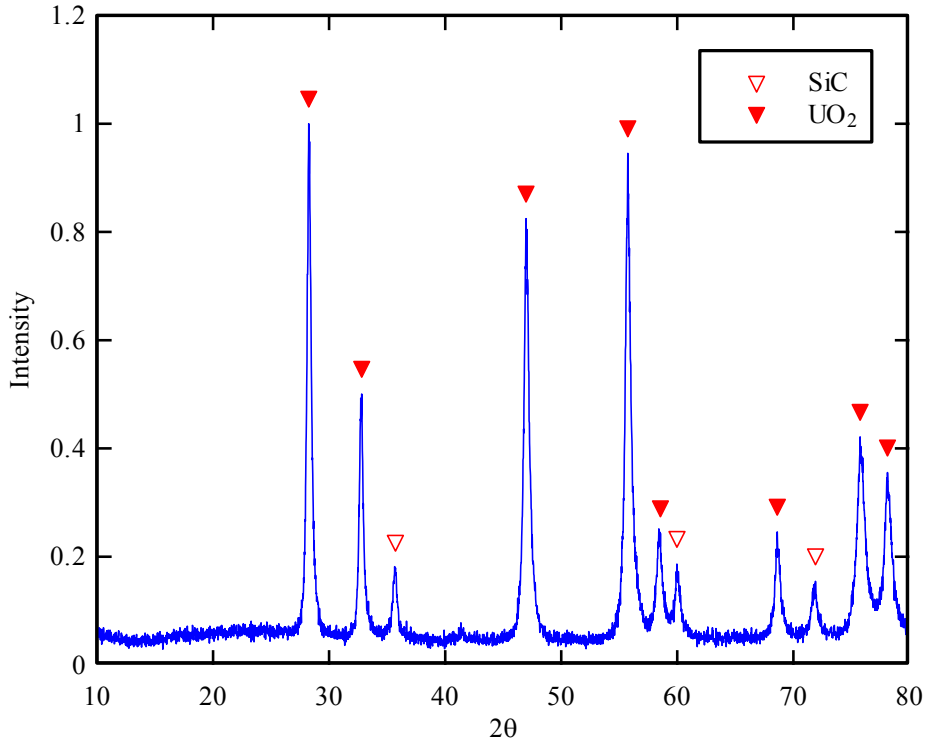

Figure 4-10. X-ray diffraction pattern of UO_2-SiC pellet after sintering at 1300 °C.

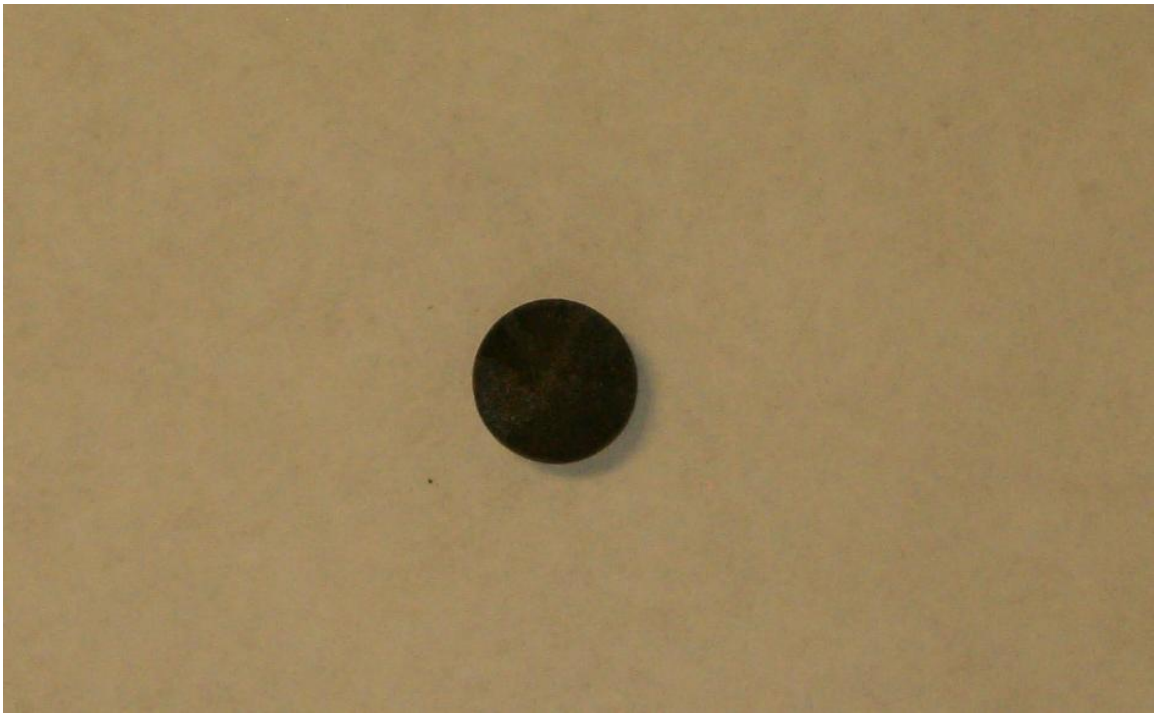

Figure 4-11. Uranium dioxide-silicon caribide pellet after sintering at 1650 °C.

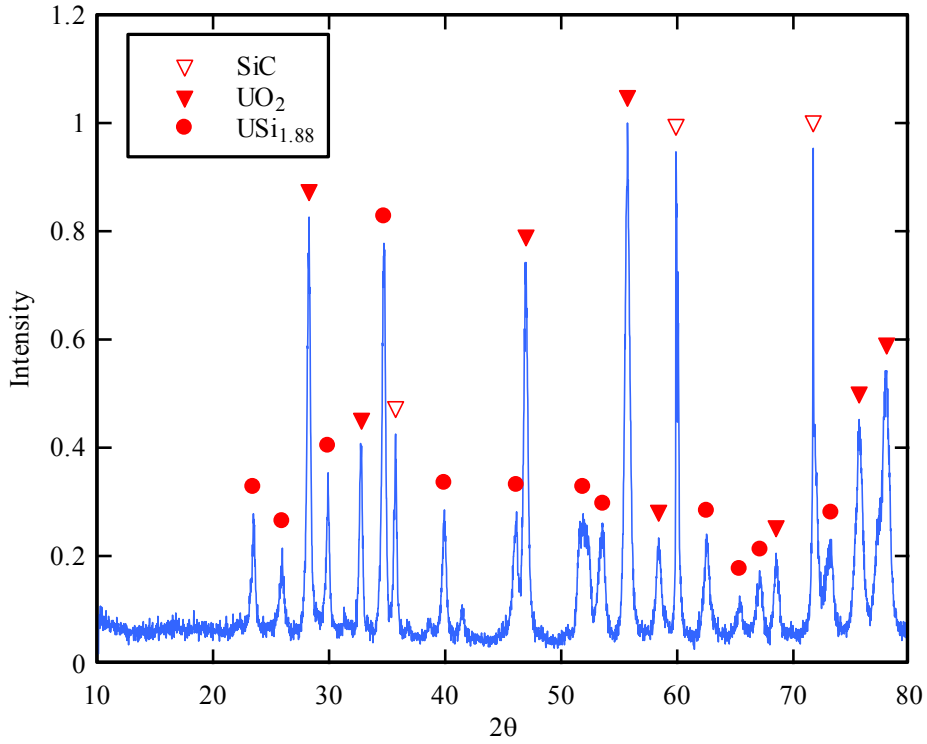

Figure 4-12. X-ray diffraction pattern of UO_2-SiC pellet after sintering at 1650 °C.

CHAPTER 5
LOW TEMPERATURE SINTERING OF URANIUM DIOXIDE

Background

Uranium dioxide (UO_2) pellets are usually produced by sintering the green pellets at about 1700 ^oC in hydrogen atmosphere [13, 14, 37-40]. The high sintering temperature around 1700 ^oC is necessary to achieve the required high density of over 95% of theoretical. However, sintering at a temperature around 1700 ^oC is expensive due to the furnace cost and maintenance cost.

Several studies have shown that UO_2 pellets with high density can be achieved at lower sintering temperature. Fuhrman et al. [13] have reported that UO_2 pellets of 95 to 97% theoretical density (TD) were achieved by sintering at 1200 ^oC in nitrogen for 1 hour followed by 1 hour reduction in hydrogen, while using uranium oxide powder with extra oxygen (O/U ~ 2.37). They also mentioned that UO_2 pellets of 95% TD were achieved at temperatures as low as 1000 ^oC using the same method, though the result was not consistent. Langrod [14] has reported that UO_2 pellets of above 95% TD was achieved by sintering at 1300 ^oC in nitrogen atmosphere for 2 hours followed by reduction in hydrogen, using mixture of UO_2 and U_3O_8 (O/U ~ 2.30). Ayaz et al. [39] have sintered UO_2 pellets of 95% TD at 1150 ^oC in CO_2 and water vapor atmosphere for 4 hour, followed by reduction in Ar+8% H_2 for 1hour, using uranium oxide powder with extra oxygen (O/U = 2.15). Williams et al. [41] have sintered uranium oxide with different O/U ratio in argon, nitrogen, carbon dioxide and vacuum and achieved UO_2 pellets of 94% TD at temperatures lower than 1400 ^oC in various gases.

Excess oxygen was believed to be the key factor to decrease the sintering temperature. Fuhrman et al. [13] indicated that a minimum O/U ratio of 2.25 to 2.28 was required to achieve a density above 95% of theoretical. In the sintering process, the uranium oxide particles undergo solid state diffusion. Based on the theory by Williams et al. [41], the rate of the diffusion of

uranium ions determines the rate of the sintering process. The diffusion of uranium ions in non-stoichiometric uranium oxides is more rapid than in stoichiometric UO_2 because the extra oxygen in non-stoichiometric uranium oxides lowers the lattice binding energies.

The uranium oxide powder was oxidized in air to increase the oxygen to uranium ratio. The rate and degree of oxidation of UO_2 versus temperature studied by Langrod [14] is shown in Figure 5-1. Langrod [14] also found that the sintering behavior of UO_2 powder blended with U_3O_8 was identical with the air oxidized UO_2 powder of the same O/U ratio.

The non-stoichiometric pellets must be further processed to bring the oxygen to uranium ratio back to 2.0 by soaking the pellets in hydrogen environment. Fuhrman et al. [13] reported that 1100 ^oC was required to remove the excess oxygen in a reasonable time.

The study by Fuhrman et al. [13] showed that the grain size of the UO_2 pellet sintered at low temperature is smaller than the grain size of the UO_2 pellet sintered at high temperature. The result was confirmed by Ayaz et al. [39].

Experiments and Results

A UO_2 pellet was first sintered in hydrogen atmosphere at high temperature. The received uranium oxide powder was cold pressed in a 13 mm die at 200 MPa. The green pellet was sintered at 1650 ^oC for 4 hours in hydrogen (balanced with argon) atmosphere. The density of sintered pellet was 96.03% TD, which was measured by the Archimedes method (Archimedes principle). The pellet is shown in Figure 5-2. The grain size of the pellet is in the range of 5 to 20 micron, as shown in the scanning electron microscopy (SEM) image (Figure 5-3).

The received uranium oxide powder was oxidized in air at 140 ^oC for 24 hours to increase the O/M ratio to $UO_{2.27}$. The $UO_{2.27}$ powder was then cold compacted in a 13mm die at 200 MPa pressure. The green pellet was sintered at 1200 ^oC for 1 hour in argon atmosphere, followed by the reduction in Ar+5% H_2 at 1200 ^oC for one hour. The picture of the sintered pellet is shown in

Figure 5-4. The density of the pellet measured by the Archimedes method was 95.71%TD. The SEM image of the pellet is shown in Figure 5-5. The grain size of the pellet is in the range of 5 to 10 micron.

Another UO_2 pellet was sintered at low temperature with pressure. The $UO_{2.27}$ powder was cold compacted in a 13mm die at 200 MPa pressure. The green pellet was then sintered at 1200 ^oC with 10 MPa pressure for 1 hour in argon atmosphere, followed by the reduction in Ar+5% H_2 at 1200 ^oC for one hour. (The detailed experiment apparatus of sintering process with pressure will be explained in chapter 8.) The picture of the sintered pellet is shown in Figure 5-6. The density of the pellet measured by the Archimedes method was 97.99%TD. The SEM image of the pellet is shown in Figure 5-7. The grain size of the pellet is in the range of 5 to 10 micron, but larger than the grain size of the UO_2 pellet sintered at low temperature without pressure.

Discussion

Uranium dioxide fuel pellets with high density (>95%TD) can be achieved at 1200 ^oC, which is lower than the temperature at which the reaction between UO_2 and SiC occurs. So the low temperature sintering method can be used to avoid the reaction between UO_2 and SiC.

The density of the UO_2 pellet sintered at 1200 ^oC is less than the density of the UO_2 pellet sintered at 1650 ^oC; the density of the UO_2 pellet sintered at 1200 ^oC with pressure is larger than the density of the UO_2 pellet sintered at 1650 ^oC. The grain size of the UO_2 pellet sintered at low temperature is smaller than the grain size of the UO_2 pellet sintered at 1650 ^oC. The pressure applied during the sintering process increased the grain size. The grain size was still smaller than the grain size of the UO_2 pellet sintered at 1650 ^oC. A larger grain size is desired to lower the amount of fission gas release because the fission gas has to diffuse longer distance to the grain boundary.

The rate of fission gas release is related to the fuel temperature. The SiC additives are expected to increase the thermal conductivity and lower the fuel temperature, thus lower the fission gas release and offset the negative effect of smaller grain of UO_2 pellet sintered at low temperature.

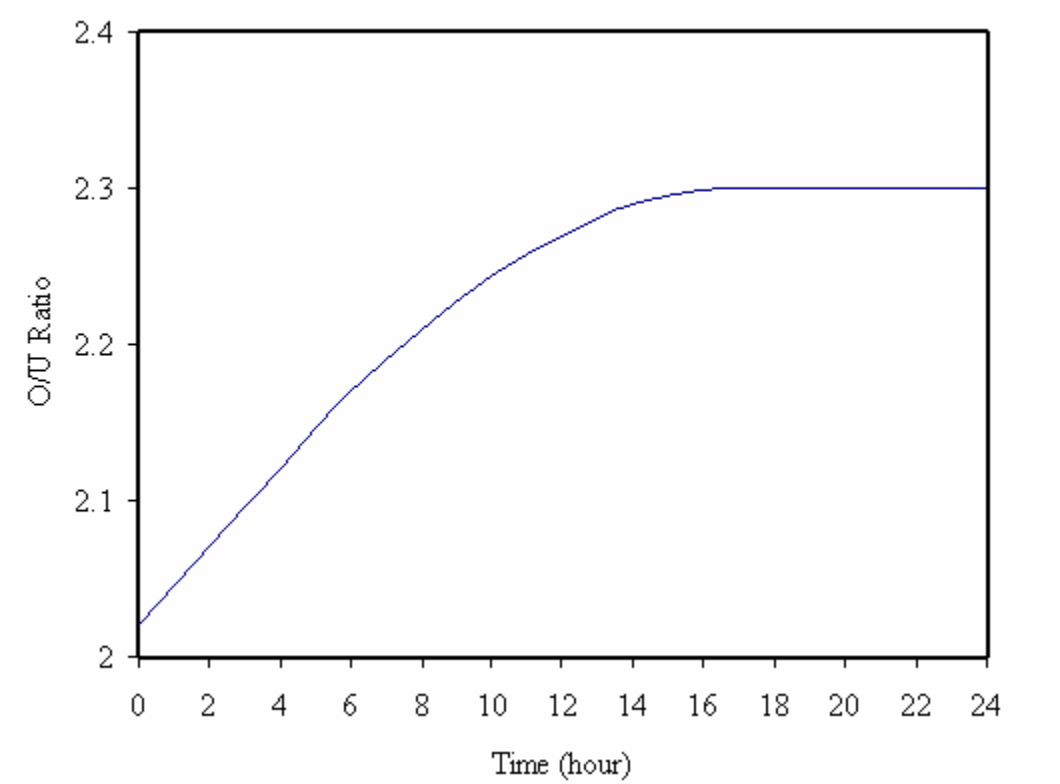

Figure 5-1. Oxygen to uranium ratio of UO_2 powder oxidized in air at 140 ^{o}C [14].

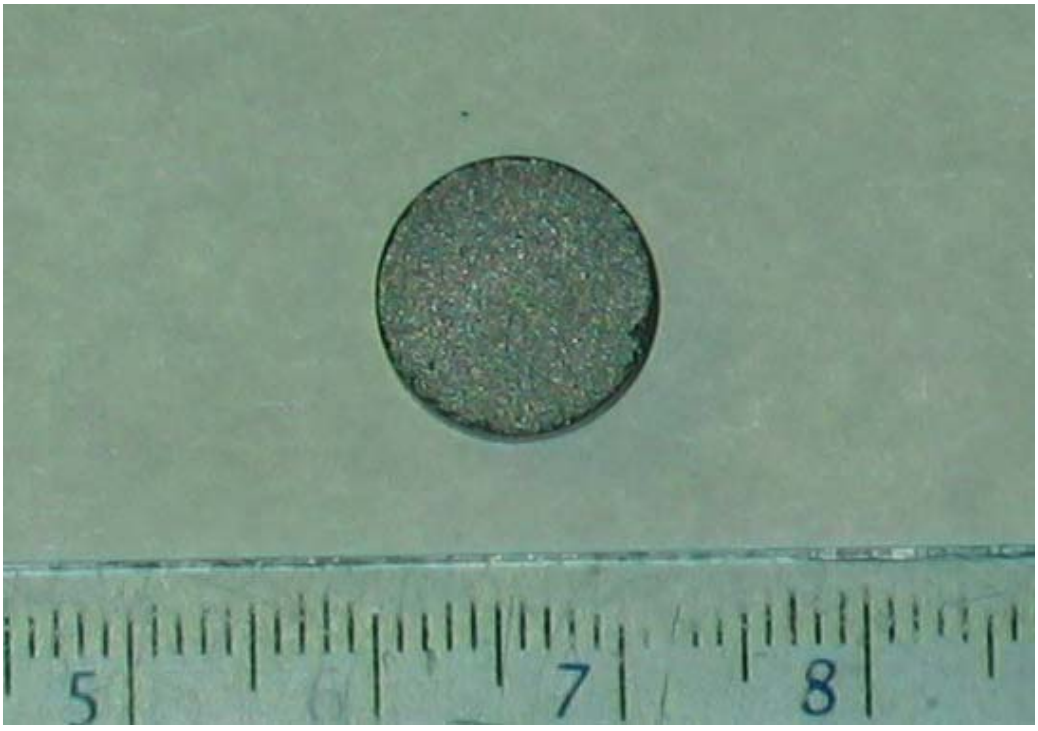

Figure 5-2. Uranium dioxide pellet sintered at 1650 ^{o}C.

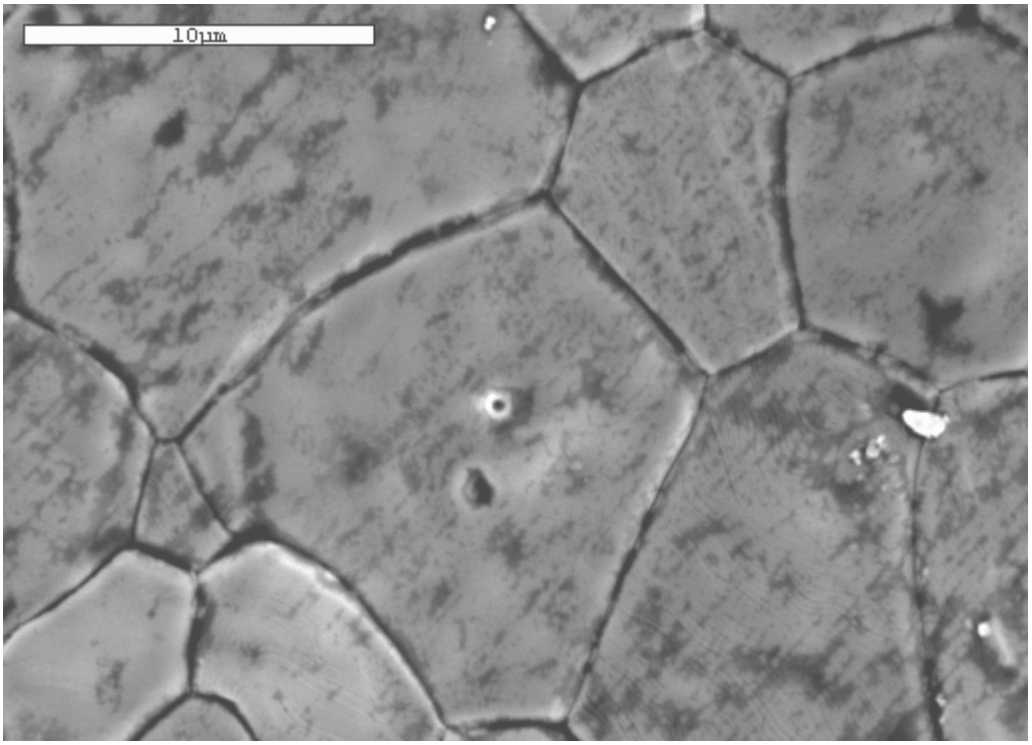

Figure 5-3. Scanning electron microscopy image of UO_2 pellet sintered at 1650 ^{o}C (5,000X).

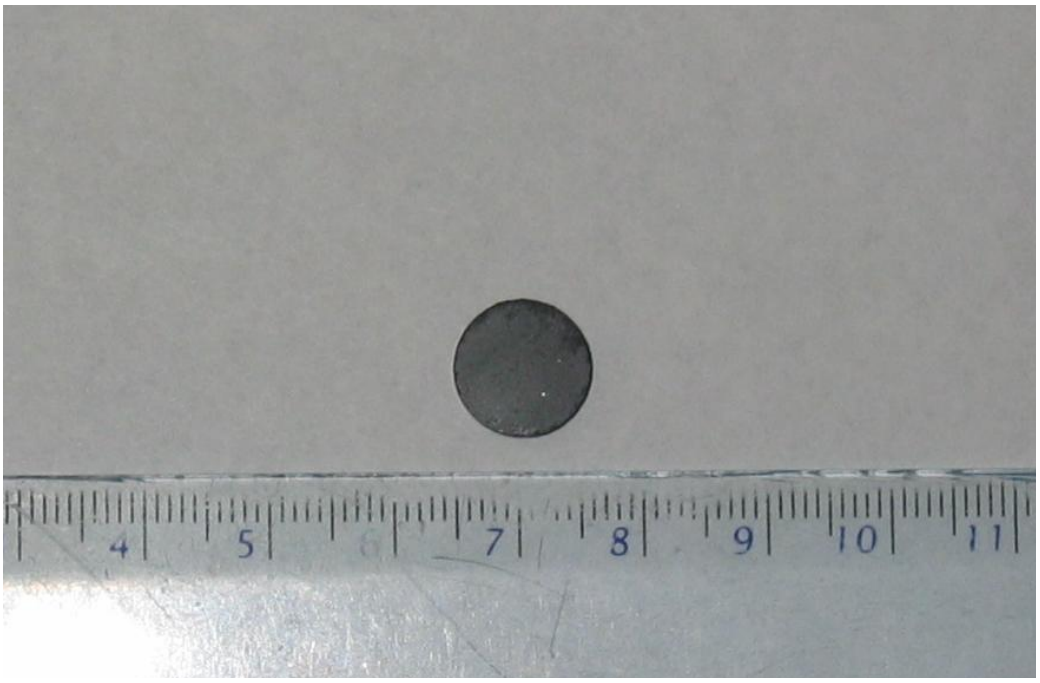

Figure 5-4. Uranium dioxide pellet sintered at 1200 ^{o}C.

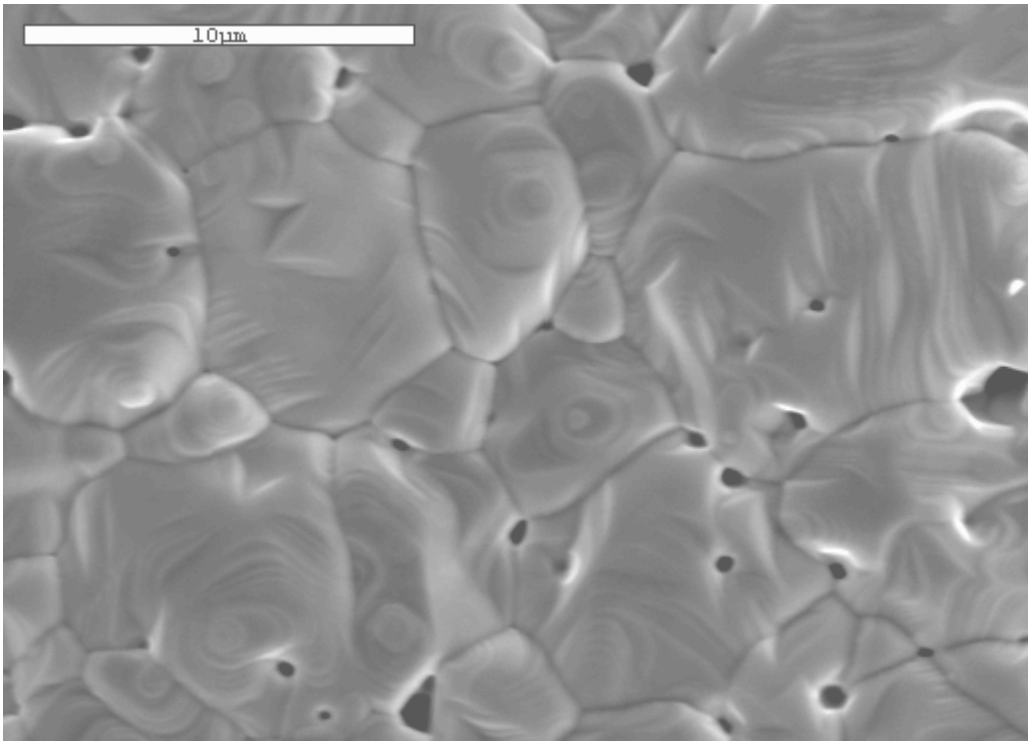

Figure 5-5. Scanning electron microscopy image of UO_2 pellet sintered at 1200 ^{o}C (5,000X).

Figure 5-6. Uranium dioxide pellet sintered at 1200 ^{o}C with pressure.

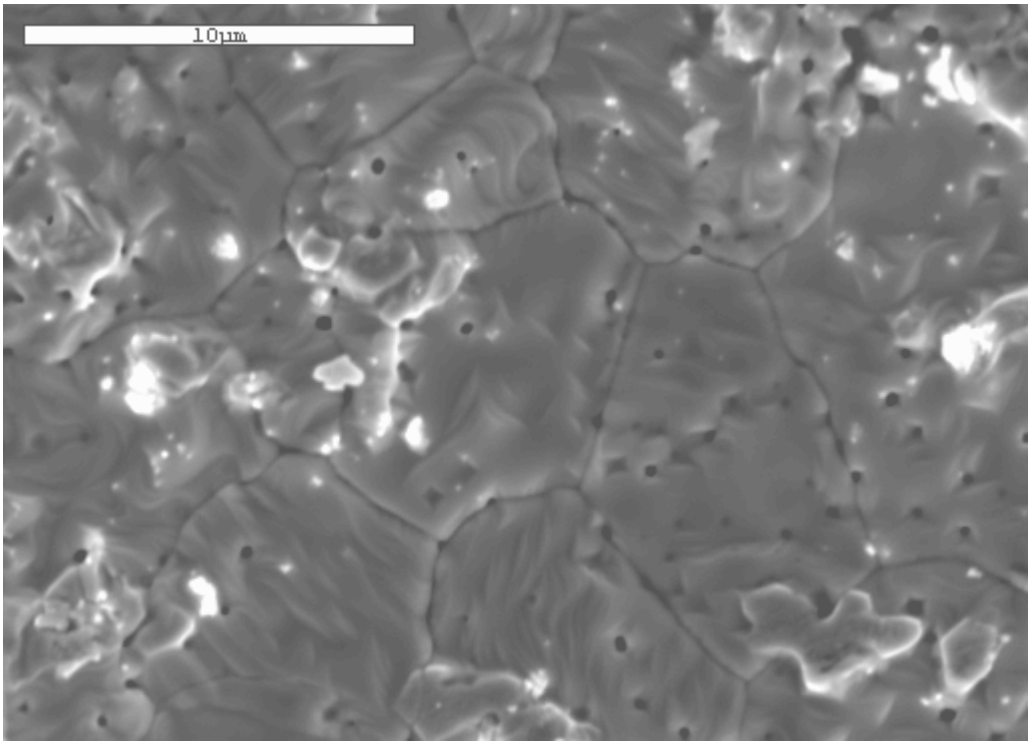

Figure 5-7. Scanning electron microscopy image of UO_2 pellet sintered at 1200 ^{o}C with pressure (5,000X).

CHAPTER 6
SILICON CARBIDE COATING BY CHEMICAL VAPOR DEPOSITION

Background

The chemical vapor deposition (CVD) is a chemical process to produce high purity solid materials by dissociation and /or chemical reactions of gaseous reactants (precursors) in an active (heat, light, plasma etc) environment. The CVD process has the advantage of producing highly dense and pure materials at relative low processing temperature. For example, SiC can be produced below 1400 ^{o}C [42-47], much lower than the melting point. There are several variants of CVD methods, which are initiated using different energy sources, such as plasma enhanced CVD (PECVD) [48], photo-assisted CVD (PACVD) [49] and microwave CVD [50]. Though the use of variant energy sources may requires sophisticated system and increase the cost of the process, the cost for conventional CVD technique is reasonable [51].

The CVD process has been used to deposit a SiC layer in tristructral isotropic (TRISO) fuel particles in a fluidized bed. In general, argon-hydrogen carrier gas is bubbled through a liquid precursor, and then passed through a fluidized bed of carbon coated fuel particles maintained at 1000 to 1800 ^{o}C. [52]. Methyltrichlorosilane (CH_4SiCl_3 or MTS) was usually used as the precursor because it contains the same number of silicon and carbon. The deposition rate and microstructure of SiC were determined by the deposition temperature, MTS flow rate and argon to hydrogen ratio.

Based on the study by Gulden [52], the deposition rate of SiC is independent of temperature and only depends on the flow rate of MTS. The microstructure of SiC is strongly dependent on temperature. A relative low dense laminar structure of SiC was formed at the temperature between 1200 ^{o}C to 1400 ^{o}C and almost full dense columnar structure of SiC was formed at the temperature above 1400 ^{o}C. However, by adjustment of argon to hydrogen ratio,

theoretical dense SiC can be deposited at the temperature between 1200 to 1400 ^{o}C [53]. The crystalline size of SiC increases with increasing temperature and decreases with increasing argon to hydrogen ratio. The study by Ford et al. [53] showed that the crystalline size of SiC was 0.25 micron at 1700 ^{o}C, using only hydrogen and 0.03 micron at 1300 ^{o}C, using an argon-hydrogen mixture.

The CVD process has also been used to produce SiC electronic devices in semiconductor industry. Steckl et al. [42] have successfully investigated the growth of β-SiC on silicon substrate using silacyclobutane ($C_3H_6SiH_2$ or SCB) at the temperatures as low as 800 ^{o}C in a low pressure CVD system. Lin et al. [43] have successfully deposited SiC film on sapphire substrate using trimethylsilane (C_3H_9SiH or TMS) at 1100 ^{o}C in a low pressure CVD system. Kunstmann et al. [44] have reported the growth of β-SiC films using MTS at 1200 ^{o}C. Madapura et al. [45] have reported the growth of β-SiC using TMS at the temperature between 1100 to 1200 ^{o}C.

Silicon carbide can also be produced by CVD process using separate precursors. Yagi et al. [46] have used SiH_2Cl_2 and C_2H_2 to grow SiC on silicon substrate at 1020 ^{o}C in a low pressure CVD system. Powell et al. [47] have used SiH_4 and propane to grow SiC on silicon substrate at 1360 ^{o}C. The ratio of the gaseous precursors has to be chosen carefully to ensure the stoichiometry of SiC.

Experiment and Result

In this research, both TMS and MTS were used to deposit a SiC layer on carbon coated uranium oxide particles. The buffer carbon layer was deposited on uranium oxide particles by decomposition of propane (C_3H_8). The CVD process was carried out at 1300 ^{o}C in a Lindberg Blue high temperature tube furnace as shown in Figure 6-1. Argon and 5% H_2 gas was used as carrier gas at a constant flow rate of 140 cm^3 per minute. The precursor, TMS or MTS, flowed

through the furnace at the flow rate of 5 cm^3 per minute at the temperature of 1300 ^oC for 30 minutes. Figure 6-2 is the temperature profile of the CVD process

The powder after the CVD process is shown in Figure 6-3. Fourier Transform Infrared Spectroscopy (FTIR) and X-ray Diffraction (XRD) were used to characterize the SiC coating. FTIR was used to obtain information about the chemical bonding in the material; XRD was used to identify the crystalline structure. The FTIR result is shown in Figure 6-4. The powder after CVD process has a peak at the same position as β-SiC powder, which indicates the formation of Si-C bond. The XRD result is shown in Figure 6-5. There are no SiC peaks found in Figure 6-5 and all of the peaks in Figure 6-5 are UO_2 peaks.

Discussion

The possible reason for no SiC peaks found in XRD result was that the precursor, TMS or MTS, had already decomposed before reaching the carbon coated UO_2 particles. The furnace tube was about four feet long and the UO_2 powder was placed in the middle of the furnace tube, so the gaseous precursor had to travel two feet before reaching the powder. TMS or MTS might have already decomposed and deposited on the inside of the furnace tube. A colored layer can be seen on the inside wall of the furnace tube in Figure 6-6. The peak in FTIR result might be some contamination containing Si-C bond.

There was another possibility that β-SiC was not detected on the carbon coated uranium oxide particles. The amount of SiC was small and uranium oxide is a strong X-ray absorber, so the X-ray diffracted from β-SiC was absorbed in UO_2 and the peaks of SiC were not shown in the XRD result.

Even if there was a β-SiC layer formed on the carbon coated UO_2 powder, the powder will be hard to sinter. The powder can be seen as SiC in the sintering process because SiC is the outside layer and there are two SiC layers between two particles. The low temperature sintering

method of UO_2 can not be used. Temperature above 1900 ^oC is required to achieve a high density SiC pellet, which is above the temperature at which SiC reacts with UO_2. The CVD process was not further studied because of the potential problem for sintering and the success in making the SiC whiskers-UO_2 composite.

Figure 6-1. Lindberg high temperature furnace.

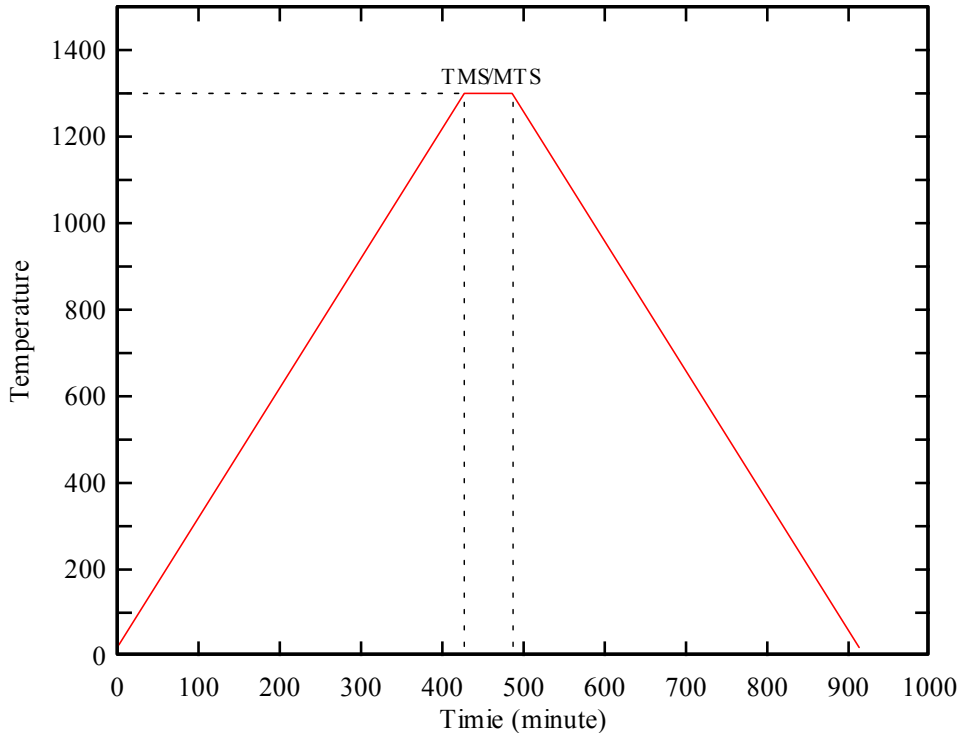

Figure 6-2. Temperature profile of the CVD process.

Figure 6-3. Uranium oxide powder after CVD process.

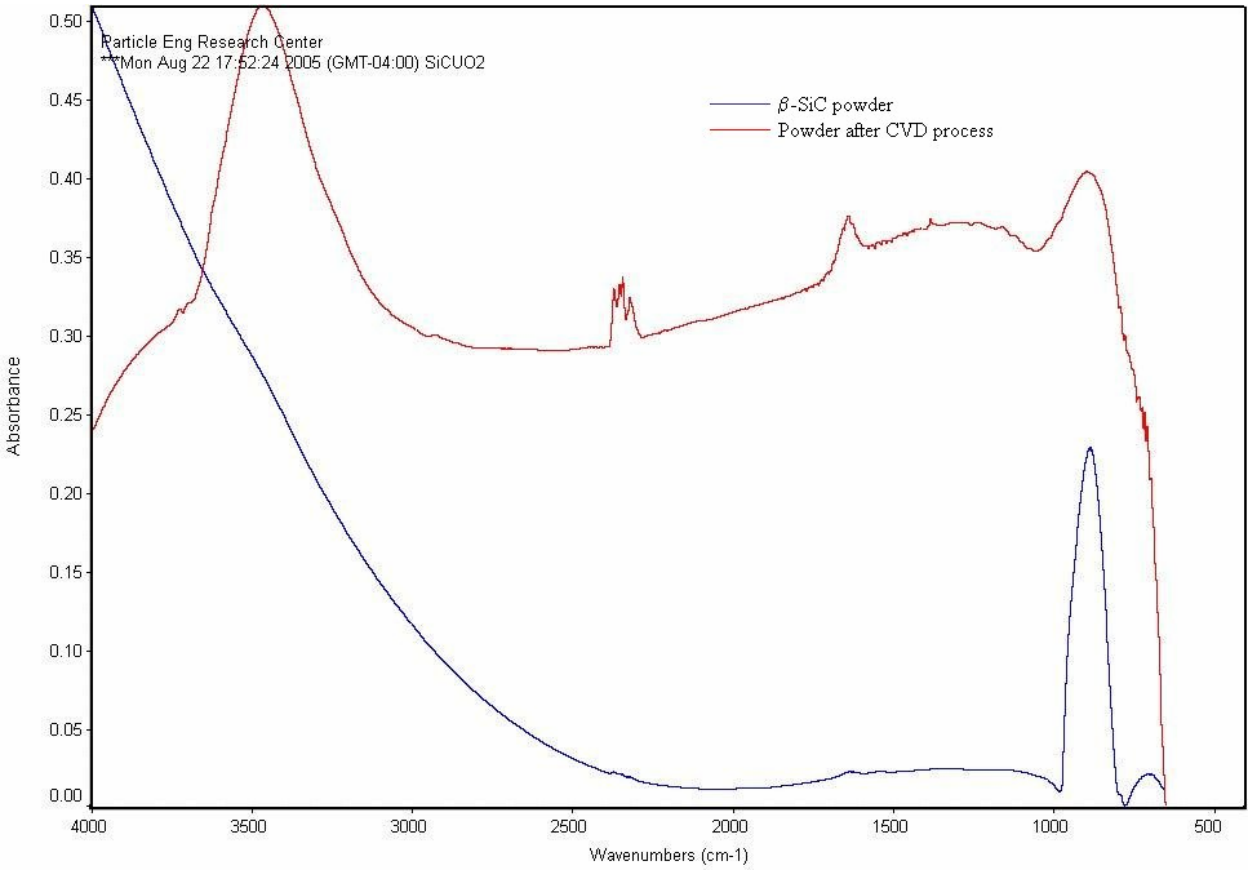

Figure 6-4. Fourier transform infrared spectroscopy result of the powder after the CVD process.

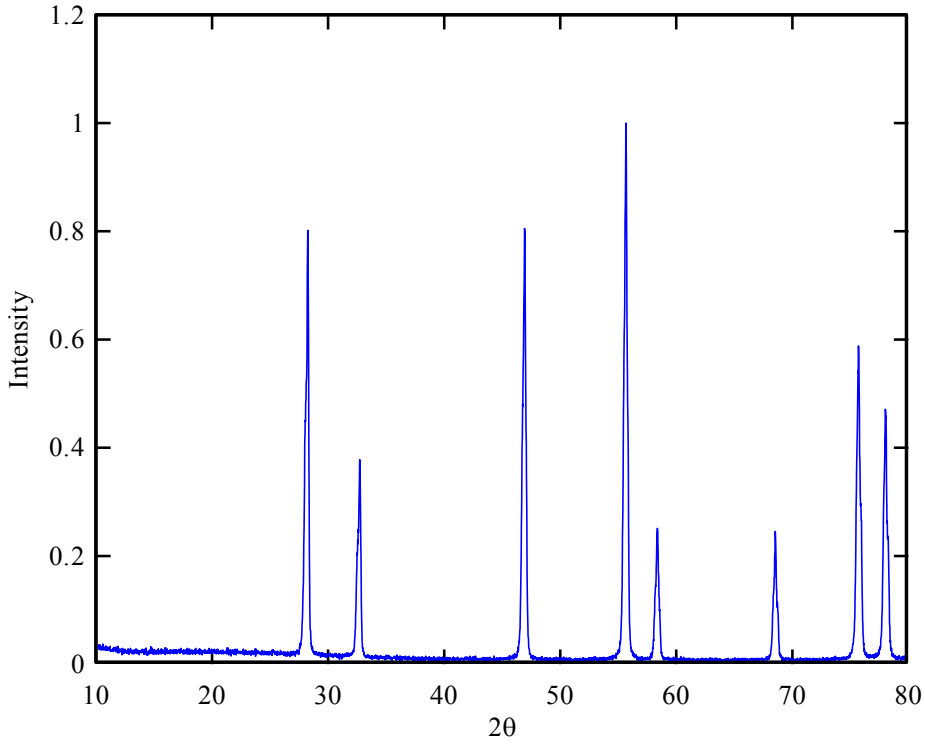

Figure 6-5. X-ray diffraction result of the powder after CVD process.

Figure 6-6. Furnace tube after CVD process.

CHAPTER 7
SILICON CARBIDE COATING FROM PRECERAMIC POLYMER

Background

Silicon carbide (SiC) can be produced by a pre-ceramic polymer. Grigoriev et al. [54] have successfully deposit an amorphous SiC coating on alumina and zirconia substrate using a ter-polysilane polymer at 900 ^{o}C. Zheng et al. [55] have reported the growth of SiC whiskers by Allylhydridopolycarbosilane (AHPCS) and SiC powder in the temperature range of 1250 ^{o}C to 1350 ^{o}C. Berton et al. [56] have used AHPCS to make carbon/ silicon carbide composite by polymer infiltration and pyrolysis (PIP). Solomon et al. [10] have also used AHPCS in the PIP process to make SiC/UO_2 composite. The conversion of pre-ceramic polymer to ceramic is a relatively easy and low cost process compared with chemical vapor deposition (CVD) process.

Experiments and Results

The SiC pre-ceramic polymer used in this research is AHPCS, also called "SMP-10" by the manufacturer Starfires Systems Inc. AHPCS is a liquid with bright orange color, as shown in Figure 7-1. According to the manufacturer, amorphous SiC forms at 850 ^{o}C with 75 to 82% ceramic yield and nano-crystalline β-SiC forms at 1250 to 1700 ^{o}C with 75 to 80% yield.

AHPCS was first used to make a SiC pellet. The SiC powder (1 μ) purchased from Alfa Aesar was mixed with 10 w% AHPCS in Hexane (C_6H_{14}). After Hexane was dried, the mixed powder was cold pressed in a 13 mm die at 200 MPa. The green pellet was then sintered in a Lindberg furnace (Figure 7-2) in argon atmosphere following the sintering procedure provided by Starfires Systems Inc (Figure 7-3). The sintered pellet made from1 μ powder is shown in Figure 7-4 and the SEM image of the pellet is shown in Figure 7-5. The density measured by the Archimedes method was 98.7%TD, which was far different from 66.7%TD, the density calculated by mass and volume.

Uranium oxide ($UO_{2.27}$) was mixed with 10 weight % AHPCS in hexane. After the hexane evaporated, the mixed powder was cold pressed in an alumina die (¼ inch in diameter) at 200 MPa. Then both the pellet and the alumina die were heated in an argon atmosphere in the same Lindberg furnace. During the sintering process, about 5 MPa pressure was applied on the pellet. The pressure was provided by two springs located at the end of the furnace tube, which was sealed by stainless steel end caps. The pellet after sintering broke into pieces when it was taken out of the alumina die.

Discussion

The reason for the large difference between the density measured by the Archimedes method and the density calculated by mass and volume is that the Archimedes method is not suitable for measuring the density of a pellet with large open porosity. The density of a pellet with large open porosity measured by the Archimedes method is the density of the "skeleton" of the pellet, which can be close to the theoretical density. The density calculated by mass and volume is relative close to the real value compare to the result by the Archimedes method.

There is an easy way to tell whether the pellet is suitable for the Archimedes method. If there are a lot of bubbles coming out of the pellet when immersed into liquid, the pellet is porous and not suitable for the Archimedes method; otherwise, the pellet is low in porosity and suitable for the density measurement by the Archimedes method. The density of the SiC pellet sintered by pressureless sintering is low because of the relative low yield of the pre-ceramic polymer. There were large pores in the SiC pellet, as shown in Figure 7-5.

The reason for the break up of the pellet may be that the pre-ceramic polymer was oxidized by the $UO_{2.27}$ powder. The polymer precursor could be oxidized by the extra oxygen in uranium oxide powder before it can be converted to silicon carbide. Because the extra oxygen is essential

for the low temperature sintering method of UO_2, the oxidation of the pre-ceramic polymer is inevitable and the process of pre-ceramic coating on uranium oxide particles is not successful.

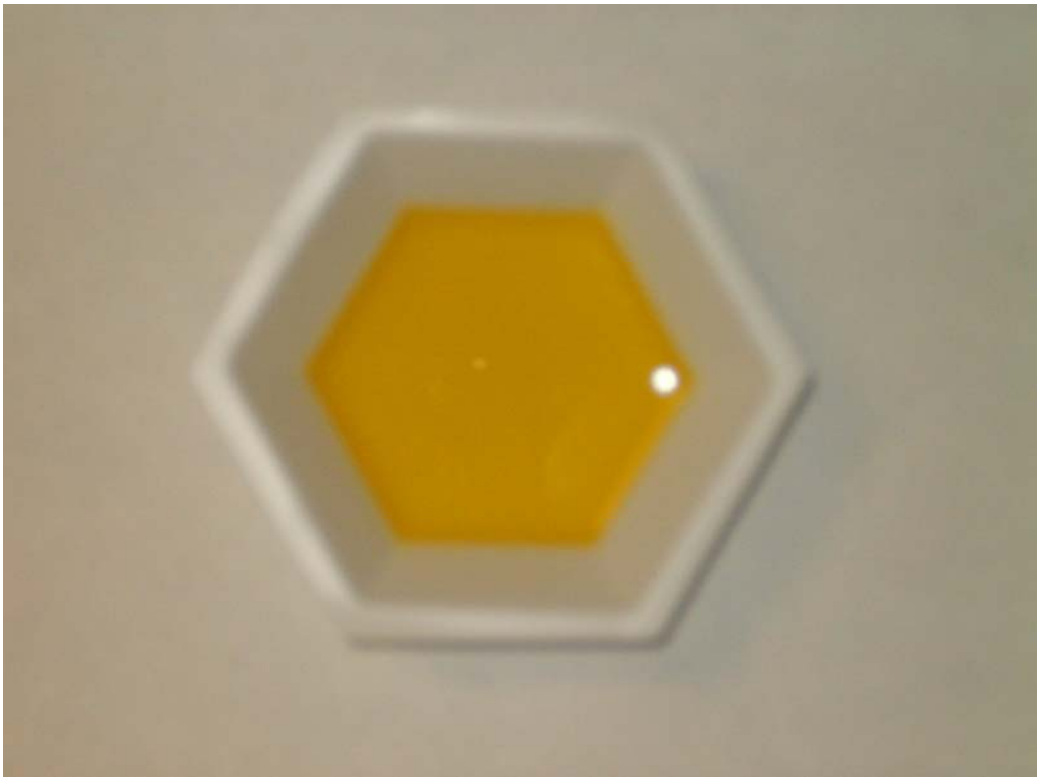

Figure 7-1. Allylhydridopolycarbosilane (AHPCS), the SiC pre-ceramic polymer.

Figure 7-2. Lindberg/Blue Mini-Mite 1100 ^{o}C furnace.

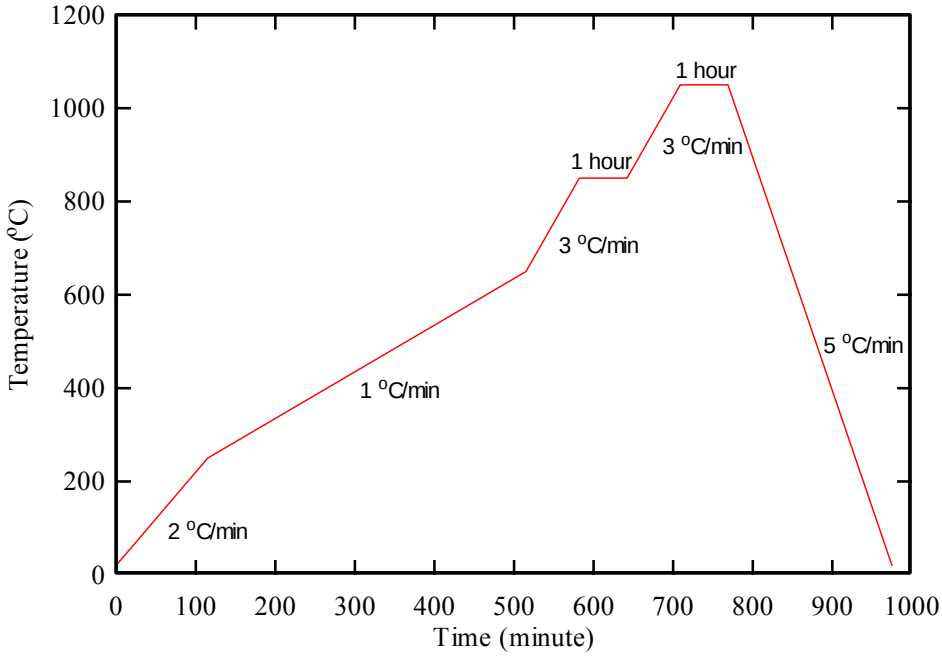

Figure 7-3. The temperature profile of sintering process.

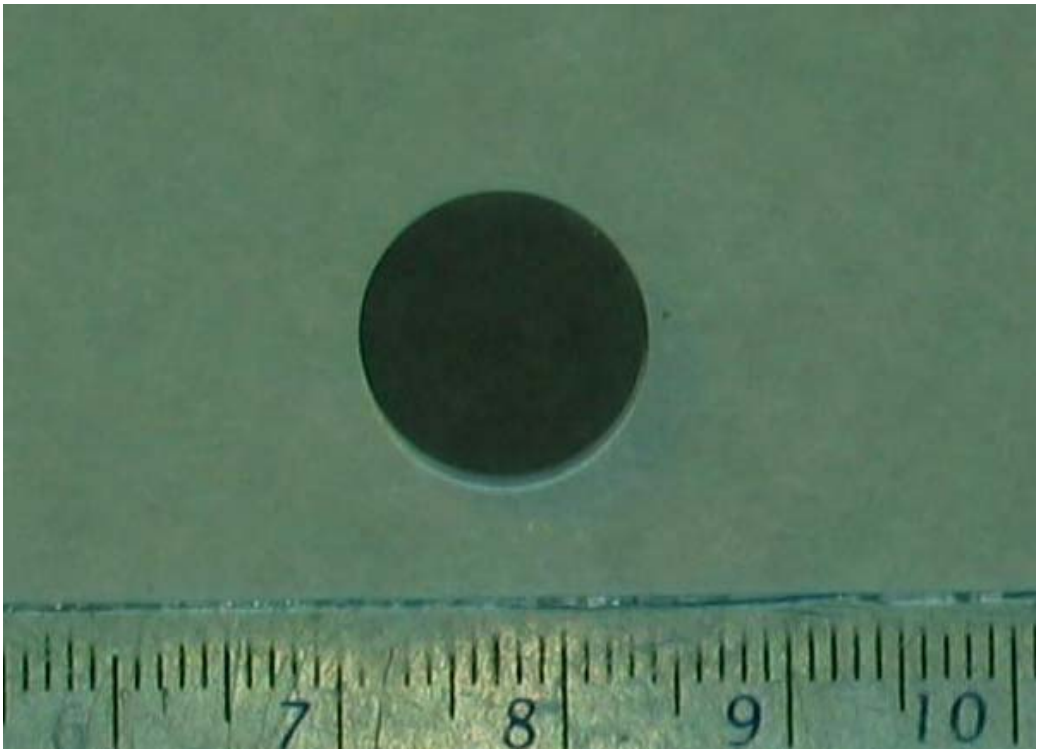

Figure 7-4. Silicon carbide pellet made by SiC powder (1 μ) and AHPCS.

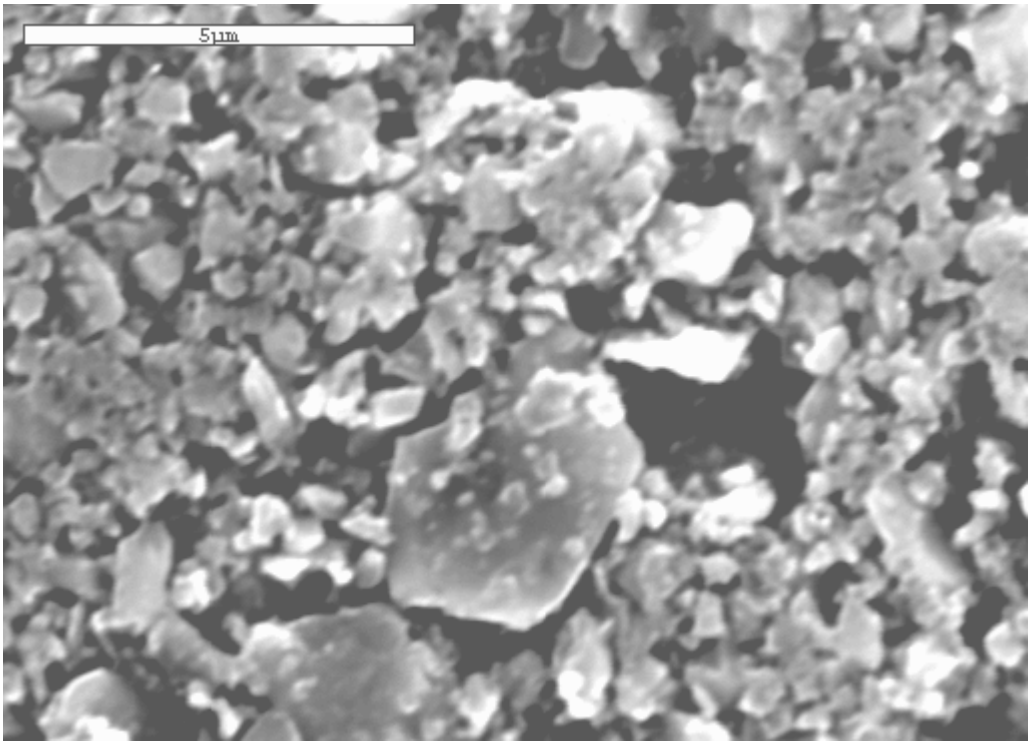

Figure 7-5. Scanning electron microscopy image of the SiC pellet made by SiC powder (1 µ) and AHPCS.

CHAPTER 8
SILICON CARBIDE WHISKERS – URANIUM DIOXIDE COMPOSITE

Background

Silicon carbide (SiC) whiskers are usually used as a reinforce material to improve the mechanical properties, such as strength and fracture toughness, of matrix materials. Wei et al. [34] used SiC whiskers to reinforce aluminum oxide (Al_2O_3) to improve the fracture toughness. Sun et al. [35] used SiC whiskers to improve the fracture toughness and high temperature strength of molybdenum disilicide ($MoSi_2$).

Silicon carbide whiskers are commonly made by either rice hull or vapor-liquid-solid (VLS) process. The SiC whiskers produced from rice hull process are typically less than 1 micron in diameter and range from 10 to 50 micron in length; the SiC whiskers produced from VLS process are typically 5-6 micron in diameter and up to 100 mm in length [57]. Silicon carbide whiskers are single crystal, which means fewer flaws than polycrystalline, so the thermal conductivity and strengths are very high.

The commercially available SiC whiskers are commonly in an agglomerated form. The agglomeration must be broken before mixing with the matrix to ensure homogenously dispersion of SiC whiskers. Wei et al. [34] reported that SiC whiskers and ceramic powder were mixed in hexane in a blender and then dispersed using an ultrasonic homogenizer; the hexane was then dried by evaporation with constant agitation under flowing air.

Hot pressing was found to be required to achieve a high density pellet with greater than 5 vol% SiC whiskers, because the SiC whiskers interfered with matrix particle rearrangement during sintering. During hot press sintering, SiC whiskers are preferentially oriented in a plane perpendicular to the hot pressing direction [7-9, 34].

Several studies have shown that SiC whiskers can also increase the thermal conductivity of matrix materials. Russell et al. [7] reported the thermal conductivity of 30 vol% VLS SiC whisker-mullite composite is three times higher at room temperature than that of single phase mullite in perpendicular direction to the hot pressing direction and two times higher in parallel direction. Johnson et al. [8] reported that the thermal conductivity of 30 vol% SiC whisker-osumilite glass composite is four times higher at room temperature than that of single phase mullite in perpendicular direction to the hot pressing direction and two times higher in parallel direction. Hesselman et al. [9] showed the thermal conductivity of 30 vol% VLS SiC whisker-lithium aluminosilicate glass composite is five times higher at room temperature than that of lithium aluminosilicate glass in perpendicular direction to the hot pressing direction and three times higher in parallel direction. Hesselman et al. [9] suggested that a SiC whisker "percolation" pathway was formed and heat was conducted through SiC whiskers, bypassing the matrix.

Experiments and Results

Characterization of Silicon Carbide Whiskers

The silicon carbide whiskers are commercially available from Alfa Aesar (Alfa) and Advanced Composite Materials (ACM). The whiskers from Alfa Aesar are 1.5 micron in diameter and about 18 micron in length (no detailed information available); the Whiskers from Advanced Composite Materials are 0.45-0.65 micron in diameter and 5-80 micron in length. Both of the whiskers are single crystal β-SiC. The received SiC whiskers were in the form of agglomerates. The scanning electron microscope (SEM) images of the received SiC whiskers from Alfa Aesar are shown in Figure 8-1 and Figure 8-2. The X-ray diffraction pattern of SiC whiskers from Alfa Aesar is shown in Figure 8-3. The SEM images of the received SiC whiskers from Advanced Composite Materials are shown in Figure 8-4 and Figure 8-5. The X-ray diffraction pattern of SiC whiskers from Advanced Composite Materials is shown in Figure 8-6.

Mixing of SiC Whiskers and Uranium Oxide Powder

The received SiC whiskers were blended with hexane in a blender for 3 minutes to break the agglomeration. A small amount of the mixture was dropped on the SEM sample holder and the hexane was left to evaporate, leaving only the separated SiC whiskers. Figure 8-8 and Figure 8-9 are the SEM images of dispersed SiC whisker from Alfa Aesar and Advanced Composite Materials, respectively. Based on the SEM images, the SiC whiskers were successfully dispersed by the blending. The separated SiC whiskers were then mixed with $UO_{2.27}$ particles (25 μ to 45 μ) in an ultrasonic mixer for 10 minutes. After hexane was dried, the mixed powder was ground by a mortar and a pestle.

Pressureless Sintering of SiC Whiskers and Uranium Oxide Powder

The mixed powder of UO_2 and SiC whiskers from Advanced Composite Materials was cold pressed in an alumina (Al_2O_3) die (1/4" in diameter) at 200MPa. The green pellet and the Al_2O_3 die were sintered at 1200 ^oC in argon atmosphere for 1 hour. The pellet of UO_2 with 5 vol% SiC is shown in Figure 8-9. The SEM images of the pellet are shown in Figure 8-10 and Figure 8-11. The density of the pellet was 98.6% TD, which was measured by the Archimedes method. The pellet of UO_2 with 10 vol% SiC is shown in Figure 8-12. The SEM images of the pellet are shown in Figure 8-13 and Figure 8-14. The density of the pellet was 82.2% TD, which was also measured by the Archimedes method. The density of the pellet decreases sharply with increasing the amount of SiC whiskers.

Hot Press Sintering of SiC Whiskers and Uranium Oxide Powder

The mixed powder of UO_2 and SiC whiskers from Advanced Composite Materials was cold pressed in an alumina die at 200MPa. The alumina die was made by an alumina tube and two alumina rods, as shown in Figure 8-15. After cold pressing, the mixed powder and alumina die were placed in a sample holder surrounded by a graphite tube at the position of mixed

powder, as shown in Figure 8-16. The geometry of the alumina die and graphite tube was shown in Figure 8-17. The mixed powder was then hot press sintered in a hot press sintering system, which included a sintering chamber, a high voltage alternating current (AC) generator and a pyrometer, as shown in Figure 8-19. The high voltage AC generator was connected to a copper coil inside the sintering chamber. An alternating electromagnetic field was generated inside the coil with AC current flowing through it. The changing electromagnetic field induced currents in an electrical conductor as it was placed inside the coil. The induced currents (Eddy current) generated heat inside the conductor due to the resistance. The alumina die and graphite tube was placed inside the coil. Eddy currents were induced inside the graphite tube, which is an electrical conductive material. Alumina and uranium oxide are poor electrical conductors, so no Eddy currents were generated inside them. The surface temperature of the graphite tube was measured by an optical pyrometer. Figure 8-18 shows the heated graphite observed through the pyrometer. The pyrometer communicated with the high voltage AC generator to keep the surface temperature of the graphite tube constant. The mixed powder was sintered at 1201.4 ^{o}C for 1hour in argon atmosphere. (The detailed sintering temperature calculation is in Appendix B.) The pressure applied by the lead bricks on top during the sintering process was about 10 MPa. The pellets after hot process sintering were soaked in hydrogen atmosphere to reduce the oxygen to uranium ratio to 2.0. The densities of the pellets after reduction, which were measured by the Archimedes method, are shown in Table 8-1.

The pellet of UO_2 with 5 vol% SiC is shown in Figure 8-20. The SEM images of the pellet are shown in Figure 8-21 and Figure 8-22 and the XRD result is shown in Figure 8-23. The pellet of UO_2 with 10 vol% SiC is shown in Figure 8-24. The SEM images of the pellet are shown in Figure 8-25 and Figure 8-26 and the XRD result is shown in Figure 8-27. The pellet of UO_2 with

15 vol% SiC is shown in Figure 8-28. The SEM images of the pellet are shown in Figure 8-29 and Figure 8-30 and the XRD result is shown in Figure 8-31.

The pellet of UO_2 (<25 μ) with 15 vol% SiC from Advanced Composite Materials (Figure 8-32) was made by hot press sintering to study the effect of UO_2 particle size on the final density. The SEM images of the pellet are shown in Figure 8-33 and Figure 8-34 and the XRD result is shown in Figure 8-35. The density of the pellet measured by Archimedes method was 95.6% TD.

The pellet of UO_2 (25 μ to 45 μ) with 15 vol% SiC from Alfa Aesar (Figure 8-36) was also made by hot press sintering to study the effect of different SiC whiskers on the final density. The SEM images of the pellet are shown in Figure 8-37 and Figure 8-38 and the XRD result is shown in Figure 8-39. The density of the pellet measured by Archimedes method was 96.0% TD.

Discussion

The densities of the pellets, which were made by pressureless sintering, decreased sharply with increasing the amount of SiC whiskers. The density of the pellet of UO_2 with 10 vol% SiC whiskers was only 82.2%, compared to 98.6% of the pellet of UO_2 with 5 vol% SiC whisker. The SiC whiskers hinder the process of UO_2 particles joining together to form large grains. It is more difficult for pellet to densify with increasing amount of SiC whiskers. High density is usually not possible with greater than 5 vol% SiC whiskers. The grain size of UO_2 with 10 vol% SiC whiskers in Figure 8-14 is smaller than that of UO_2 with 5 vol% SiC whiskers in Figure 8-11.

The densities of the pellets made by hot press sintering were all close to 95% TD. The density of the pellet of UO_2 with 10 vol% SiC whiskers was 94.7% TD, which was slightly less than the density of the pellet of UO_2 with 5 vol% SiC whiskers, 95.4% TD. It is reasonable because the SiC whiskers hinder the process of UO_2 particles joining together to form large

grains. It is more difficult for pellet to densify with increasing amount of SiC whiskers. The density of the pellet of UO_2 with 15 vol% SiC whiskers was 95.9%, which was larger than the density of the pellet of UO_2 with 10 vol% SiC whiskers and even larger than the density of the pellet of UO_2 with 5 vol% SiC whiskers. The reason for the unusual increase in the density may be that the SiC whiskers were not well dispersed in UO_2. Some UO_2 islands can be found in the SEM image of the pellet of UO_2 and 15 vol% SiC whiskers (Figure 8-29 and Figure 8-30). The UO_2 islands increased the density of the pellet. Some UO_2 islands can also be found in the SEM images of the pellet of UO_2 and 5 vol% or 10 vol% SiC whisker. It is more difficult to disperse SiC whiskers homogeneously in UO_2 with increasing amount of SiC whiskers.

The density of the pellet of UO_2 (<25 μ) with 15 vol% SiC from Advanced Composite Materials was 95.6% TD. The density of the pellet of UO_2 (25 μ to 45 μ) with 15 vol% SiC from Alfa Aesar was 96.0% TD. The two densities were very close to the density of UO_2 (25 μ to 45 μ) with 15 vol% SiC from Advanced Composite Materials, so the UO_2 particle size and the SiC whiskers are not decisive factors for the density of the pellet after hot press sintering.

Due to the nature of material transport and flow during hot press sintering, the SiC whiskers exhibited a preferential orientation. The SEM images of the cross section of UO_2 with 30 vol% SiC whiskers after hot press sintering are shown in Figure 8-40 and Figure 8-41. The SiC whiskers are oriented in a plane which is perpendicular to the direction of hot pressing. This preferential orientation of the SiC whiskers is desired because the preferential orientation increases the probability of the contact of SiC whiskers, thus increase the probability of the formation of the percolation pathway for heat to flow out of the pellet.

Table 8-1. Densities of the pellets of UO_2 and SiC whiskers after hot press sintering.

	UO_2 with 5 vol% SiC whiskers	UO_2 with 10 vol% SiC whiskers	UO_2 with 15 vol% SiC whiskers
Density (% TD)	95.4	94.7	95.9

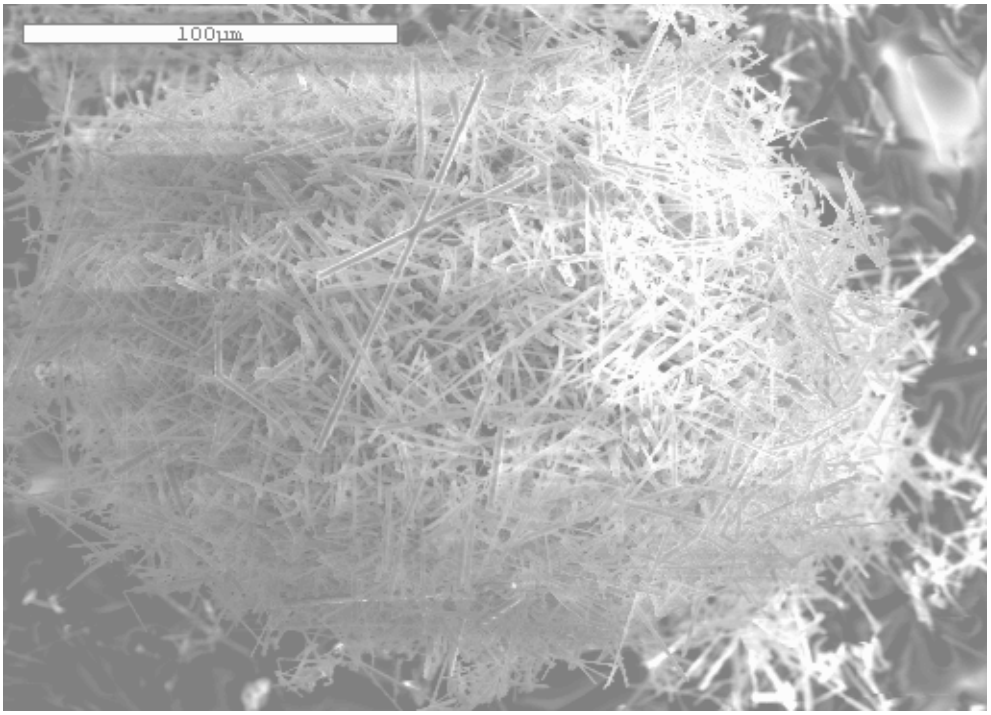

Figure 8-1. Scanning electron microscopy image of SiC whiskers as received from Alfa Aesar (500X).

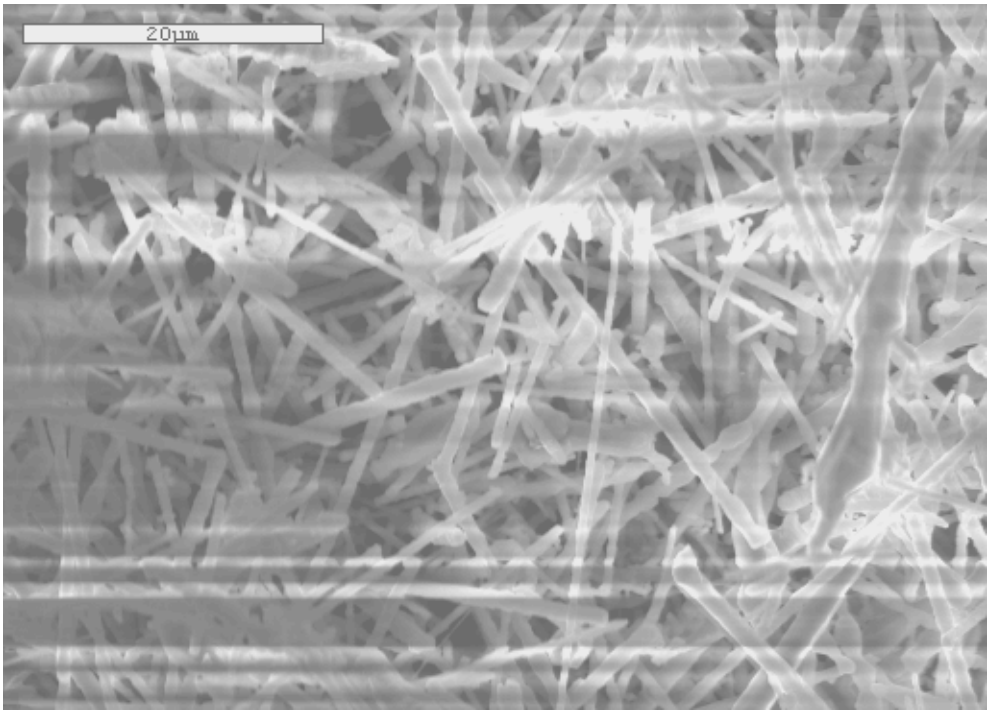

Figure 8-2. Scanning electron microscopy image of SiC whiskers as received from Alfa Aesar (2,000X).

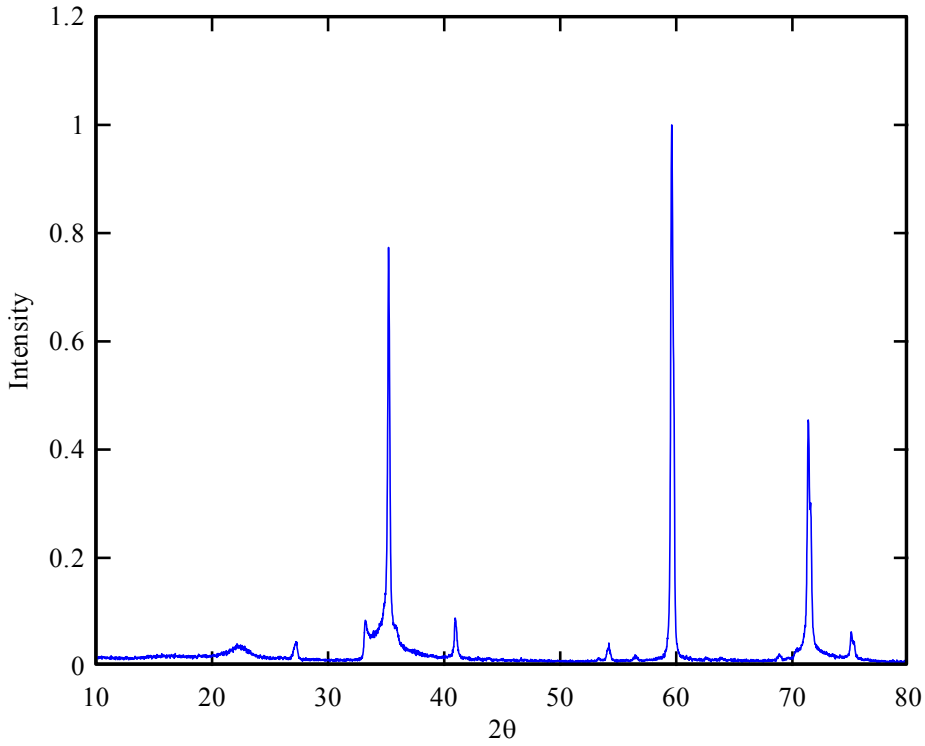

Figure 8-3. X-ray diffraction pattern of SiC whiskers from Alfa Aesar.

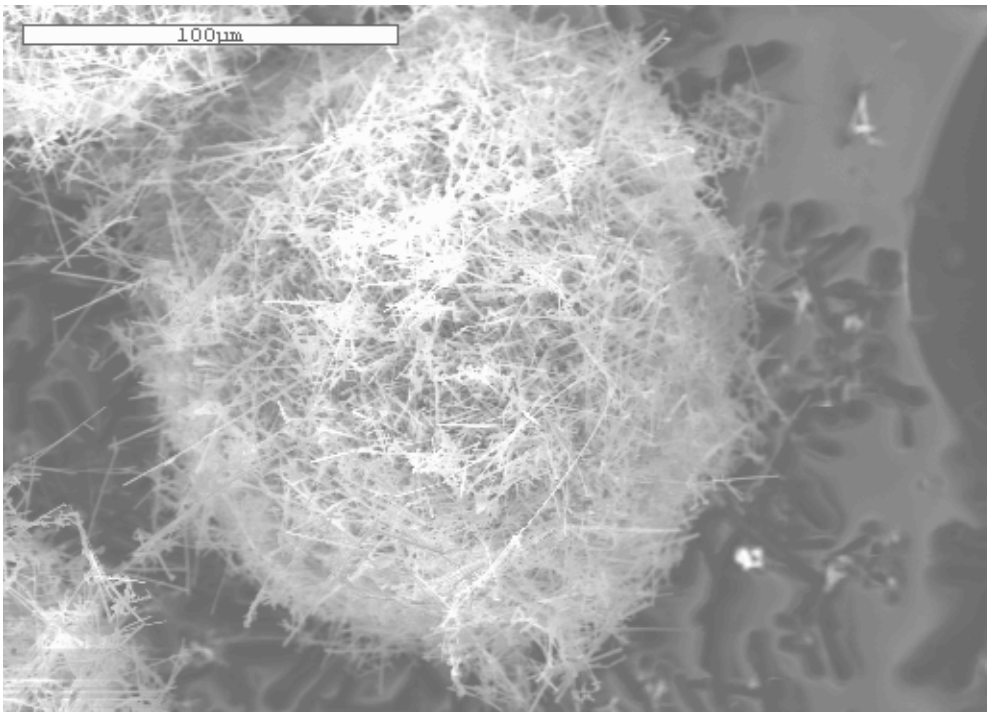

Figure 8-4. Scanning electron microscopy image of SiC whiskers as received from Advanced Composite Materials (500X).

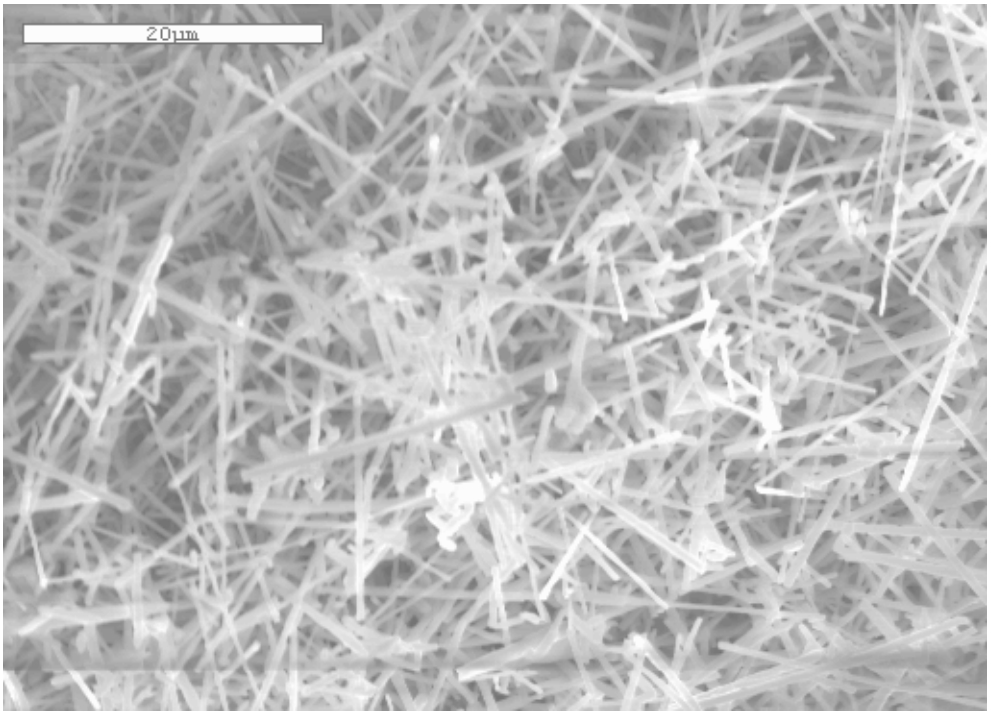

Figure 8-5. Scanning electron microscopy image of SiC whiskers as received from Advanced Composite Materials (2,000X).

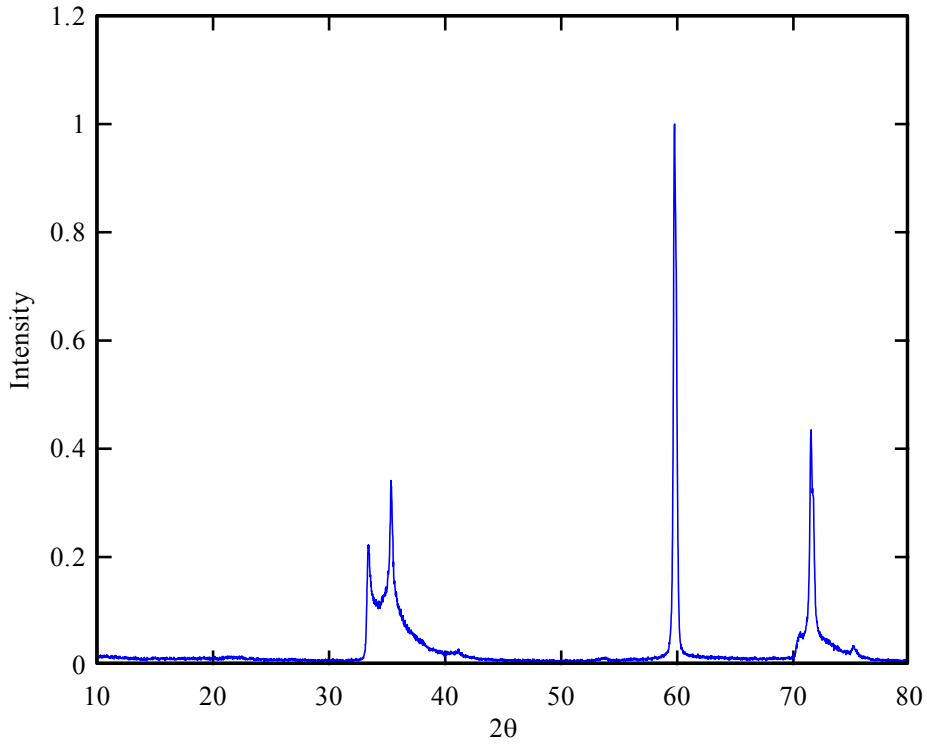

Figure 8-6. X-ray diffraction pattern of SiC whiskers from Advanced Composite Materials.

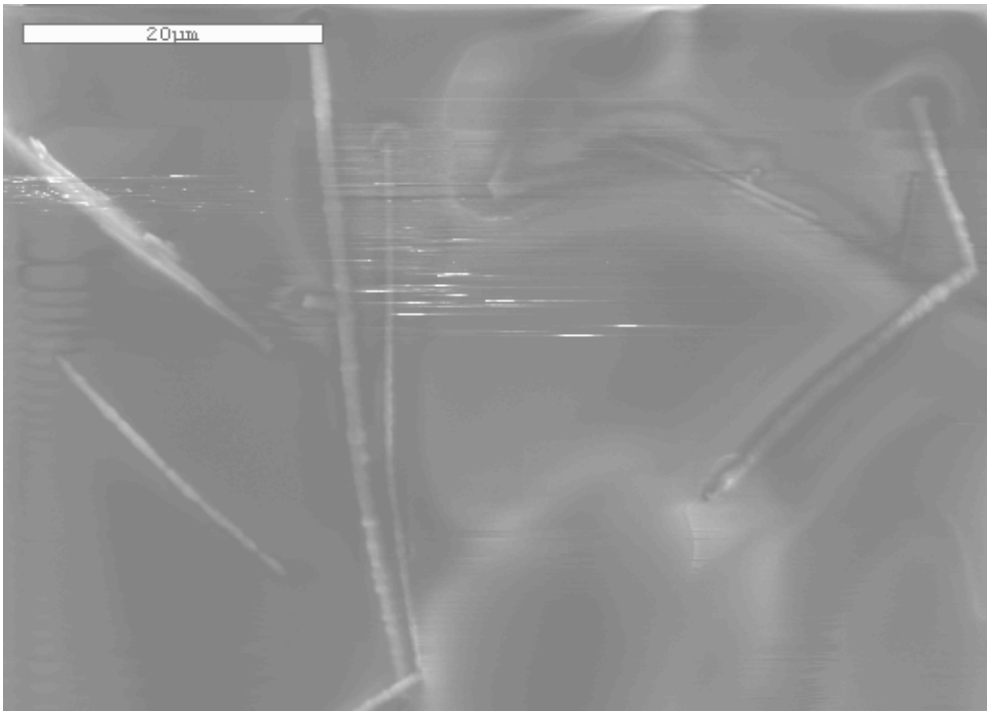

Figure 8-7. Scanning electron microscopy image of SiC whiskers from Alfa Aesar after dispersion (2,000X).

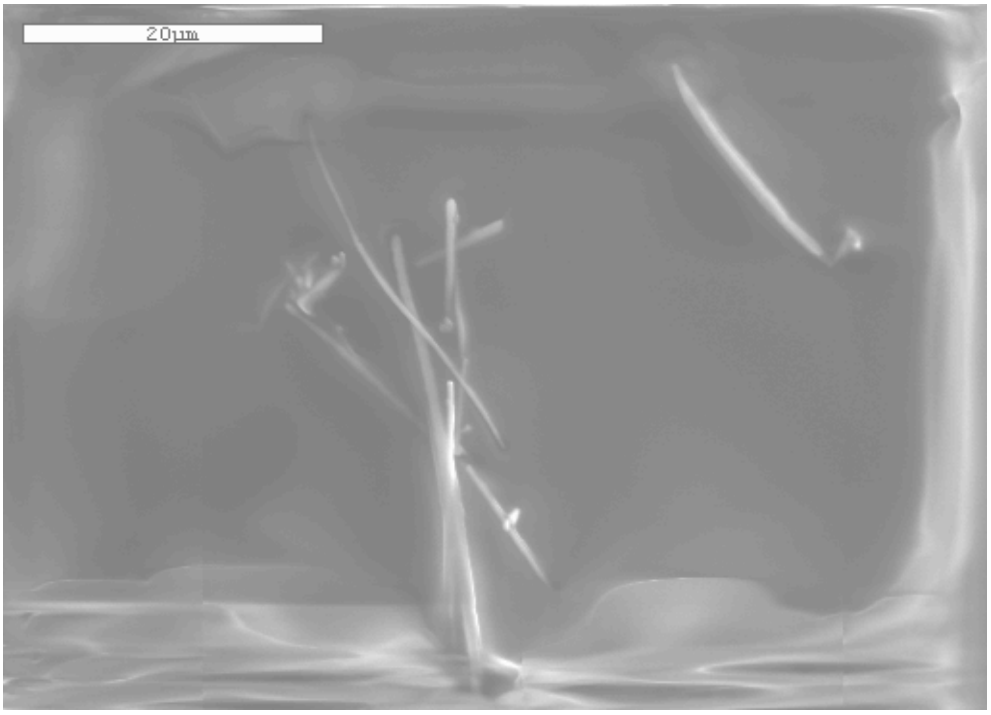

Figure 8-8. Scanning electron microscopy image of SiC whiskers from Advanced Composite Materials after dispersion (2,000X).

Figure 8-9. The pellet of UO_2 with 5 vol% SiC whiskers after pressureless sintering.

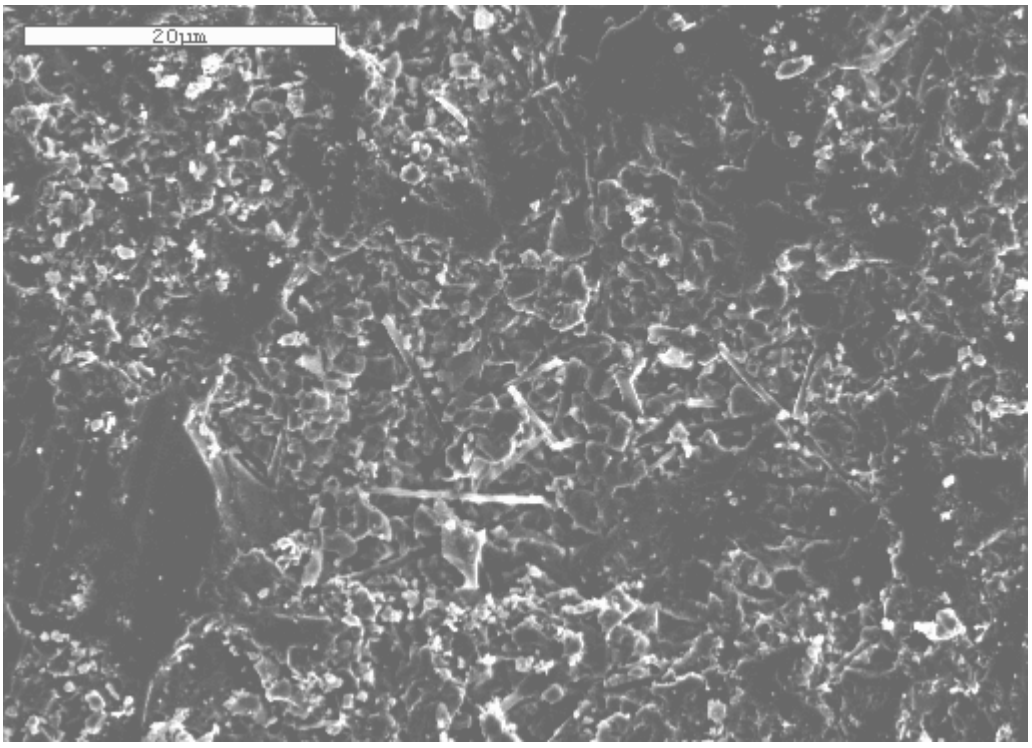

Figure 8-10. Scanning electron microscopy image of UO_2 with 5 vol% SiC whiskers after pressureless sintering, (2,000X).

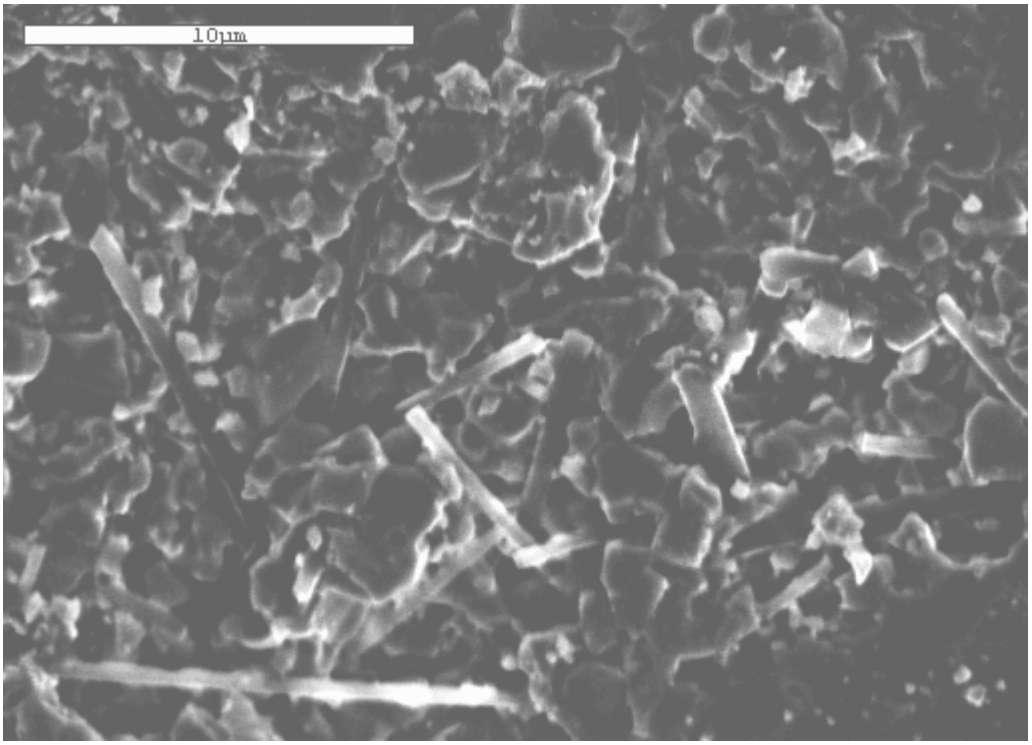

Figure 8-11. Scanning electron microscopy image of UO_2 with 5 vol% SiC whiskers after pressureless sintering, (5,000X).

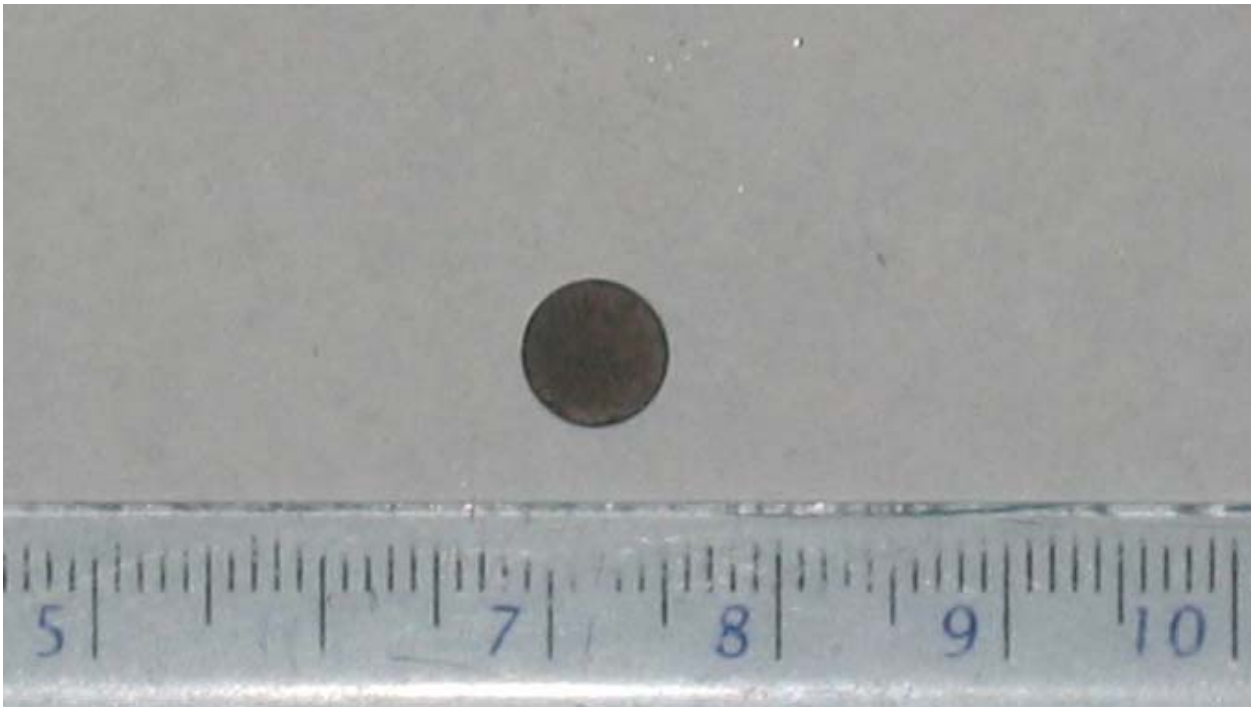

Figure 8-12. The pellet of UO_2 with 10 vol% SiC whiskers after pressureless sintering.

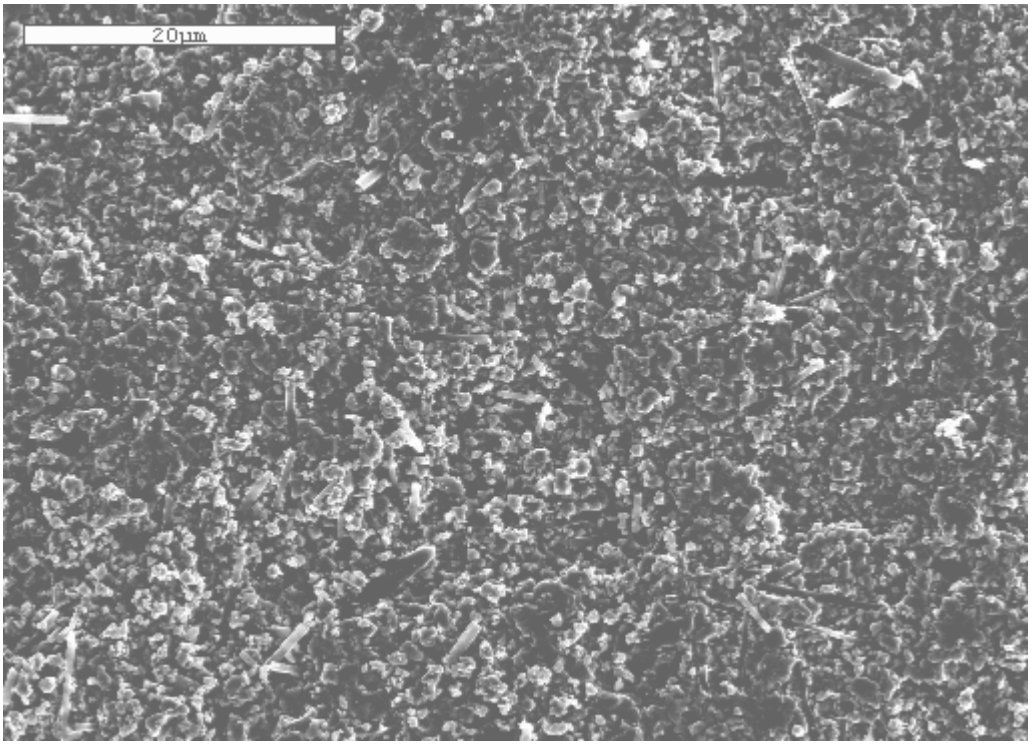

Figure 8-13. Scanning electron microscopy image of UO_2 with 10 vol% SiC whiskers after pressureless sintering, (2,000X).

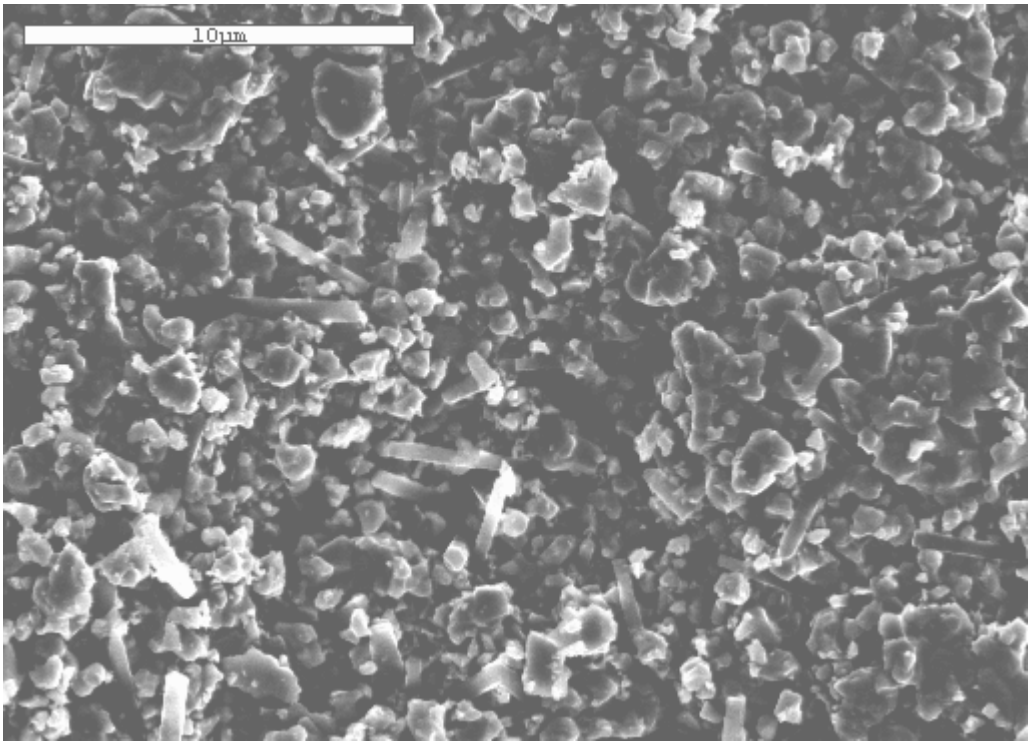

Figure 8-14. Scanning electron microscopy image of UO_2 with 10 vol% SiC whiskers after pressureless sintering, (5,000X).

Figure 8-15. Alumina die for hot press sintering.

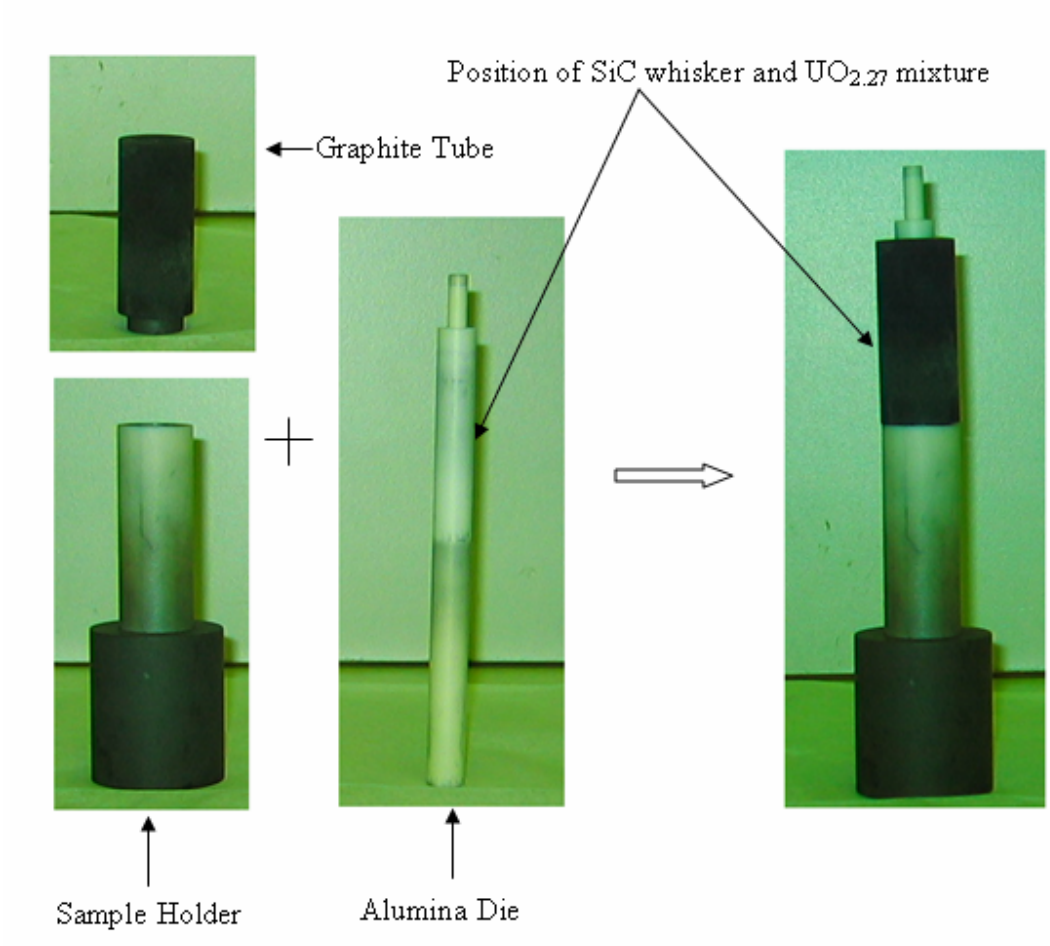

Figure 8-16. Alumina die, graphite tube and sample holder.

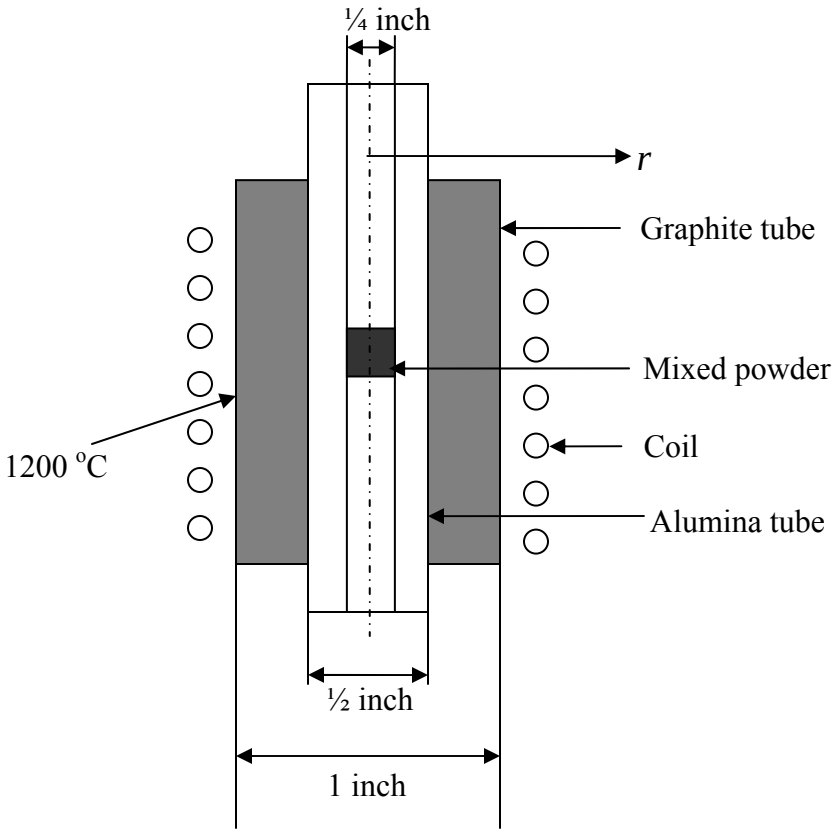

Figure 8-17. Geometry of the alumina die and graphite tube.

Figure 8-18. Heated graphite tube observed through the optical pyrometer.

Figure 8-19. Hot press sintering apparatus.

Figure 8-20. The pellet of UO_2 with 5 vol% SiC whiskers after hot press sintering.

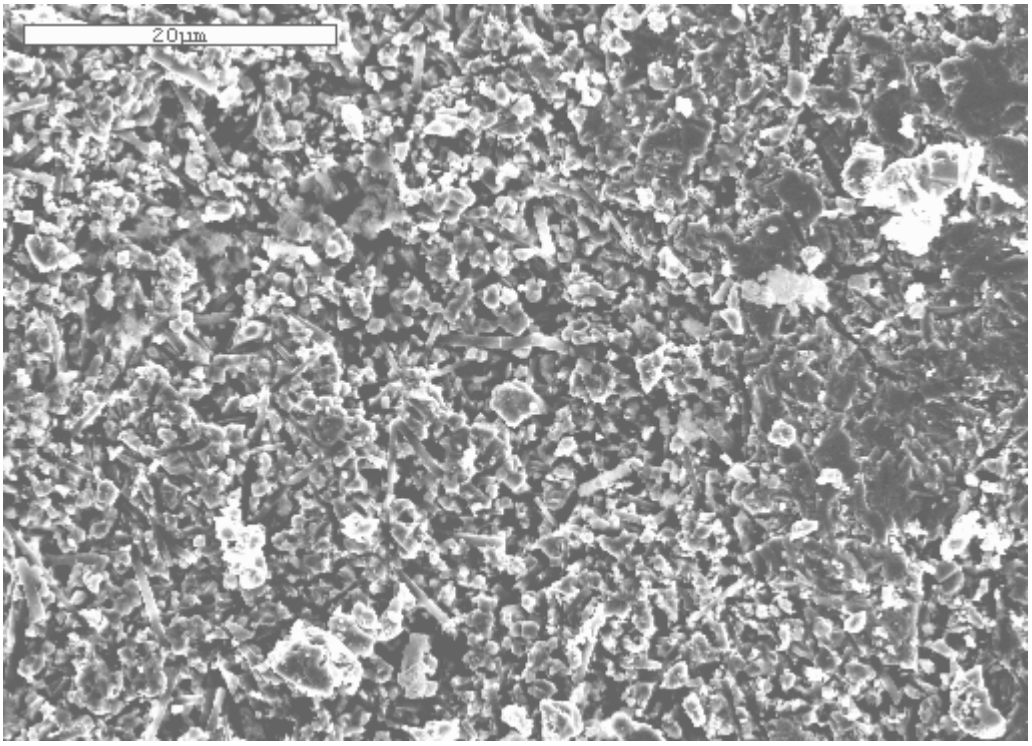

Figure 8-21. Scanning electron microscopy image of UO_2 with 5 vol% SiC whiskers after hot press sintering, (2,000X).

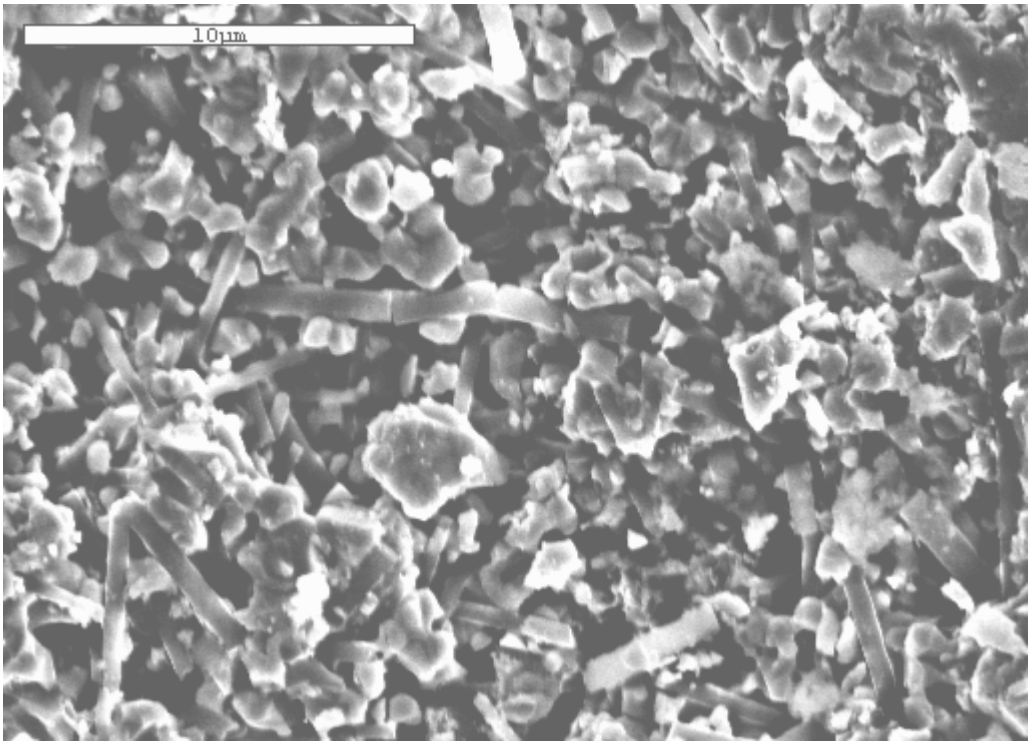

Figure 8-22. Scanning electron microscopy image of UO_2 with 5 vol% SiC whiskers after hot press sintering, (5,000X).

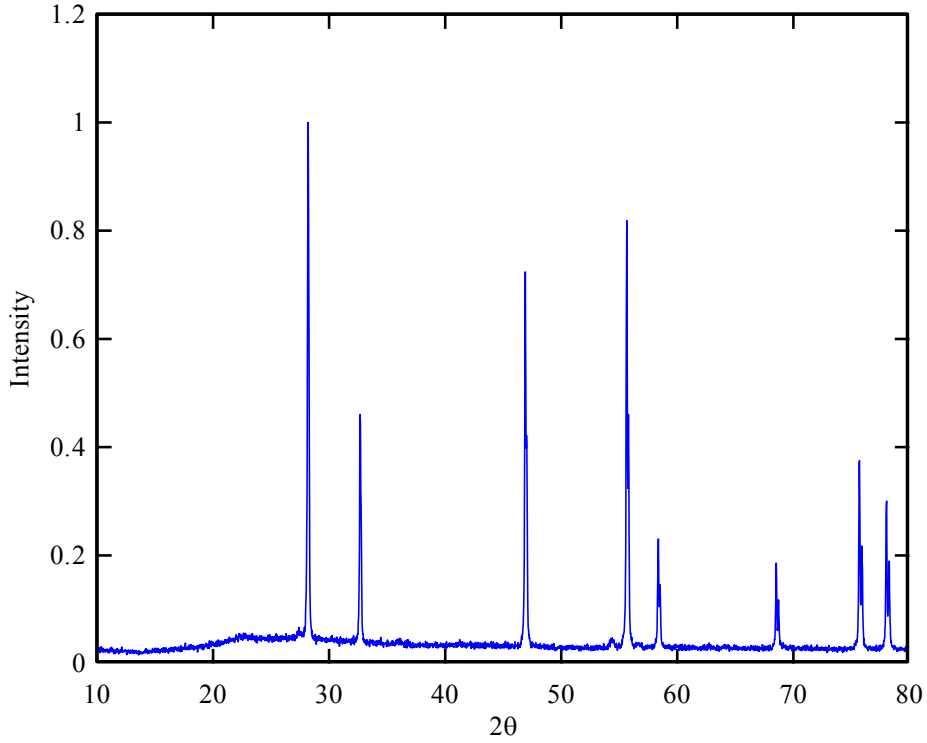

Figure 8-23. X-ray diffraction result of UO_2 with 5 vol% SiC whiskers after hot press sintering.

Figure 8-24. The pellet of UO_2 with 10 vol% SiC whiskers after hot press sintering.

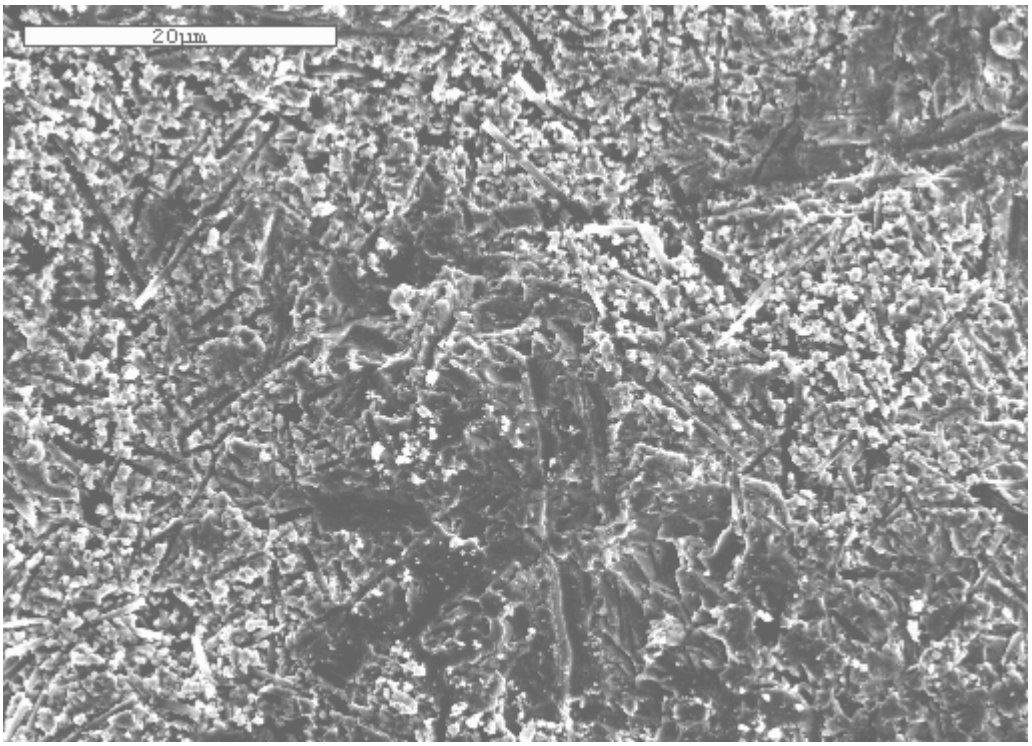

Figure 8-25. Scanning electron microscopy image of UO_2 with 10 vol% SiC whiskers after hot press sintering, (2,000X).

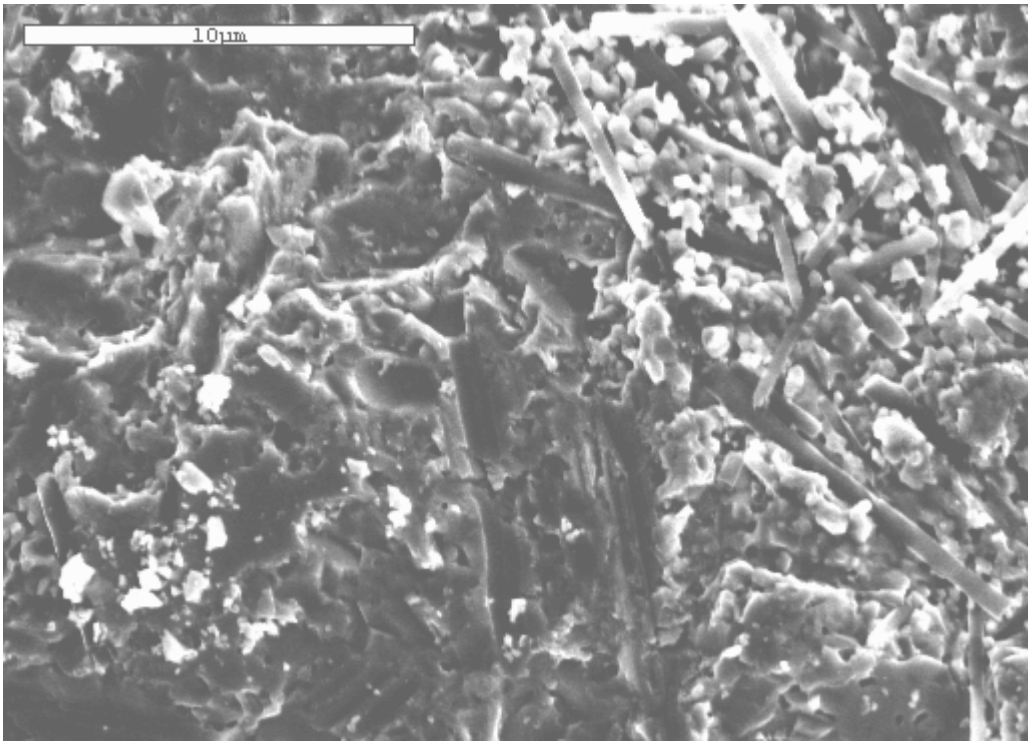

Figure 8-26. Scanning electron microscopy image of UO_2 with 10 vol% SiC whiskers after hot press sintering, (5,000X).

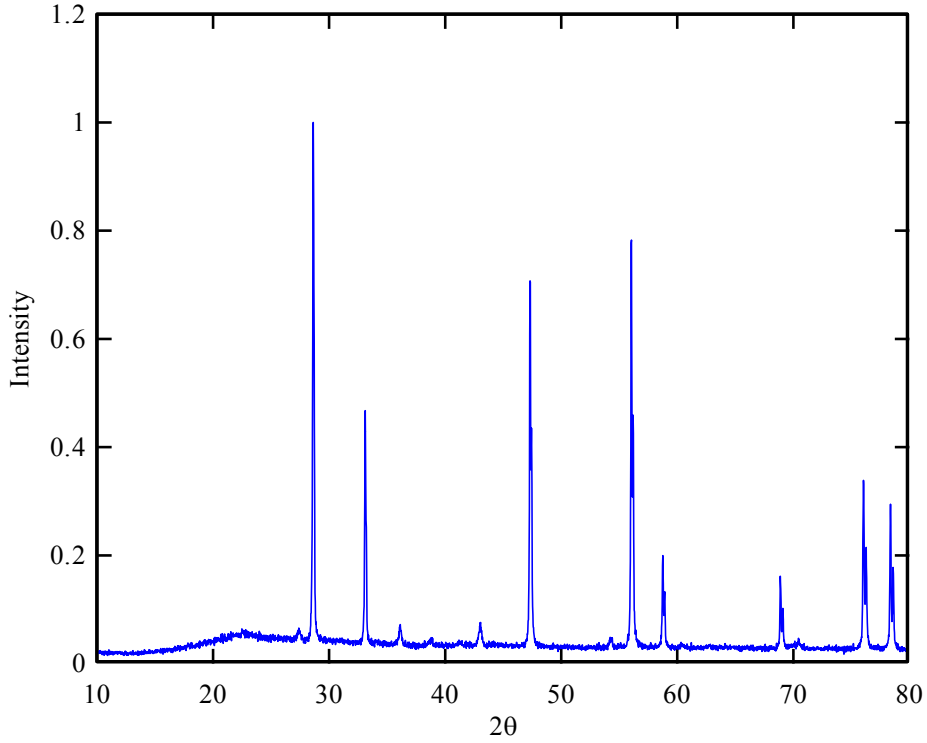

Figure 8-27. X-ray diffraction result of UO_2 with 10 vol% SiC whiskers after hot press sintering.

Figure 8-28. The pellet of UO_2 with 15 vol% SiC whiskers after hot press sintering.

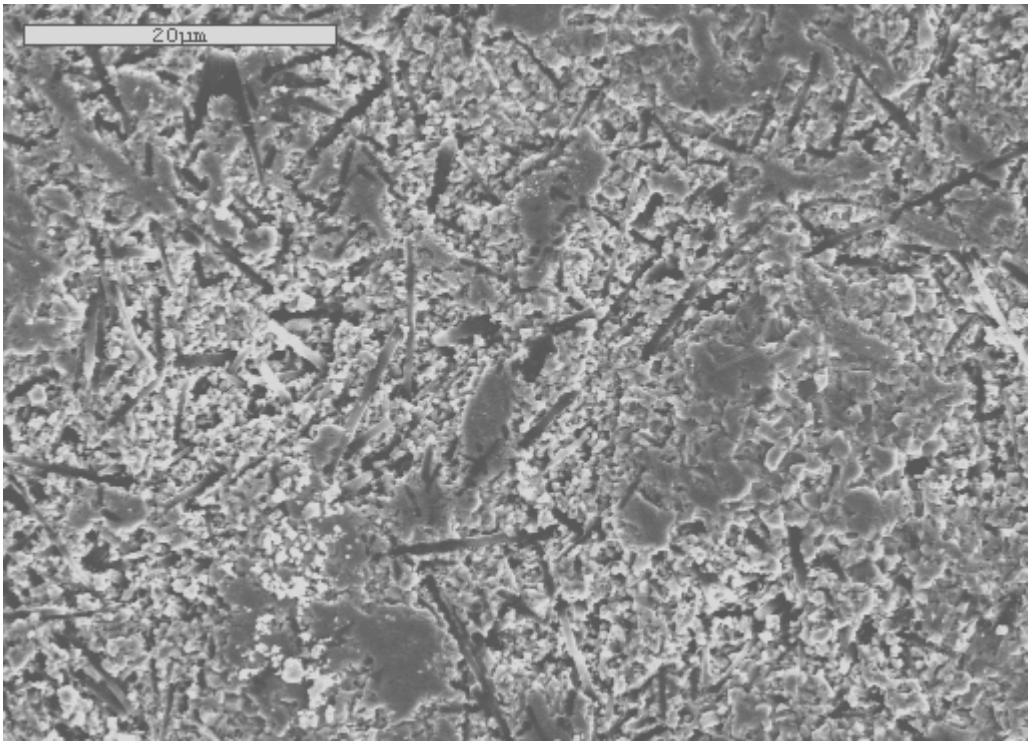

Figure 8-29. Scanning electron microscopy image of UO_2 with 15 vol% SiC whiskers after hot press sintering, (2,000X).

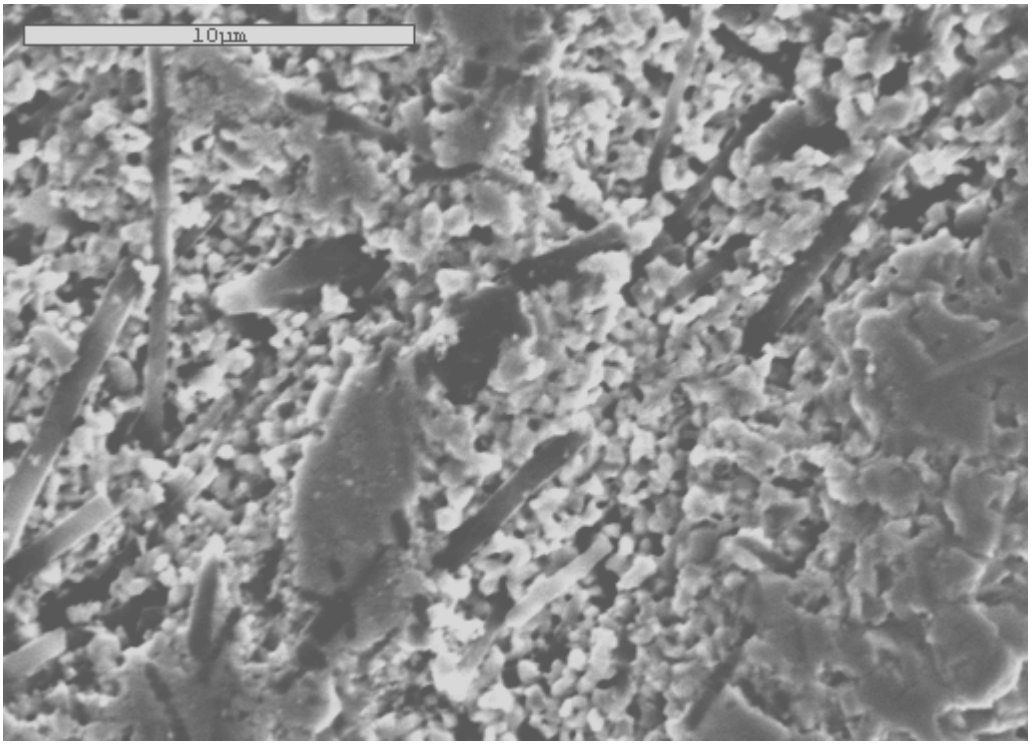

Figure 8-30. Scanning electron microscopy image of UO_2 with 15 vol% SiC whiskers after hot press sintering, (5,000X).

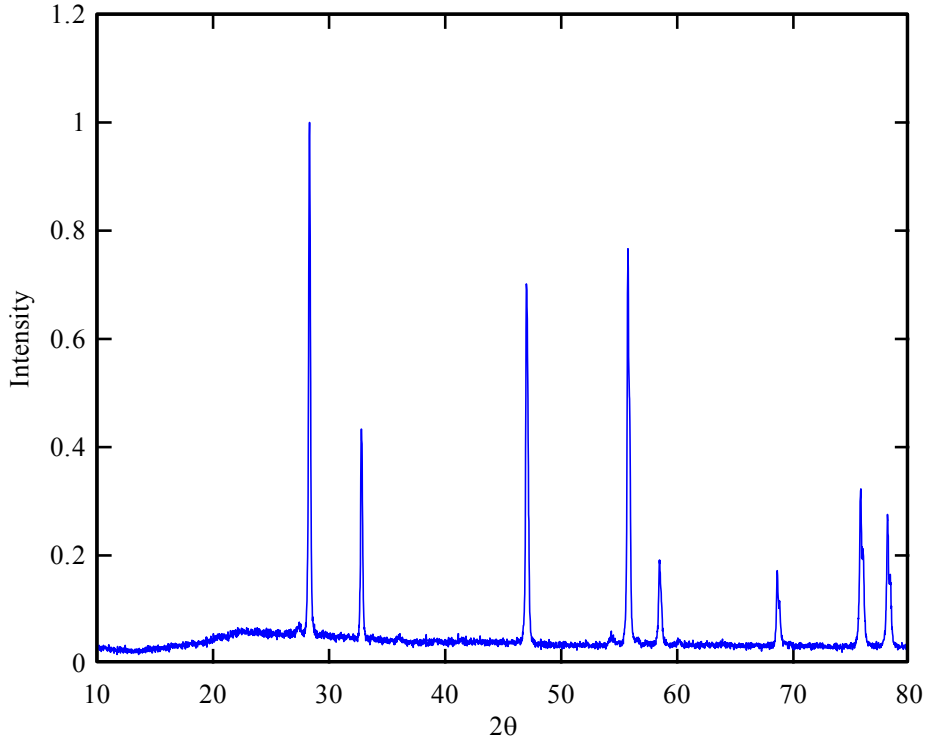

Figure 8-31. X-ray diffraction result of UO_2 with 15 vol% SiC whiskers after hot press sintering.

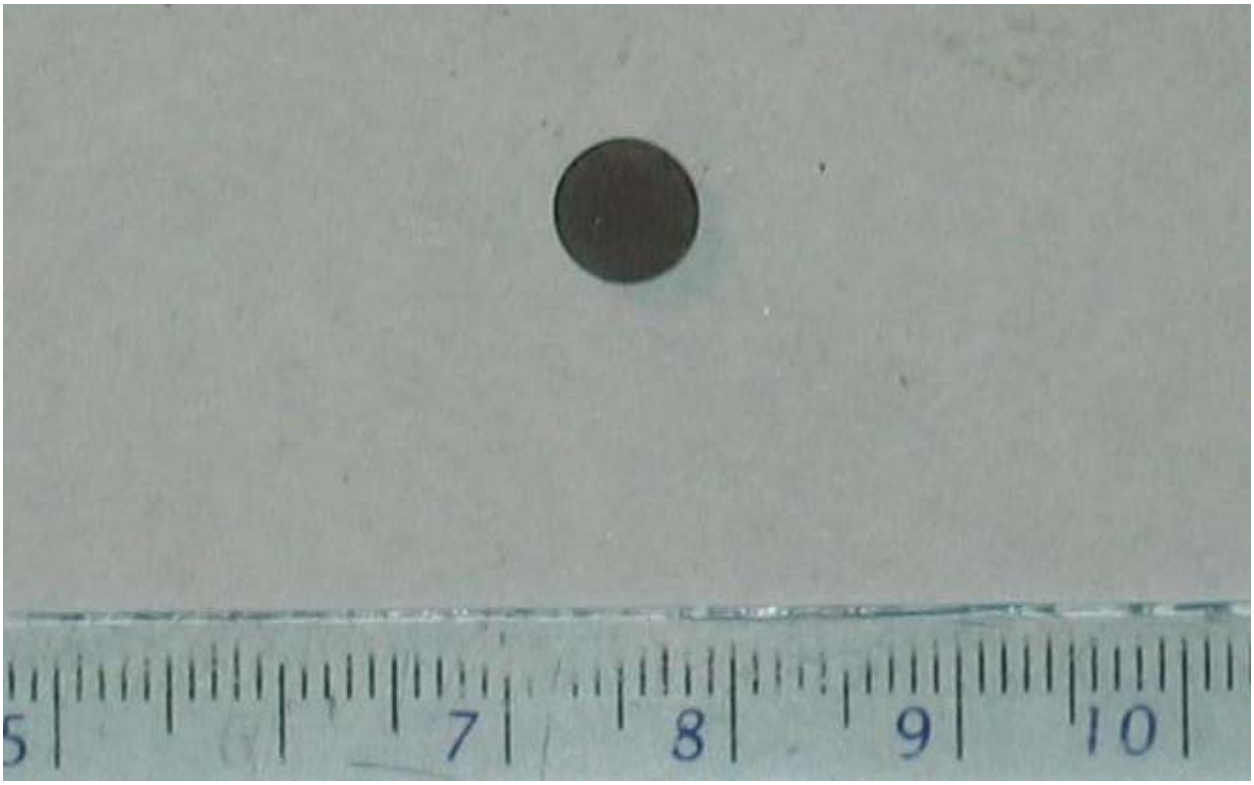

Figure 8-32. The pellet of UO_2 (<25 μ) with 15 vol% SiC whiskers after hot press sintering.

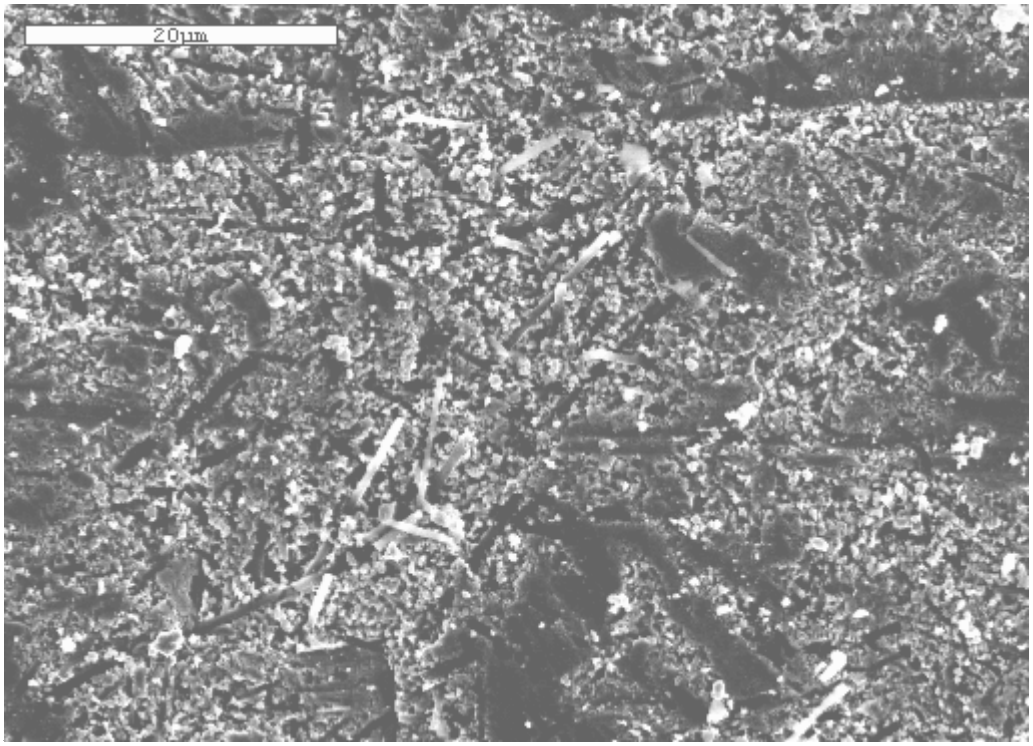

Figure 8-33. Scanning electron microscopy image of UO_2 (<25 μ) with 15 vol% SiC whiskers after hot press sintering, (2,000X).

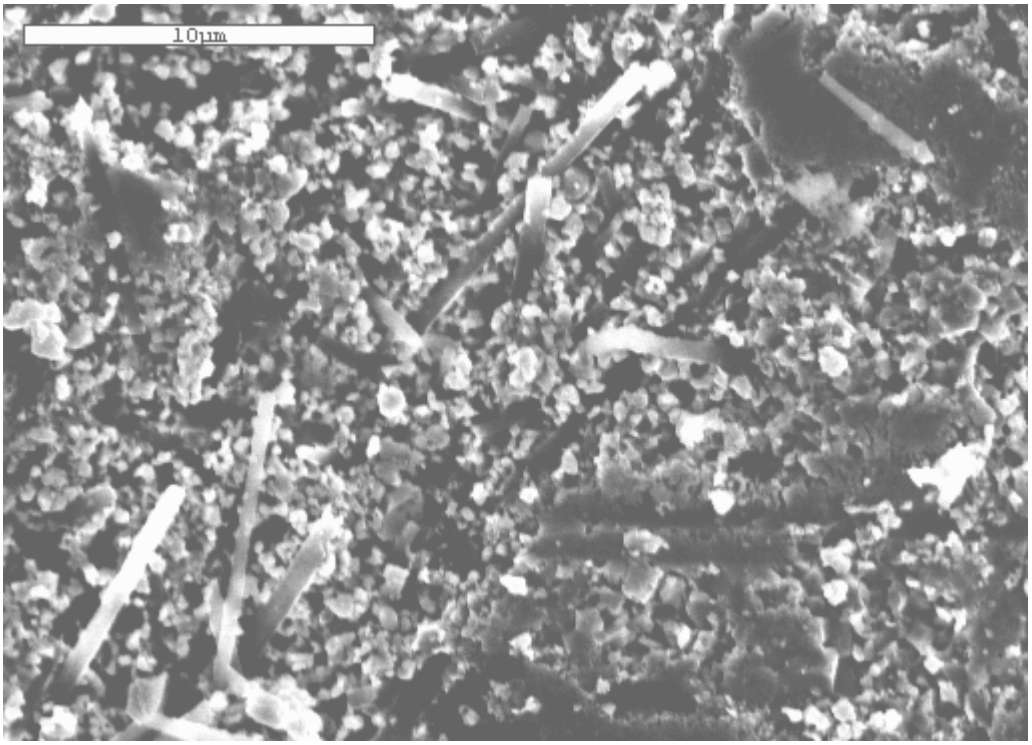

Figure 8-34. Scanning electron microscopy image of UO_2 (<25 µ) with 15 vol% SiC whiskers after hot press sintering, (5,000X).

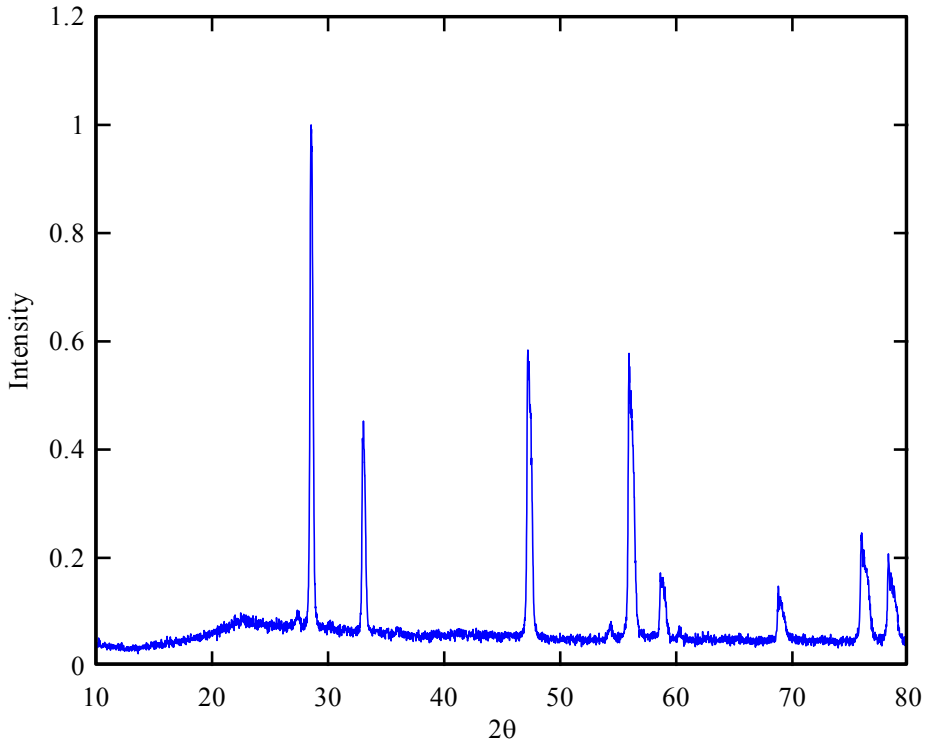

Figure 8-35. X-ray diffraction result of UO_2 (<25 μ) with 15 vol% SiC whiskers after hot press sintering.

Figure 8-36. The pellet of UO_2 with 15 vol% SiC whiskers (from Alfa Aesar) after hot press sintering.

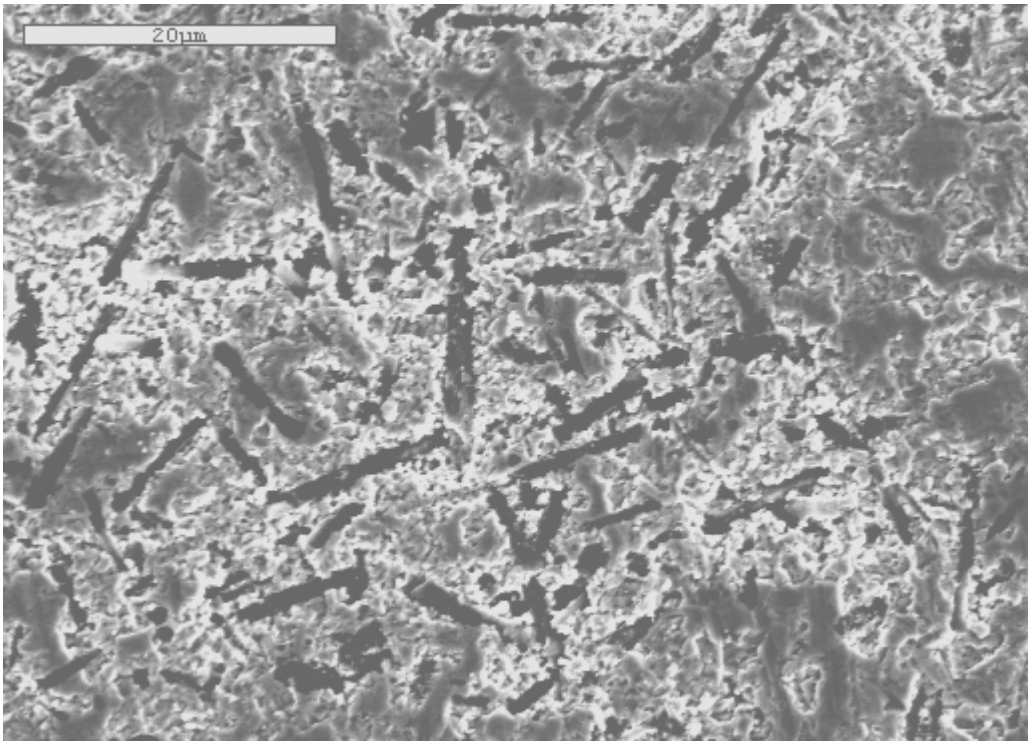

Figure 8-37. Scanning electron microscopy image of UO_2 with 15 vol% SiC whiskers (from Alfa Aesar) after hot press sintering, (2,000X).

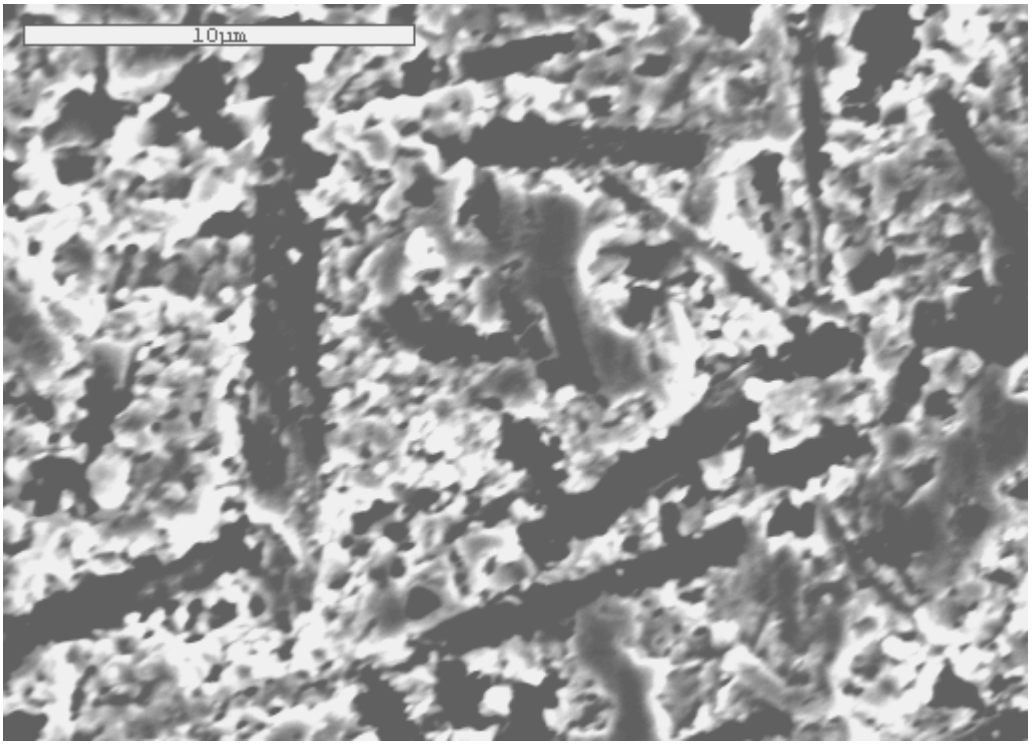

Figure 8-38. Scanning electron microscopy image of UO_2 with 15 vol% SiC whiskers (from Alfa Aesar) after hot press sintering, (5,000X).

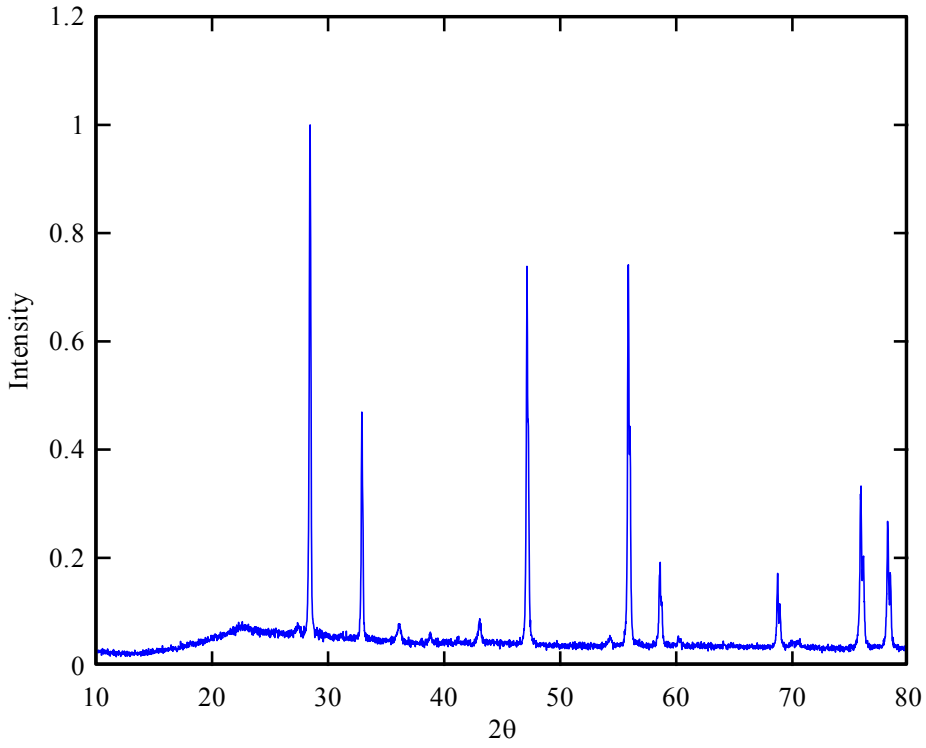

Figure 8-39. X-ray diffraction result of UO_2 with 15 vol% SiC whiskers (from Alfa Aesar) after hot press sintering.

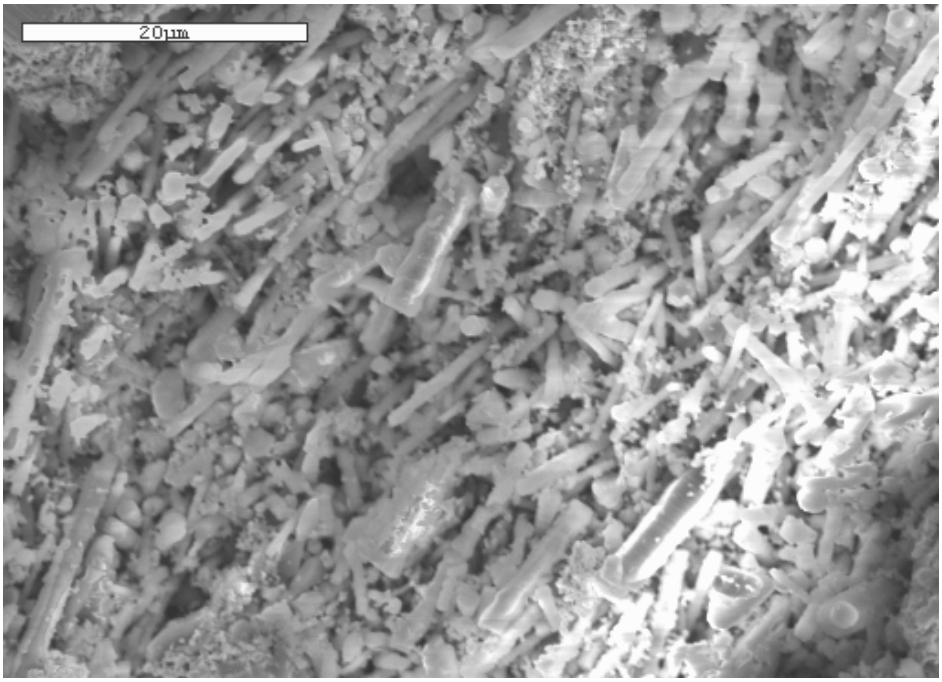

Figure 8-40. Scanning electron microscopy image of the cross section of UO_2 with 30 vol% SiC whiskers after hot press sintering, (2,000X).

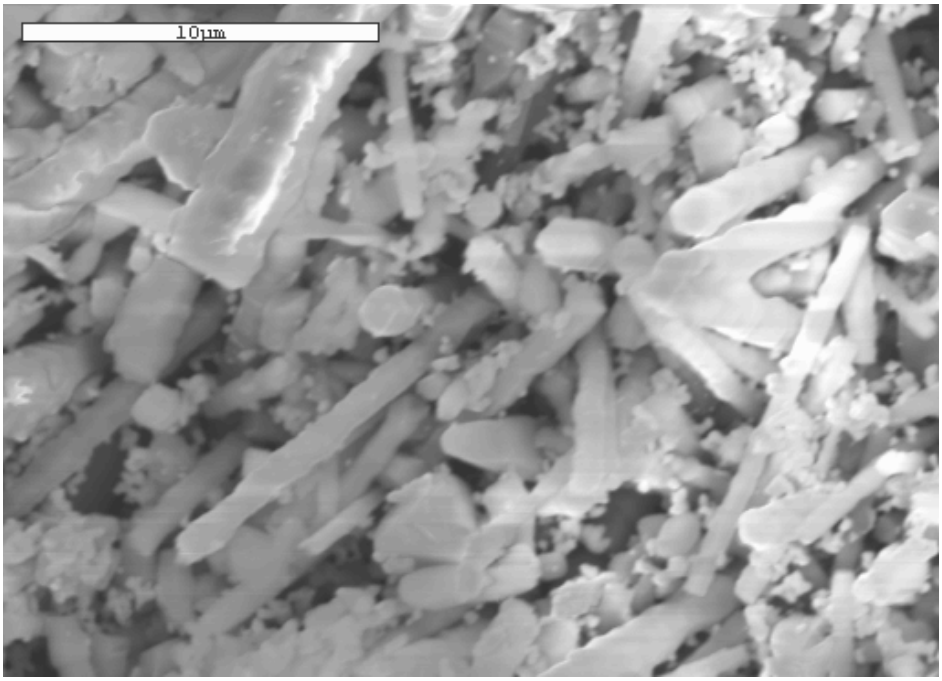

Figure 8-41. Scanning electron microscopy image of the cross section of UO_2 with 30 vol% SiC whiskers after hot press sintering, (5,000X).

CHAPTER 9
CONCLUSIONS AND FUTURE WORK

Conclusion

In this research, the silicon carbide (SiC) whisker-uranium dioxide (UO_2) composite was successfully fabricated by low temperature sintering method of UO_2. High density pellets were achieved at 1200 ^oC by pressureless sintering of UO_2 with 5 vol% SiC whiskers and hot press sintering of UO_2 with 5 vol%, 10 vol% and 15 vol% SiC whiskers. Based on the work by Russell et al. [7], Johnson et al. [8] and Hesselman et al. [9], The thermal conductivity of SiC whisker-UO_2 composite is higher than the thermal conductivity of UO_2.

Two other methods to incorporate SiC into UO_2, the chemical vapor deposition (CVD) process to coat uranium oxide particles with SiC and the pre-ceramic polymer coating on uranium oxide particles process, were not successful.

Because SiC whiskers replace UO_2, there is a reactivity penalty at the end of life (EOL). The neutronic calculation showed the K-infinity of UO_2 with 5 vol%, 10 vol% and 15 vol% SiC are about 2.4%, 4.9% and 7.6% less than the K-infinity of UO_2 fuel at 60 GWD/MTU burnup. The amount of SiC whiskers was limited to 15 vol% in this research to ensure the neutronic properties of the fuel pellet. The neutronic calculation also proved the UO_2 with up to 15 vol% SiC additives can be operate safely in a reactor core because of the negative Doppler coefficient and moderator temperature coefficient.

During the fabrication process of SiC whisker – UO_2 pellet, the low temperature sintering method of UO_2 was used to avoid the reaction between silicon carbide and UO_2 at the temperature above 1377 ^oC. The density of the SiC whisker-UO_2 pellet fabricated by hot press sintering was not significantly affected by the particle size of uranium oxide particle and the type

of SiC whiskers. The SiC whiskers after hot press sintering exhibited a preferential orientation, which is perpendicular to the direction of hot pressing.

Future Work

There are several aspects of this research can be improved or studied in the future work. The thermal conductivity of the UO_2-SiC pellets need to be measured to study the effect of SiC whiskers on the thermal conductivity of UO_2.

The process of mixing SiC whiskers and UO_2 particles need to be improved to make a homogeneous mixture. The UO_2 islands in the SiC whiskers-UO_2 pellet can cause local heat spot, which is highly undesired in the operation of the reactor.

The effect of whiskers orientation, aspect ratio of whiskers, particle size of the matrix and interfacial thermal barrier resistance, if any, on the thermal conductivity of the composite need to be studied. Because the thermal conductivity of single crystal drops significantly after radiation, the change of the thermal conductivity of SiC whiskers-UO_2 pellet under radiation also need to be studied.

APPENDIX A
CASMO INPUT FILES

This appendix contains all of the CASMO-3 input files used to determine the effect of silicon carbide additives on the neutronic properties of uranium dioxide fuel.

The CASMO-3 Input File for Uranium Dioxide Fuel

```
*Crystal River-3 15X15 Assembly UO2 Fuel
TIT TFU=1000  TMO=588  BOR=0 IDE='P32' *Mark-B10E
FUE 1 10.5216/4.66  *FUEL COMP. #, DENSITY/ENRICHMENT
PIN 1 .4699 .4788 .5461/ '1' 'AIR' 'CAN'
PIN 7 .632 .6731/ 'COO' 'CAN'  *Center water hole
PWR 15 1.443 21.81 * PWR with pitch 1.443
FUM 2.778-04  2
PDE 29.36
XEN 0
LPI
7
1 1
1 1 7
1 1 1 1
1 1 1 1 7
1 1 7 1 1 1
1 1 1 1 1 1 1
1 1 1 1 1 1 1 1
DEP 0.0 0.5 5 10 15 20 25 30 35 40 45 50 55 60
STA
TIT *+ , FUEL TEMP BRANCHES
RES 'P32', 0.0 0.5 5 10 15 20 25 30 35 40 45 50 55 60
TFU 900 1000 1100
NLI,STA
TIT *+ , MOD TEMP BRANCHES
RES 'P32', 0.0 0.5 5 10 15 20 25 30 35 40 45 50 55 60
TMO 563 588 613
NLI,STA
END
```

The CASMO-3 Input File for Uranium Dioxide Fuel with 5 w% Silicon Carbide

```
*Crystal River-3 15X15 Assembly UO2 Fuel with 5 w% SiC
TIT TFU=1000  TMO=588  BOR=0 IDE='P32' *Mark-B10E
FUE 1 9.4458/3.9023 92238=79.8384 8000=11.2593 6000=1.4963 14000=3.5037
*FUEL COMP. #, DENSITY/ENRICHMENT
PIN 1 .4699 .4788 .5461/ '1' 'AIR' 'CAN'
PIN 7 .632 .6731/ 'COO' 'CAN'  *Center water hole
PWR 15 1.443 21.81 * PWR with pitch 1.443
FUM 2.778-04  2
PDE 34.43
XEN 0
LPI
7
1 1
1 1 7
1 1 1 1
1 1 1 1 7
1 1 7 1 1 1
1 1 1 1 1 1 1
1 1 1 1 1 1 1 1
DEP 0.0 0.59 5.86 11.73 17.59 23.45 29.31 35.18
    41.04 46.90 52.76 58.63 64.49 70.35
STA
TIT *+ , FUEL TEMP BRANCHES
RES 'P32', 0.0 0.59 5.86 11.73 17.59 23.45 29.31 35.18
     41.04 46.90 52.76 58.63 64.49 70.35
TFU 900 1000 1100
NLI,STA
TIT *+ , MOD TEMP BRANCHES
RES 'P32', 0.0 0.59 5.86 11.73 17.59 23.45 29.31 35.18
     41.04 46.90 52.76 58.63 64.49 70.35
TMO 563 588 613
NLI,STA
END
```

The CASMO-3 Input File for Uranium Dioxide Fuel with 10 w% Silicon Carbide

```
*Crystal River-3 15X15 Assembly UO2 Fuel with 10 w% SiC
TIT TFU=1000  TMO=588  BOR=0 IDE='P32' *Mark-B10E
FUE 1 8.5696/3.6969 92238=75.6364 8000=10.6667 6000=2.9925 14000=7.0075
*FUEL COMP. #, DENSITY/ENRICHMENT
PIN 1 .4699 .4788 .5461/ '1' 'AIR' 'CAN'
PIN 7 .632 .6731/ 'COO' 'CAN'  *Center water hole
PWR 15 1.443 21.81 * PWR with pitch 1.443
FUM 2.778-04  2
PDE 40.06
XEN 0
LPI
7
1 1
1 1 7
1 1 1 1
1 1 1 1 7
1 1 7 1 1 1
1 1 1 1 1 1 1
1 1 1 1 1 1 1 1
DEP 0.0 0.68 6.82 13.64 20.46 27.28 34.10 40.93
    47.75 54.57 61.39 68.21 75.03 81.85
STA
TIT *+ , FUEL TEMP BRANCHES
RES 'P32', 0.0 0.68 6.82 13.64 20.46 27.28 34.10 40.93
     47.75 54.57 61.39 68.21 75.03 81.85
TFU 900 1000 1100
NLI,STA
TIT *+ , MOD TEMP BRANCHES
RES 'P32', 0.0 0.68 6.82 13.64 20.46 27.28 34.10 40.93
     47.75 54.57 61.39 68.21 75.03 81.85
TMO 563 588 613
NLI,STA
END
```

The CASMO-3 Input File for Uranium Dioxide Fuel with 5 vol% Silicon Carbide

```
*Crystal River-3 15X15 Assembly UO2 Fuel with 5 vol% SiC
TIT TFU=1000  TMO=588  BOR=0 IDE='P32' *Mark-B10E
FUE 1 10.156/4.0428 92238=82.7123 8000=11.6646 6000=0.4729 14000=1.1074
*FUEL COMP. #, DENSITY/ENRICHMENT
PIN 1 .4699 .4788 .5461/ '1' 'AIR' 'CAN'
PIN 7 .632 .6731/ 'COO' 'CAN'  *Center water hole
PWR 15 1.443 21.81 * PWR with pitch 1.443
FUM 2.778-04  2
PDE 30.91
XEN 0
LPI
7
1 1
1 1 7
1 1 1 1
1 1 1 1 7
1 1 7 1 1 1
1 1 1 1 1 1 1
1 1 1 1 1 1 1 1
DEP 0.0 0.53 5.26 10.53 15.79 21.05 26.32 31.58
    36.84 42.11 47.37 52.63 57.89 63.16
STA
TIT *+ , FUEL TEMP BRANCHES
RES 'P32', 0.0 0.53 5.26 10.53 15.79 21.05 26.32 31.58
     36.84 42.11 47.37 52.63 57.89 63.16
TFU 900 1000 1100
NLI,STA
TIT *+ , MOD TEMP BRANCHES
RES 'P32', 0.0 0.53 5.26 10.53 15.79 21.05 26.32 31.58
     36.84 42.11 47.37 52.63 57.89 63.16
TMO 563 588 613
NLI,STA
END
```

The CASMO-3 Input File for Uranium Dioxide Fuel with 10 vol% Silicon Carbide

```
*Crystal River-3 15X15 Assembly UO2 Fuel with 10 vol% SiC
TIT TFU=1000  TMO=588  BOR=0 IDE='P32' *Mark-B10E
FUE 1 9.7904/3.9730 92238=81.2850 8000=11.4633 6000=0.9812 14000=2.2975
*FUEL COMP. #, DENSITY/ENRICHMENT
PIN 1 .4699 .4788 .5461/ '1' 'AIR' 'CAN'
PIN 7 .632 .6731/ 'COO' 'CAN'  *Center water hole
PWR 15 1.443 21.81 * PWR with pitch 1.443
FUM 2.778-04  2
PDE 32.63
XEN 0
LPI
7
1 1
1 1 7
1 1 1 1
1 1 1 1 7
1 1 7 1 1 1
1 1 1 1 1 1 1
1 1 1 1 1 1 1 1
DEP 0.0 0.56 5.56 11.11 16.67 22.22 27.78 33.33
    38.89 44.44 50.00 55.56 61.11 66.67
STA
TIT *+ , FUEL TEMP BRANCHES
RES 'P32', 0.0 0.56 5.56 11.11 16.67 22.22 27.78 33.33
     38.89 44.44 50.00 55.56 61.11 66.67
TFU 900 1000 1100
NLI,STA
TIT *+ , MOD TEMP BRANCHES
RES 'P32', 0.0 0.56 5.56 11.11 16.67 22.22 27.78 33.33
     38.89 44.44 50.00 55.56 61.11 66.67
TMO 563 588 613
NLI,STA
END
```

The CASMO-3 Input File for Uranium Dioxide Fuel with 15 vol% Silicon Carbide

```
*Crystal River-3 15X15 Assembly UO2 Fuel with 15 vol% SiC
TIT TFU=1000  TMO=588  BOR=0 IDE='P32' *Mark-B10E
FUE 1 9.4249/3.8978 92238=79.7470 8000=11.2464 6000=1.5288 14000=3.5800
*FUEL COMP. #, DENSITY/ENRICHMENT
PIN 1 .4699 .4788 .5461/ '1' 'AIR' 'CAN'
PIN 7 .632 .6731/ 'COO' 'CAN'  *Center water hole
PWR 15 1.443 21.81 * PWR with pitch 1.443
FUM 2.778-04  2
PDE 34.55
XEN 0
LPI
7
1 1
1 1 7
1 1 1 1
1 1 1 1 7
1 1 7 1 1 1
1 1 1 1 1 1 1
1 1 1 1 1 1 1 1
DEP 0.0 0.59 5.88 11.76 17.65 23.53 29.41 35.29
    41.18 47.06 52.94 58.82 64.71 70.59
STA
TIT *+ , FUEL TEMP BRANCHES
RES 'P32', 0.0 0.59 5.88 11.76 17.65 23.53 29.41 35.29
     41.18 47.06 52.94 58.82 64.71 70.59
TFU 900 1000 1100
NLI,STA
TIT *+ , MOD TEMP BRANCHES
RES 'P32', 0.0 0.59 5.88 11.76 17.65 23.53 29.41 35.29
     41.18 47.06 52.94 58.82 64.71 70.59
TMO 563 588 613
NLI,STA
END
```

The CASMO-3 Input File for Uranium Dioxide Fuel with 5 vol% Silicon Carbide at Lower Fuel Temperature

```
*Crystal River-3 15X15 Assembly UO2 Fuel with 5 vol% SiC
TIT TFU=800  TMO=588  BOR=0 IDE='P32' *Mark-B10E
FUE 1 10.156/4.0428 92238=82.7123 8000=11.6646 6000=0.4729 14000=1.1074
*FUEL COMP. #, DENSITY/ENRICHMENT
PIN 1 .4699 .4788 .5461/ '1' 'AIR' 'CAN'
PIN 7 .632 .6731/ 'COO' 'CAN'  *Center water hole
PWR 15 1.443 21.81 * PWR with pitch 1.443
FUM 2.778-04  2
PDE 30.91
XEN 0
LPI
7
1 1
1 1 7
1 1 1 1
1 1 1 1 7
1 1 7 1 1 1
1 1 1 1 1 1 1
1 1 1 1 1 1 1 1
DEP 0.0 0.53 5.26 10.53 15.79 21.05 26.32 31.58
    36.84 42.11 47.37 52.63 57.89 63.16
STA
TIT *+ , FUEL TEMP BRANCHES
RES 'P32', 0.0 0.53 5.26 10.53 15.79 21.05 26.32 31.58
     36.84 42.11 47.37 52.63 57.89 63.16
TFU 700 800 900
NLI,STA
TIT *+ , MOD TEMP BRANCHES
RES 'P32', 0.0 0.53 5.26 10.53 15.79 21.05 26.32 31.58
     36.84 42.11 47.37 52.63 57.89 63.16
TMO 563 588 613
NLI,STA
END
```

The CASMO-3 Input File for Uranium Dioxide Fuel with 10 vol% Silicon Carbide at Lower Fuel Temperature

```
*Crystal River-3 15X15 Assembly UO2 Fuel with 10 vol% SiC
TIT TFU=800  TMO=588  BOR=0 IDE='P32' *Mark-B10E
FUE 1 9.7904/3.9730 92238=81.2850 8000=11.4633 6000=0.9812 14000=2.2975
*FUEL COMP. #, DENSITY/ENRICHMENT
PIN 1 .4699 .4788 .5461/ '1' 'AIR' 'CAN'
PIN 7 .632 .6731/ 'COO' 'CAN'  *Center water hole
PWR 15 1.443 21.81 * PWR with pitch 1.443
FUM 2.778-04  2
PDE 32.63
XEN 0
LPI
7
1 1
1 1 7
1 1 1 1
1 1 1 1 7
1 1 7 1 1 1
1 1 1 1 1 1 1
1 1 1 1 1 1 1 1
DEP 0.0 0.56 5.56 11.11 16.67 22.22 27.78 33.33
    38.89 44.44 50.00 55.56 61.11 66.67
STA
TIT *+ , FUEL TEMP BRANCHES
RES 'P32', 0.0 0.56 5.56 11.11 16.67 22.22 27.78 33.33
     38.89 44.44 50.00 55.56 61.11 66.67
TFU 700 800 900
NLI,STA
TIT *+ , MOD TEMP BRANCHES
RES 'P32', 0.0 0.56 5.56 11.11 16.67 22.22 27.78 33.33
     38.89 44.44 50.00 55.56 61.11 66.67
TMO 563 588 613
NLI,STA
END
```

The CASMO-3 Input File for Uranium Dioxide Fuel with 15 vol% Silicon Carbide at Lower Fuel Temperature

```
*Crystal River-3 15X15 Assembly UO2 Fuel with 15 vol% SiC
TIT TFU=800  TMO=588  BOR=0 IDE='P32' *Mark-B10E
FUE 1 9.4249/3.8978 92238=79.7470 8000=11.2464 6000=1.5288 14000=3.5800
*FUEL COMP. #, DENSITY/ENRICHMENT
PIN 1 .4699 .4788 .5461/ '1' 'AIR' 'CAN'
PIN 7 .632 .6731/ 'COO' 'CAN'  *Center water hole
PWR 15 1.443 21.81 * PWR with pitch 1.443
FUM 2.778-04  2
PDE 34.55
XEN 0
LPI
7
1 1
1 1 7
1 1 1 1
1 1 1 1 7
1 1 7 1 1 1
1 1 1 1 1 1 1
1 1 1 1 1 1 1 1
DEP 0.0 0.59 5.88 11.76 17.65 23.53 29.41 35.29
    41.18 47.06 52.94 58.82 64.71 70.59
STA
TIT *+ , FUEL TEMP BRANCHES
RES 'P32', 0.0 0.59 5.88 11.76 17.65 23.53 29.41 35.29
     41.18 47.06 52.94 58.82 64.71 70.59
TFU 700 800 900
NLI,STA
TIT *+ , MOD TEMP BRANCHES
RES 'P32', 0.0 0.59 5.88 11.76 17.65 23.53 29.41 35.29
     41.18 47.06 52.94 58.82 64.71 70.59
TMO 563 588 613
NLI,STA
END
```

The CASMO-3 Input File for Uranium Dioxide Fuel with 5 vol% Silicon Carbide at Lower Fuel Temperature and Boron Let Down

```
*Crystal River-3 15X15 Assembly UO2 Fuel with 5 vol% SiC
TIT TFU=800  TMO=588  BOR=1400 IDE='P32' *Mark-B10E
FUE 1 10.156/4.0428 92238=82.7123 8000=11.6646 6000=0.4729 14000=1.1074
*FUEL COMP. #, DENSITY/ENRICHMENT
PIN 1 .4699 .4788 .5461/ '1' 'AIR' 'CAN'
PIN 7 .632 .6731/ 'COO' 'CAN'  *Center water hole
PWR 15 1.443 21.81 * PWR with pitch 1.443
FUM 2.778-04  2
PDE 30.91
XEN 0
LPI
7
1 1
1 1 7
1 1 1 1
1 1 1 1 7
1 1 7 1 1 1
1 1 1 1 1 1 1
1 1 1 1 1 1 1 1
PVD 'BOR'
    0      1400
    26.32  10
    26.33  1400
    47.37  10
    47.38  1400
    63.16  10
DEP 0.0 0.53 5.26 10.53 15.79 21.05 26.32 26.33 26.74 30.53 34.74
    38.95 43.16 47.37 47.38 47.68 50.53 53.68 56.84 60.0 63.16
STA
TIT *+ , FUEL TEMP BRANCHES
RES 'P32', 0.0 0.53 5.26 10.53 15.79 21.05 26.32 26.33 26.74 30.53
    34.74 38.95 43.16 47.37 47.38 47.68 50.53 53.68 56.84 60.0 63.16
TFU 700 800 900
NLI,STA
TIT *+ , MOD TEMP BRANCHES
RES 'P32', 0.0 0.53 5.26 10.53 15.79 21.05 26.32 26.33 26.74 30.53
    34.74 38.95 43.16 47.37 47.38 47.68 50.53 53.68 56.84 60.0 63.16
TMO 563 588 613
NLI,STA
END
```

The CASMO-3 Input File for Uranium Dioxide Fuel with 10 vol% Silicon Carbide at Lower Fuel Temperature and Boron Let Down

```
*Crystal River-3 15X15 Assembly UO2 Fuel with 10 vol% SiC
TIT TFU=800  TMO=588  BOR=1400 IDE='P32' *Mark-B10E
FUE 1 9.7904/3.9730 92238=81.2850 8000=11.4633 6000=0.9812 14000=2.2975
*FUEL COMP. #, DENSITY/ENRICHMENT
PIN 1 .4699 .4788 .5461/ '1' 'AIR' 'CAN'
PIN 7 .632 .6731/ 'COO' 'CAN'  *Center water hole
PWR 15 1.443 21.81 * PWR with pitch 1.443
FUM 2.778-04  2
PDE 32.63
XEN 0
LPI
7
1 1
1 1 7
1 1 1 1
1 1 1 1 7
1 1 7 1 1 1
1 1 1 1 1 1 1
1 1 1 1 1 1 1 1
PVD 'BOR'
    0      1400
    27.78  10
    27.79  1400
    50.0   10
    50.01  1400
    66.67  10
DEP 0.0 0.56 5.56 11.11 16.67 22.22 27.78 27.79 28.22 32.22 36.67
    41.11 45.56 50.0 50.01 50.33 53.33 56.67 60.0 63.33 66.67
STA
TIT *+ , FUEL TEMP BRANCHES
RES 'P32', 0.0 0.56 5.56 11.11 16.67 22.22 27.78 27.79 28.22 32.22
    36.67 41.11 45.56 50.0 50.01 50.33 53.33 56.67 60.0 63.33 66.67
TFU 700 800 900
NLI,STA
TIT *+ , MOD TEMP BRANCHES
RES 'P32', 0.0 0.56 5.56 11.11 16.67 22.22 27.78 27.79 28.22 32.22
    36.67 41.11 45.56 50.0 50.01 50.33 53.33 56.67 60.0 63.33 66.67
TMO 563 588 613
NLI,STA
END
```

The CASMO-3 Input File for Uranium Dioxide Fuel with 10 vol% Silicon Carbide at Lower Fuel Temperature and Boron Let Down

```
*Crystal River-3 15X15 Assembly UO2 Fuel with 15 vol% SiC
TIT TFU=800  TMO=588  BOR=1400 IDE='P32' *Mark-B10E
FUE 1 9.4249/3.8978 92238=79.7470 8000=11.2464 6000=1.5288 14000=3.5800
*FUEL COMP. #, DENSITY/ENRICHMENT
PIN 1 .4699 .4788 .5461/ '1' 'AIR' 'CAN'
PIN 7 .632 .6731/ 'COO' 'CAN'  *Center water hole
PWR 15 1.443 21.81 * PWR with pitch 1.443
FUM 2.778-04  2
PDE 34.55
XEN 0
LPI
7
1 1
1 1 7
1 1 1 1
1 1 1 1 7
1 1 7 1 1 1
1 1 1 1 1 1 1
1 1 1 1 1 1 1 1
PVD 'BOR'
    0      1400
    29.41  10
    29.42  1400
    52.94  10
    52.95  1400
    70.59  10
DEP 0.0 0.59 5.88 11.76 17.65 23.53 29.41 29.42 29.88 34.12 38.82
    43.53 48.24 52.94 52.95 53.29 56.47 60.0 63.53 67.06 70.59
STA
TIT *+ , FUEL TEMP BRANCHES
RES 'P32', 0.0 0.59 5.88 11.76 17.65 23.53 29.41 29.42 29.88 34.12
    38.82 43.53 48.24 52.94 52.95 53.29 56.47 60.0 63.53 67.06 70.59
TFU 700 800 900
NLI,STA
TIT *+ , MOD TEMP BRANCHES
RES 'P32', 0.0 0.59 5.88 11.76 17.65 23.53 29.41 29.42 29.88 34.12
    38.82 43.53 48.24 52.94 52.95 53.29 56.47 60.0 63.53 67.06 70.59
TMO 563 588 613
NLI,STA
END
```

APPENDIX B
HOT PRESS SINTERING TEMPERATURE CALCULATION

The surface temperature of the graphite tube is 1200 ^{o}C. The geometry of the alumina die and the graphite tube is shown in Figure 8-17. The steady state temperatures of the alumina tube and mixed powder were calculated base on Equation B-1 and Equation B-5.

For graphite tube,

$$\frac{1}{r}\frac{d}{dr}(r\frac{dT}{dr})+\frac{q'''}{k_g}=0 \quad \text{(B-1)}$$

Where q''' is the rate of heat production per unit volume and K_g is the thermal conductivity of graphite.

The two boundary conditions of the graphite tubs are Equation 3-2 and Equation 3-3.

$$\frac{dT}{dr}=0 \text{ at } r=0.25 \text{ inch} \quad \text{(B-2)}$$

$$T\,(r=0.5 \text{ inch})=1200\ ^{o}\text{C} \quad \text{(B-3)}$$

The heat flux on the surface of the graphite tube can be calculated by Equation 3-4.

$$q'' = \varepsilon\sigma T^4 \quad \text{(B-4)}$$

Where ε is the emissivity, which is 0.95 for graphite, σ is the Stefan-Boltzmann constant, which equals to 5.67x10^{-8} W/m^2·K^4.

The calculated graphite temperature at r = 0.25 inch is 1201.4 ^{o}C.

For alumina tube,

$$\frac{1}{r}\frac{d}{dr}(r\frac{dT}{dr})=0 \quad \text{(B-5)}$$

The two boundary conditions of the graphite tubs are Equation 3-6 and Equation 3-7.

$$\frac{dT}{dr}=0 \text{ at } r=0.125 \text{ inch} \quad \text{(B-6)}$$

$T\,(r = 0.25 \text{ inch}) = 1201.4\ ^{o}\text{C}$ (B-7)

The calculated temperature of alumina tube is a constant, 1201.4 ^{o}C.

For mixed powder,

$$\frac{1}{r}\frac{d}{dr}\left(r\frac{dT}{dr}\right) = 0 \quad \text{(B-8)}$$

The two boundary conditions of the graphite tubs are Equation 3-6 and Equation 3-7.

$$\frac{dT}{dr} = 0 \text{ at } r = 0 \quad \text{(B-9)}$$

$T\,(r = 0.125 \text{ inch}) = 1201.4\ ^{o}\text{C}$ (B-10)

The calculated temperature of mixed powder is also a constant, 1201.4 ^{o}C.

LIST OF REFERENCES

[1] J. K. Fink, Journal of Nuclear Materials 279 (2000) 1-18.

[2] S.-H. Kim, C.-Y. Joung, H.-S. Kim, Y.-W. Lee, H.-J. Ryu, D.-S. Sohn, D.-J. Kim, Journal of Nuclear Materials 352 (2006) 151-156.

[3] S. Ishimoto, M. Hirai, K. Ito, Y. Korei, Journal of Nuclear Science and Technology 33 (1996) 134-140.

[4] G. A. Slack, Journal of Applied Physics 35 (1964) 3460-3466.

[5] R. A. Verrall, M. D. Vlajic, V. D. Krstic, Journal of Nuclear Materials 274 (1999) 54-60.

[6] M. Edenius, A. Ahlin, Nuclear Science and Engineering 100 (1988) 342-351.

[7] L. M. Russell, L. F. Johnson, D. P. H. Hasselman, R. Ruh, Journal of the American Ceramic Society 70 (1987) 226-229.

[8] L. F. Johnson, D. P. H. Hasselman, K. Chyung, Journal of the American Ceramic Society 70 (1987) 135-138.

[9] D. P. H. Hasselman, K. Y. Donaldson, J. R. Thomas, Jr., J. J. Brennan, Journal of the American Ceramic Society 79 (1996) 742-748.

[10] A. A. Solomon, J. Fourcade, S.-G. Lee, S. Kuchibhotla, S. Revankar, R. Latta, P. L. Holman, J. K. McCoy, The polymer impregnation and pyrolysis method for producing enhanced conductivity LWR fuels, in: American Nuclear Society, La Grange Park, IL 60526, United States, Orlando, FL, United States, 2004, pp. 146-155.

[11] K. H. Sarma, J. Fourcade, S. G. Lee, A. A. Solomon, Journal of Nuclear Materials 352 (2006) 324-333.

[12] G. C. Allen, J. A. Crofts, T. Swan, pp 630-639 of Reactivity of Solids. Anderson, J.S. (ed.). London ;Chapman and Hall Ltd., 1972.; From 7. international symposium on the reactivity of solids, Bristol, UK, 17 Jul 1972.

[13] N. Fuhrman, J. L. C. Hower, R. B. Holden, American Ceramic Society -- Journal 46 (1963) 114-121.

[14] K. Langrod, American Ceramic Society Bulletin (U.S.); Vol: 39 (1960) Pages: 366-369.

[15] A. Turos, R. Falcone, A. Drigo, A. Sambo, L. Nowicki, N. Madi, J. Jagielski, H. Matzke, Nuclear Instruments and Methods in Physics Research Section B: Beam Interactions with Materials and Atoms 118 (1996) 659-662.

[16] K. Kapoor, A. Ahmad, A. Laksminarayana, G. V. S. Hemanth Rao, Journal of Nuclear Materials 366 (2007) 87-98.

[17] J. J. Carbajo, G. L. Yoder, S. G. Popov, V. K. Ivanov, Journal of Nuclear Materials 299 (2001) 181-198.

[18] S. Glasstone, A. Sesonske, Nuclear Reactor Engineering, Van Nostrand Reinhold, 1980.

[19] R. J. McEachern, P. Taylor, Journal of Nuclear Materials 254 (1998) 87-121.

[20] S. Siegel, Acta Crystallographica 8 (1955) 617-619.

[21] I. C. Hobson, R. Taylor, J. B. Ainscough, Journal of Physics D: Applied Physics 7 (1974) 1003-1015.

[22] H. Bailly, D. Menessier, C. Prunier, The Nuclear Fuel of Pressurized Water Reactors and Fast Neutron Reactors: Design and Behavior, Lavoisier Publishing, France, 1999.

[23] E. A. Schaefer, J. O. Hibbits, Anal. Chem., 41: 254-9(Feb. 1969). (1969).

[24] P. G. Lucuta, H. Matzke, I. J. Hastings, Journal of Nuclear Materials 232 (1996) 166-180.

[25] G. L. Harris, Properties of Silicon Carbide, Institution of Electrical Engineers, 1995.

[26] H. Etherington, Nuclear Engineering Handbook, McGraw-Hill Book Company, Inc, New York, 1958.

[27] R. J. Price, Nuclear Technology 35 (1977) 320-336.

[28] R. J. Price, Journal of Nuclear Materials 46 (1973) 268-272.

[29] L. L. Snead, J. C. Hay, Journal of Nuclear Materials 273 (1999) 213-220.

[30] H. Hirayama, T. Kawakubo, A. Goto, T. Kaneko, Journal of the American Ceramic Society 72 (1989) 2049-2053.

[31] K. Minato, K. Fukuda, Journal of Nuclear Materials 149 (1987) 233-246.

[32] J. Zheng, M. Akinc, Journal of the American Ceramic Society 84 (2001) 2479-2483.

[33] D. Belitskus, Fiber and Whisker Reinforced Ceramics for Structural Applications, Marcel Dekker, Inc, New York, 1993.

[34] G. C. Wei, P. F. Becher, American Ceramic Society Bulletin 64 (1985) 298-304.

[35] L. Sun, J.-S. Pan, Y.-J. Liu, Journal of Materials Science Letters 20 (2001) 1421-1423.

[36] W. Lippmann, J. Knorr, R. Noring, M. Umbreit, Nuclear Engineering and Design 205 (2001) 13-22.

[37] C. Ganguly, U. Basak, Journal of Nuclear Materials 178 (1991) 179-183.

[38] K. W. Song, K. S. Kim, K. W. Kang, Y. H. Jung, Journal of Nuclear Materials 317 (2003) 204-211.

[39] B. Ayaz, A. N. Bilge, Journal of Nuclear Materials 280 (2000) 45-50.

[40] Y. Harada, Journal of Nuclear Materials 245 (1997) 217-223.

[41] J. Williams, E. Barnes, R. Scott, A. Hall, Journal of Nuclear Materials 1 (1959) 28-38.

[42] A. J. Steckl, C. Yuan, J. P. Li, M. J. Loboda, Applied Physics Letters 63 (1993) 3347.

[43] C. Lin, C. Lin, A. J. Steckl, J. Scofield, Electron Devices, IEEE Transactions on 50 (2003) 2159-2164.

[44] T. Kunstmann, S. Veprek, Applied Physics Letters 67 (1995) 3126.

[45] S. Madapura, A. J. Steckl, M. Loboda, Journal of the Electrochemical Society 146 (1999) 1197-1202.

[46] K. Yagi, H. Nagasawa, Journal of Crystal Growth 174 (1997) 653-657.

[47] J. A. Powell, L. G. Matus, M. A. Kuczmarski, Journal of the Electrochemical Society 134 (1987) 1558-1565.

[48] M. J. Loboda, Microelectronic Engineering 50 (2000) 15-23.

[49] H. Sankur, Thin Solid Films 218 (1992) 161-169.

[50] P. Mandracci, S. Ferrero, G. Cicero, F. Giorgis, C. F. Pirri, G. Barucca, R. Reitano, P. Musumeci, L. Calcagno, G. Foti, Thin Solid Films 383 (2001) 169-171.

[51] K. L. Choy, Progress in Materials Science 48 (2003) 57-170.

[52] T. D. Gulden, Journal of the American Ceramic Society 51 (1968) 424-427.

[53] L. H. Ford, N. S. Hibbert, D. G. Martin, Journal of Nuclear Materials 45 (1972) 139-149.

[54] D. A. Grigoriev, M. J. Edirisinghe, X. Bao, J. R. G. Evans, Z. B. Luklinska, Philosophical Magazine Letters 81 (2001) 285-291.

[55] J. Zheng, M. J. Kramer, M. Akinc, Journal of the American Ceramic Society 83 (2000) 2961-2966.

[56] M. Berbon, M. Calabrese, Journal of the American Ceramic Society 85 (2002) 1891-1893.

[57] R. Warren, Ceramic-Matrix Composites, Blackie Academic and Professional, New York, 1992.

BIOGRAPHICAL SKETCH

Jiwei Wang was born in 1978 in Anshan City, Liaoning Province, People's Republic of China. His parents are Li Wang and Shaofen Liu. He has an older sister, Jihong Wang. Jiwei graduated with a Bachelor of Science in nuclear engineering from Tsinghua University in July 2001. After that, he took the TOEFL and GRE tests and prepared to pursue a graduate degree in United States. Jiwei enrolled in nuclear and radiological engineering's graduate program at the University of Florida in January 2003. He received a non thesis Master of Science degree in December 2006. He is scheduled to graduate with a Doctor of Philosophy degree in August 2008.